GEOCHEMICAL CHARACTERIZATION OF GEOTHERMAL SYSTEMS IN TURKEY AS NATURAL ANALOGUES FOR GEOLOGICAL STORAGE OF CO_2

A THESIS SUBMITTED TO
THE GRADUATE SCHOOL OF NATURAL AND APPLIED SCIENCES
OF
MIDDLE EAST TECHNICAL UNIVERSITY

BY

SANEM ELİDEMİR

IN PARTIAL FULFILLMENT OF THE REQUIREMENTS
FOR
THE DEGREE OF MASTER OF SCIENCE
IN
GEOLOGICAL ENGINEERING

SEPTEMBER 2014

Approval of the thesis:

GEOCHEMICAL CHARACTERIZATION OF GEOTHERMAL SYSTEMS IN TURKEY AS NATURAL ANALOGUES FOR GEOLOGICAL STORAGE OF CO_2

submitted by **SANEM ELİDEMİR** in partial fulfillment of the requirements for the degree of **Master of Science in Geological Engineering Department, Middle East Technical University** by,

Prof. Dr. Canan Özgen _____
Dean, Graduate School of **Natural and Applied Science**

Prof. Dr. Erdin Bozkurt _____
Head of Department, **Geological Engineering**

Prof. Dr. Nilgün Güleç _____
Supervisor, **Geological Engineering Dept., METU**

Examining Committee Members:

Prof. Dr. Ender Okandan _____
Petroleum and Natural Gas Engineering Dept., METU

Prof. Dr. Nilgün Güleç _____
Geological Engineering Dept., METU

Prof. Dr. Nurkan Karahanoğlu _____
Geological Engineering Dept., METU

Prof. Dr. Halim Mutlu _____
Geological Engineering Dept., Ankara University

Assist. Prof. Dr. Fatma Toksoy Köksal _____
Geological Engineering Dept., METU

Date: 02.09.2014

I hereby declare that all information in this document has been obtained and presented in accordance with academic rules and ethical conduct. I also declare that, as required by these rules and conduct, I have fully cited and referenced all material and results that are not original to this work.

Name, Last name : Sanem Elidemir

Signature :

ABSTRACT

GEOCHEMICAL CHARACTERIZATION OF GEOTHERMAL SYSTEMS IN TURKEY AS NATURAL ANALOGUES FOR GEOLOGICAL STORAGE OF CO_2

Elidemir, Sanem

M.S., Department of Geological Engineering

Supervisor: Prof. Dr. Nilgün Güleç

September 2014, 150 pages

To mitigate the unfavourable effect of CO_2 emission on global warming and climate change, geological storage of CO_2 is currently regarded to be one of the major strategies. Deep saline formations constitute one of the alternative reservoirs for hosting the injected CO_2 and the information about the behaviour of these reservoirs is provided via the studies of natural analogues.

This thesis is concerned with the geothermal systems of Turkey as natural analogues for CO_2 storage sites and the evaluation of their geochemical characteristics in terms of possible hydrogeochemical processes involved in CO_2 storage. For the selected geothermal fields from western, eastern and northern Anatolia, the hydrogeochemical processes and potential trapping mechanisms controlling the systems are determined with the assistance of various geochemical approaches including the geochemical characterization of the system, speciation-

solubility calculations, estimation of relative contribution of carbonate and sulphate minerals to the system, and modelling studies (such as inverse modelling, dedolomitization modelling) depending on the behaviour of the field. The results lead to the recognition of three different groups of geothermal systems with respect to the dominant trapping mechanisms: mineral trapping, solubility trapping and mineral ± solubility trapping. In some of the fields from western Anatolia, mineral trapping seems to be the major mechanism, while the others show the effects of both mineral and solubility trapping; a special mechanism named dedolomitization is also identified for Emet geothermal field. For eastern Anatolian fields, and for the fields located along the North Anatolian Fault Zone, solubility trapping is the dominant mechanism.

Keywords: CO_2 storage, geothermal system, trapping mechanism, dedolomitization, hydrogeochemistry.

ÖZ

CO_2 DEPOLAMA SAHALARININ DOĞAL BENZERLERİ OLARAK TÜRKİYE'DEKİ JEOTERMAL SİSTEMLERİN JEOKİMYASAL KARAKTERİZASYONU

Elidemir, Sanem
Yüksek Lisans, Jeoloji Mühendisliği Bölümü
Tez Yöneticisi: Prof. Dr. Nilgün Güleç

Eylül 2014, 150 sayfa

CO_2 emisyonunun küresel ısınma ve iklim değişimi üzerindeki olumsuz etkisini azaltmak için, gündemde olan başlıca stratejilerden biri CO_2 gazının yeraltı katmanlarında depolanmasıdır. Derin tuzlu akiferler, enjekte edilen CO_2'in depolanması için alternatif rezervuarlardan birini oluşturur ve bu rezervuarların davranışı hakkındaki bilgi doğal benzerleri üzerindeki çalışmalarla sağlanır.

Bu tez çalışması, CO_2 depolama sahalarının doğal benzerleri olan Türkiye'deki jeotermal sistemlere ve bu sistemlerin jeokimyasal özelliklerinin CO_2 depolama sırasında gelişebilecek muhtemel hidrojeokimyasal süreçler açısından değerlendirilmesine ilişkindir. Batı, doğu ve kuzey Anadolu'dan seçilmiş jeotermal sistemler için bu sistemleri kontrol eden hidrojeokimyasal süreçler ve potansiyel kapanlanma mekanizmaları, sistemin jeokimyasal karakterizasyonu, türleşme-çözünürlük hesaplamaları, karbonat ve sülfat minerallerinin göreceli olarak sisteme

katkısının tahmini ve saha davranışına göre (tersine modelleme, dedolomitleşme modellemesi gibi) modelleme çalışmalarını içeren çeşitli jeokimyasal yöntemlerle belirlenmiştir. Sonuçlar baskın kapanlanma mekanizmalarına göre üç farklı grubun tanımlanmasına yol açmıştır: mineral kapanlanması, çözünürlük kapanlanması ve mineral ± çözünürlük kapanlanması. Batı Anadolu'daki bazı sahalarda mineral kapanlanması başlıca mekanizma olarak görünürken, diğerlerinde hem mineral hem çözünürlük kapanlanması etkisini göstermektedir; Emet jeotermal sahasında ise dedolomitleşme adı verilen özel bir mekanizmanın da varlığı belirlenmiştir. Doğu Anadolu'da ve Kuzey Anadolu Fay Zonu üzerinde yer alan sahalarda çözünürlük kapanlanması ana mekanizmadır.

Anahtar kelimeler: CO_2 depolama, jeotermal sistem, kapanlanma mekanizması, dedolomitleşme, hidrojeokimya.

To my beloved mother

ACKNOWLEDGEMENTS

First and foremost, I would like to express my deepest gratitude to my thesis supervisor, Prof. Dr. Nilgün Güleç, for her invaluable guidance, patience and encouragement throughout this thesis study. I am extremely grateful for her continuous support and advice, both on academic and on personal level. With her exceptional knowledge, kindness, and discipline, I have learned a lot.

I am indebted to Assist. Prof. Dr. Fatma Toksoy Köksal, for her guidance and support at an important stage of my life. I am deeply grateful.

I would like to thank my family. Not only during my thesis study, but in each part of my life, my mother and father have always been supportive, understanding, patient and encouraging. Thank you for your love and for believing in me in every step I take. I would also like to thank my sweet little Sushi, for brightening every day, being a moral support and his uncontrollable playfulness whenever I try to study.

I would like to thank my best friends Seda Kahraman and Çidem Argunhan, for their endless support, patience and being there for me whenever I need any help. I consider myself lucky to have met you two.

The friendship, assistances and encouragements of my colleagues and roommates Faruk Berber and Okay Çimen are also greatly appreciated. Special thanks go to Faruk for chocolate support and background music at the most critical times.

I would also like to thank my lunch group: Çidem Argunhan, Uğurcan Özçamur and Barış Ünal, for all those fun lunch times that turn even the most stressful day into a happy one.

Last but most certainly not least, I would like to thank Uğur Can Karakuş for always being with me, cheering me up and standing by me in the good and bad

times. Without his infinite support, encouragement, love and patience, many things wouldn’t have been possible.

TABLE OF CONTENTS

ABSTRACT v

ÖZ vii

ACKNOWLEDGEMENTS x

TABLE OF CONTENTS xii

LIST OF FIGURES xv

LIST OF TABLES xix

CHAPTERS

1. INTRODUCTION 1

1.1. Purpose and Scope 2

1.2. Geographic Setting 2

1.3. Material and Methods 3

1.4. Layout of the Thesis 5

2. LITERATURE REVIEW: SUBSURFACE STORAGE OF CO_2 7

2.1. Sites Suitable for CO_2 Storage 8

2.2. Physico – Chemical Processes of CO_2 Storage 10

2.2.1. Trapping Mechanisms 11

2.2.2. Dedolomitization 17

2.3. Monitoring the Site 18

2.4. Migration Mechanisms and Potential Impacts of CO_2 Leakage and Risk Assessment 20

3. GEOTHERMAL FIELDS IN TURKEY 25

3.1. Western Anatolia 27
3.2. Eastern Anatolia 44
3.3. Northern Anatolia 49
4. HYDROGEOCHEMICAL CHARACTERIZATION OF GEOTHERMAL FIELDS: DATA COMPILATION 53
4.1. Western Anatolia 54
4.1.1. Kızıldere, Tekkehamam and Germencik Geothermal Fields 54
4.1.2. Balçova Geothermal Field 56
4.1.3. Salihli Geothermal Field 57
4.1.4. Sındırgı Geothermal Field 60
4.1.5. Simav Geothermal Field 60
4.1.6. Emet Geothermal Field 62
4.1.7. Dikili Geothermal Field 62
4.1.8. Balıkesir Thermal Waters 63
4.1.9. Edremit Geothermal Field 64
4.2. Eastern Anatolia 64
4.2.1. Diyadin Geothermal Field 64
4.2.2. Çaldıran Geothermal Field 67
4.3. Northern Anatolia 68
5. HYDROGEOCHEMICAL MODELLING: PROCESSES CONTROLLING THE GEOCHEMICAL BEHAVIOUR OF THE SYSTEMS 73
5.1. Mineral Trapping: Group I Type Geothermal Fields 77
5.1.1. Hydrogeochemical Characteristics 77
5.1.2. Speciation – Solubility Calculations 79
5.1.3. Mass-Balance Calculations 83

5.2. Solubility ± Mineral Trapping: Group II Type Geothermal Fields 85
5.2.1. Hydrogeochemical Characteristics 85
5.2.2. Speciation – Solubility Calculations 88
5.2.3. Mass – Balance Calculations 98
5.2.4. Modelling Dedolomitization 100
5.3. Solubility Trapping: Group III Type Geothermal Fields 103
5.3.1. Hydrogeochemical Characteristics 104
5.3.2. Speciation – Solubility Calculations 106
5.3.3. Mass – Balance Calculations 110
6. CONCLUSIONS AND RECOMMENDATIONS 111
REFERENCES 115
APPENDICES
A. GEOCHEMICAL DATA COMPILED FROM PREVIOUS STUDIES 127

LIST OF FIGURES

FIGURES

Figure 1.1: Distribution of geothermal springs in Turkey (from MTA, 2012). 3
Figure 2.1: Schematic diagram of CO_2 geological storage (METI, 2010)..... 7
Figure 2.2: Existing/proposed CO_2 storage sites (IPCC, 2005). Major projects mentioned in this study are highlighted with a circle..... 9
Figure 2.3: CO_2 distribution model after 0.1, 0.5, 1.0 and 2.0 years of injection (Hovorka et al., 2001). 11
Figure 2.4: A general depiction of the development of trapping mechanisms over time (IPCC, 2005). 12
Figure 2.5: The injected CO_2 is trapped by the impermeable caprock (CCP, 2008). 13
Figure 2.6: Examples for the structural trapping: a) fault trapping; b) anticline trapping; c) facies change trapping; d) unconformity trapping (CO2CRC, 2011).. 13
Figure 2.7: Residual trapping of CO_2 within the pores of a rock (CCP, 2008)..... 14
Figure 2.8: Following physical trapping mechanisms, geochemical trapping (solubility and mineral trapping) mechanisms can take place (Solomon, 2007). ... 15
Figure 2.9: Monitoring the CO_2 plume at the Sleipner pilot with seismic imaging method [before injection (which began in 1996) and after injection] (CO2GeoNet, 2008)..... 20
Figure 2.10: Potential leakage scenarios of CO_2 storage (CO2GeoNet, 2008)..... 21
Figure 3.1: Distribution of geothermal areas and hot-springs in Turkey in relation to the major tectonic and volcanic features (from MTA, 2012)..... 27
Figure 3.2: A) Paleotectonic units and suture zones of Turkey (from Şengör, 1984) (Şimşek & Güleç, 1994)..... 29
Figure 3.3: General geologic map and location of important geothermal fields of BMG (Karakuş & Şimşek, 2013)..... 33

Figure 3.4: The Seferihisar–Balçova Geothermal system (Magri et al., 2010 and the references therein) 34
Figure 3.5: Simplified hydrogeological map of the Gediz Graben (Tarcan, 2005 and the references therein). 35
Figure 3.6: Location map of the geothermal fields in Afyon, Turkey (Şimşek & Güleç, 1994). 37
Figure 3.7: Location map of Simav geothermal area, Turkey (Palabıyık & Serpen, 2008 and the references therein) 38
Figure 3.8: Geological map of Emet geothermal field (Gemici et al., 2004 and the references therein). 40
Figure 3.9: Geological map of the Balıkesir region showing the geothermal areas (from Mutlu & Kılıç, 2009). 41
Figure 3.10: Geological map of the Biga Peninsula (Okay & Satır, 2000). 43
Figure 3.11: Maps showing a) the location, b) major tectonic units and c) geology of eastern Anatolia. (from Keskin, 2007 in Mutlu et al., 2012). 45
Figure 3.12: Location map of Diyadin geothermal field (Mutlu et al., 2013). 47
Figure 3.13: Location map of Çaldıran geothermal field (Aydın et al., 2013). 48
Figure 3.14: Location map of the sampled geothermal fields along the NAFZ (Güleç et al., 2006) 50
Figure 4.1: Schoeller diagrams of the geothermal fields of western Anatolia a) Kızıldere, b) Tekkehamam, c) Germencik, d) Balçova, e) Salihli, f) Sındırgı. 55
Figure 4.2: $\delta^{18}O$–δD diagrams for the western Anatolian waters. 58
Figure 4.3: CO_2–^3He–^4He ternary diagram for the western Anatolian fluids. 61
Figure 4.4: Schoeller diagrams of the geothermal fields of eastern Anatolia a) Diyadin, b) Çaldıran 65
Figure 4.5: $\delta^{18}O$–δD diagram for the eastern Anatolian thermal waters. 66
Figure 4.6: CO_2–^3He–^4He ternary diagram for the eastern Anatolian fluids. 67
Figure 4.7: Schoeller diagrams of the geothermal fields along the NAFZ 69
Figure 4.8: $\delta^{18}O$ vs. δD diagram of the sampled waters 70
Figure 4.9: Ternary plot of CO_2–^3He–^4He for the geothermal fields along the NAFZ 71

Figure 5.1: Concentration vs EC diagrams for geothermal fields of Kızıldere (a, b), Germencik (c, d), Balçova (e, f) and Simav (g, h). 78
Figure 5.2: Evolution of saturation indices in the thermal waters of Kızıldere (A), Germencik (B), Balçova (C) and Simav (D) vs dominant anion concentrations 81
Figure 5.3: Evolution of analytic and corrected calcium concentrations and magnesium concentrations vs. total sulphate concentrations in the thermal waters of Kızıldere (A), Germencik (B), Balçova (C) and Simav (D) (see text for further explanation) 83
Figure 5.4: Concentration vs EC diagrams for geothermal fields of Edremit (a, b), Balikesir (c, d), Dikili (e, f) and Sindirgi (g, h)..... 86
Figure 5.5: Evolution of saturation indices in the thermal waters of Edremit (A), Balıkesir (B), Dikili (C), Sındırgı (D), Emet (E), Salihli (F) and Tekkehamam (G) vs dominant anion concentrations 92
Figure 5.6: Evolution of analytic and corrected calcium concentrations and magnesium concentrations vs. total sulphate concentrations in the thermal waters of Edremit (A), Balıkesir (B), Dikili (C), Sındırgı (D), Emet (E), Sındırgı (F) and Tekkehamam (G)..... 95
Figure 5.7: Evolution of analytic and corrected magnesium and calcium concentrations vs. total sulfate concentrations in the thermal waters of Edremit (A), Balıkesir (B), Dikili (C), Sındırgı (D), Emet (E), Salihli (F) and Tekkehamam (G) (sse text for further explanation) 97
Figure 5.8: PHREEQC simulations of a less evolved Emet sample (sample no.6) water reacting with added CO_2 and gypsum 100
Figure 5.9: Modelling of dedolomitization and calcite dissolution for the geothermal fields of a) Edremit, b) Balikesir, c) Emet. Trends are modelled for different conditions of fixed PCO_2 at $10^{-1,2}$, $10^{-1,5}$, 10^{-2} and $10^{-2,7}$ as shown. 102
Figure 5.10: Concentration vs EC diagrams for geothermal fields of Çaldıran (a, b), Diyadin (c, d), NAFZ (e, f). 105
Figure 5.11: Evolution of saturation indices in the thermal waters of Çaldıran (A), Diyadin (B), and NAFZ (C) vs dominant anion concentrations 108

Figure 5.12: Evolution of analytic and corrected calcium concentrations and magnesium concentrations vs. total sulphate concentrations in the thermal waters of Çaldıran (A), Diyadin (B), and NAFZ (C). 109

LIST OF TABLES

TABLES

Table 3.1: Drilling data on the primary geothermal systems in western Anatolia .. 31
Table 3.2: Drilling data on the primary geothermal systems in eastern Anatolia ... 46
Table 3.3: Drilling data on the primary geothermal systems along the NAFZ 51
Table 5.1: Comparison of three different groups of geothermal fields in Turkey, determined for this study 76
Table 5.2: Summary of results from speciation - solubility calculations of Group I fields (spr: spring) 80
Table 5.3: Summary of results from mass-balance calculations of Group I geothermal fields 84
Table 5.4: Summary of results from speciation - solubility calculations of Group II fields 89
Table 5.5: Summary of results from mass-balance calculations of Group II geothermal fields 98
Table 5.6: Summary of results from speciation - solubility calculations of Group III fields 107
Table 5.7: Summary of results from mass-balance calculations of Group III geothermal fields 110
Table A.1: Chemical analyses of waters from geothermal fields of western Anatolia 128
Table A.2: Isotopic compositions waters from geothermal fields of western Anatolia 139
Table A.3: Chemical analyses of waters from geothermal fields of eastern Anatolia 146
Table A.4: Isotopic compositions waters from geothermal fields of eastern Anatolia 148

Table A.5: Chemical analyses of waters from geothermal fields along the NAFZ 149
Table A.6: Isotopic compositions waters from geothermal fields along the NAFZ 150

CHAPTER 1

INTRODUCTION

From the time of the industrial revolution, the atmospheric concentrations of carbon dioxide (CO_2) and other Green-House Gases (GHG) (e.g. methane and nitrous oxide) have been increasing continuously which resulted in the rise of the average global surface temperature (Shukla et al., 2010). The level of CO_2 concentration in the atmosphere during this period is reported to have dramatically increased from about 280 ppm to 396.83 ppm mainly due to the burning of fossil fuels (coal, oil, gas) (IPCC, 2007 and Scripps Institution of Oceanography, 2014). Since CO_2 is the primary greenhouse gas, scientists have been searching for techniques to be able to reduce CO_2 emissions and to mitigate the effects of global warming and climate change. For this purpose, CO_2 capture and storage is considered to be one of the main measures which is a process carried out in several stages: the separation of CO_2 from industrial and energy-related sources, the transportation to a storage location and the injection of supercritical CO_2 into deep geologic formations (such as deep saline aquifers, and depleted or active oil reservoirs) for a long-term isolation from the atmosphere.

Prior to the application of this technology, for the safety of both humans and environment it is crucial to perform safety assessment of the reservoir and to examine the behaviour of CO_2 after the injection with respect to the hosting rocks (fluid-rock interactions). Natural analogues provide a valuable source for the investigation of these elements. Gas fields and hydrothermal (geothermal) systems are the two reservoir types that are being studied as natural analogues.

In terms of the geothermal energy potential, Turkey is one of the richest countries in the world with many geothermal fields. These geothermal fields are ideal candidates to be studied as natural analogues for CO_2 storage. In this thesis study, several geothermal fields are selected from western, eastern and northern Anatolia for the application of various geochemical methodologies in order to characterize the reservoir, its potential evolution and the hydrogeochemical processes expected in geological storage. Additionally, the mechanisms that can trap the injected CO_2 are identified which are very important for a successful storage.

1.1. Purpose and Scope

This thesis study is focused on the hydrogeochemical characteristics of geothermal systems in Turkey as natural analogues for CO_2 storage. The main aim of the study is to contribute to the preliminary assessment of the geothermal fields for the potential future projects of CO_2 storage in Turkey.

To accomplish this goal, the database available for several geothermal fields from western, eastern and northern Anatolia are evaluated in terms of possible mechanisms of CO_2 trapping in hydrothermal reservoirs. This evaluation is performed via the use of speciation-solubility relations, estimation of relative contribution of carbonate and sulphate minerals to the system, and hydrogeochemical modelling studies.

1.2. Geographic Setting

Turkey, as located on a tectonically active zone, is characterized by complex geology, and by the presence of extensive volcanism, numerous grabens and active faults, resulting in the formation of large-scale thermal systems each having different characteristics. Thus, various geothermal fields from western, eastern and northern part of Turkey are chosen as natural analogues for this study. The selection of the fields is based primarily on the available and reliable hydrogeochemical data from recent publications. The selected geothermal systems from the western Anatolia are Kızıldere-Denizli, Tekkehamam-Denizli, Salavatlı-

Aydın, Germencik-Aydın, Balçova-İzmir, Seferihisar-İzmir, Salihli-Manisa, Ömer-Gecek-Afyon, Sındırgı-Balıkesir, Simav-Kütahya, Emet-Kütahya, Dikili-İzmir, Balıkesir, Tuzla-Çanakkale and Edremit-Balıkesir fields which are all associated with different grabens. From eastern Anatolia, Diyadin-Ağrı and Çaldıran-Van fields located around young volcanoes and from northern Anatolia the fields along North Anatolian Fault Zone Yalova (town centre), Efteni-Düzce, Mudurnu-Bolu, Seben-Bolu, Bolu (town centre), Kurşunlu-Çankırı, Hamamözü-Amasya, Gözlek-Amasya, and Reşadiye-Tokat are also selected (Fig 1.1).

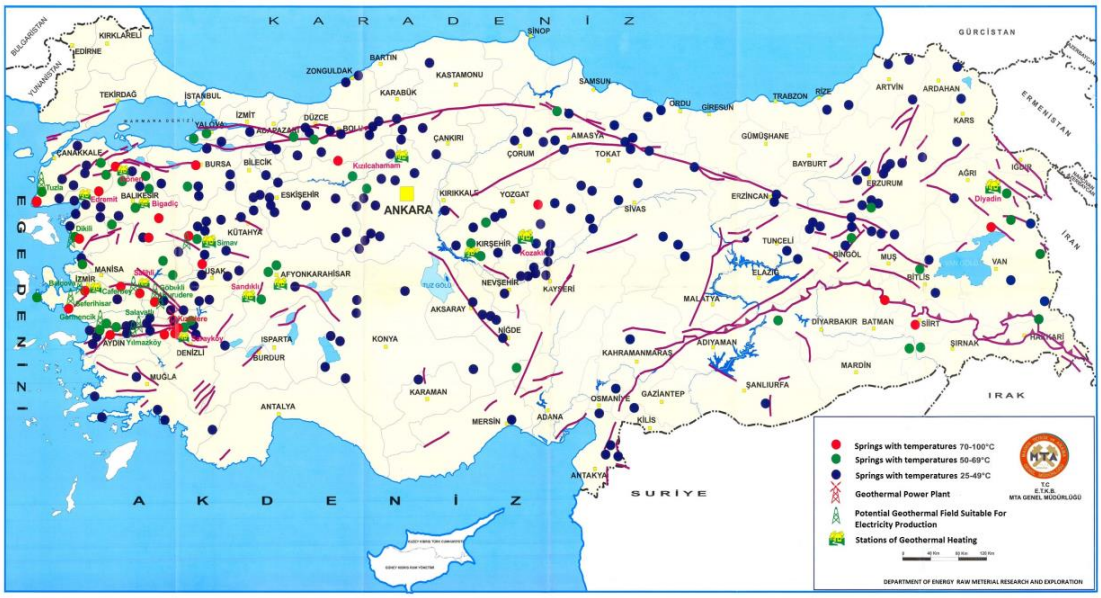

Figure 1.1: Distribution of geothermal springs in Turkey (from MTA, 2012).

1.3. Material and Methods

For the hydrogeochemical characterization of the systems and the identification of potential trapping mechanisms, various geochemical approaches are utilized. The relevant data are compiled from the previous studies conducted for the selected geothermal fields.

As a first step for the hydrogeochemical characterization, the water types are identified via Schoeller diagrams. Then, the major anion and cation contents of water samples are correlated with their electrical conductivity values, the latter being used as a tracer of the hydrogeochemical evolution of the system. Following this, speciation–solubility calculations are performed with the aid of *PHREEQC* code (Parkhurst and Appelo, 1999). *PHREEQC* performs a wide variety of aqueous geochemical calculations and is used for modelling reactions and processes, including (1) speciation and saturation-index calculations, (2) batch-reaction and one-dimensional (1D) transport calculations, and (3) inverse modelling (Parkhurst and Appelo, 2013). In this study, the features of speciation and saturation-index calculations and inverse modelling are used. Saturation index calculations helped with the identification of the minerals that are prone to be dissolved or to be precipitated. The estimation of the relative contribution of carbonate and sulphate minerals to the system is performed using the common ion Ca^{2+}. Combined evaluation of the hydrogeochemical patterns and the speciation-solubility calculations led to identification of the potential trapping mechanisms. To further verify the validity of the specified mechanisms, the mass-balance calculations (inverse modelling) are performed by using *PHREEQC* code which allows determination of the direction and magnitude of mass transfers and the potential geochemical reactions that occur between two hydraulically-connected points of a system.

The possibility of dedolomitization, which is a special trapping mechanism, (dissolution of dolomite accompanied by precipitation of calcite) is also investigated. For those systems/fields where dedolomitization appeared as a possible mechanism, additional modelling of dedolomitization is performed with the assistance of *PHREEQC* code. This modelling helped distinguishing the effects of CO_2 in systems dominated by dedolomitization from those dominated by calcite dissolution.

1.4. Layout of the Thesis

This thesis is divided into 6 chapters. Following this introduction chapter which is Chapter 1;

Chapter 2 is a literature research regarding the fundamentals of CO_2 storage process.

Chapter 3 explains the geologic characteristics of the primary geothermal systems from the western, eastern, and the northern Anatolia.

Chapter 4 is the compilation of the chemical compositions of the selected thermal waters in Turkey from previous studies and the review of their hydrogeochemical characteristics.

Chapter 5 presents the hydrogeochemical calculations and modelling studies and their interpretation in terms of the processes controlling the CO_2 trapping in the geothermal systems.

Chapter 6 gives the major conclusions derived from this thesis study.

CHAPTER 2

LITERATURE REVIEW: SUBSURFACE STORAGE OF CO_2

One of humanity's most pressing concerns is the continuous increase of CO_2 emissions in the atmosphere. Geological storage of CO_2 (Fig. 2.1) provides a way to avoid these emissions and to fight against climate change. Once CO_2 is captured from industrial facility or power plant, it is compressed into a dense supercritical form (both temperature and pressure exceed the critical point where the substance has both gas-like and liquid-like qualities), transported by either pipeline or ship and injected under pressure into suitable deep rock formations (IPCC, 2005 and CO_2GeoNet, 2008).

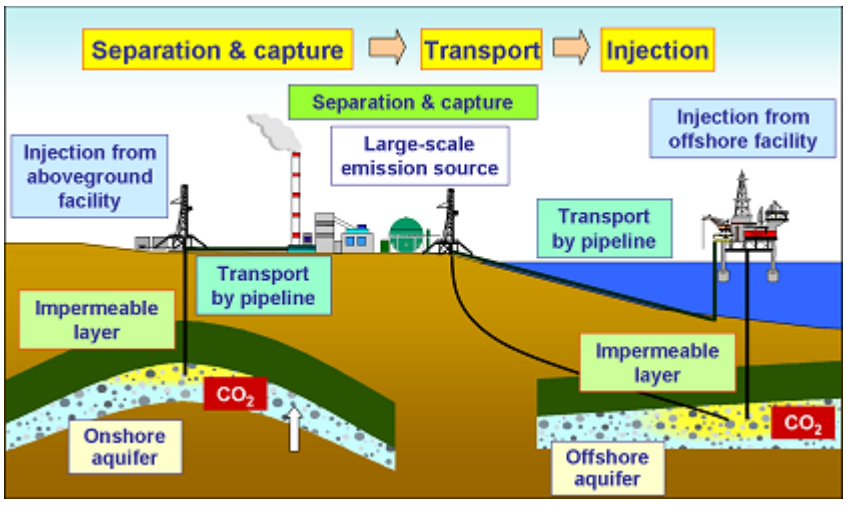

Figure 2.1: Schematic diagram of CO_2 geological storage (METI, 2010).

Since CO_2 storage is a widely accepted solution against global warming, major research programmes have been carried out in Europe, Australia, Japan, the United States, and Canada since the 1990's. Lessons learned from these investigations provide important insight regarding this topic. This chapter is the review of the information obtained from studies performed so far about the geological storage of CO_2.

2.1. Sites Suitable for CO_2 Storage

The selection of a storage site is a long and important process. Before making any injections, a detailed image of the layers below the surface is prepared via seismic surveying studies. Following these preliminary assessments, other criteria for a suitable site are examined. The fundamental ones are; (i) sufficient porosity, permeability and storage capacity, (ii) an overlying impermeable rock (the caprock of clay, marl etc.) to act like a trap mechanism for CO_2 and to prevent it from migrating upwards, (iii) the presence of other trapping mechanisms (e.g. solubility trapping, mineral trapping), (iv) a location where pressures and temperatures are high enough (deeper than 800m) to permit supercritical CO_2 to be stored, (v) the remoteness of the storage site from potable waters (CO_2GeoNet, 2008).

Three storage options are available:

1) Deep saline aquifers,
2) Depleted hydrocarbon fields,
3) Coal seams that cannot be mined.

In the special report of IPCC (2005) it is stated that deep saline aquifers are generally regarded as an effective reservoir for the CO_2 storage since they have the largest storage capacity and they are more widespread than other reservoir options.

The storage studies started in the early 1970s with the first injection of CO_2 into subsurface geological formations in Texas, USA, as part of enhanced oil recovery

(EOR) project (i.e increasing the amount of oil that can be extracted from the field via gas injection), and this and many other projects have been ongoing ever since (IPCC, 2005). Currently, the important large-scale projects include Sleipner in Norway, Weyburn in Canada, Otway in Australia and In Salah in Algeria (Fig. 2.2) (Shukla et al., 2010).

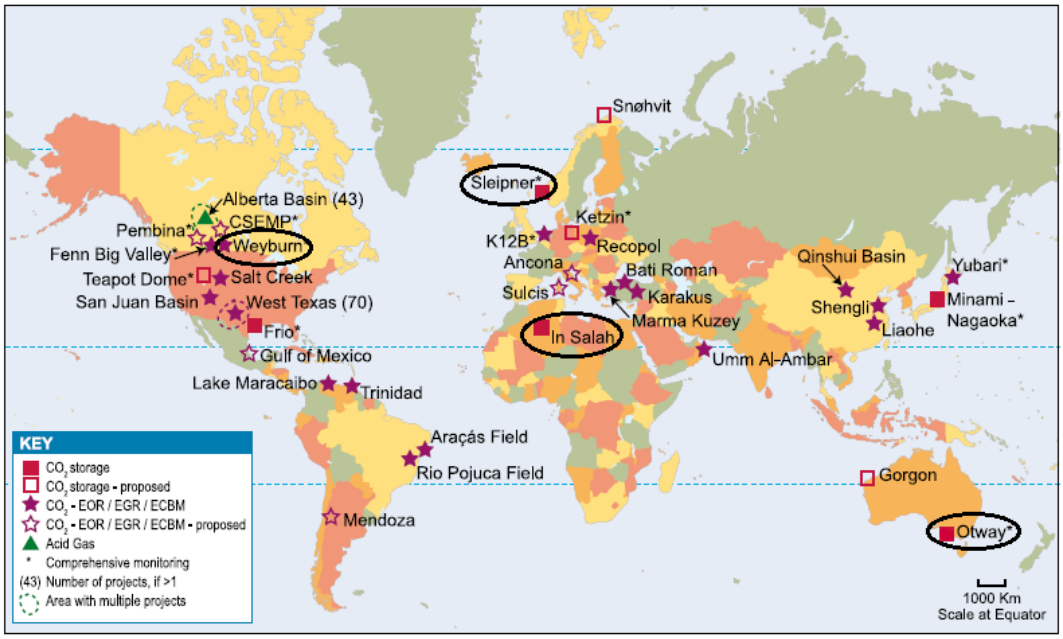

Figure 2.2: Existing/proposed CO_2 storage sites (IPCC, 2005). Major projects mentioned in this study are highlighted with a circle.

The *Sleipner* project, which is first commercial application of CO_2 storage, was launched in 1996 in a Norwegian offshore saline aquifer which is 800 m below the seabed of the North Sea. The reservoir (Utsira formation) is a 200–300 m thick sandstone saline aquifer including thin mudstone layers which provide the physical trapping for CO_2. By mid 2008, 10 Mt (Million tonnes) of CO_2 has been injected into the formation (Shukla et al., 2010). The *Weyburn* project started in the year 2000, in south Canada. The project is the injection of CO_2 into an oil field for EOR. The carbonate reservoir is composed of two aquifers capped by an anhydrite

caprock. 20 Mt of CO_2 is expected to be stored within the lifespan of the project of 20-25 years (Shukla et al., 2010). The *Otway* project which is the storage in depleted gas reservoir, started in 2008. Porous sandstone comprises the reservoir while the caprock is the thick-layered low-porosity Belfast mudstone. By June 2010, 50,000 tons of CO_2 has been successfully stored in this project (MIT Energy Initiative, 2014). The injection to a depleted gas reservoir started in 2004 in the *In Salah* project. The reservoir is composed of the Krechba Carboniferous sandstone. More than three million tons of CO_2, separated during gas production, have been securely stored into the formation. After the analysis of the reservoir, seismic and geomechanical data, the concerns about the integrity of the seal led to the decision to suspend CO_2 injection in June 2011. The future of the injection strategy is under review at present (MIT Energy Initiative, 2014). Most of these projects continue with injection and also geochemical and monitoring investigations.

2.2. Physico – Chemical Processes of CO_2 Storage

Once injected to the reservoir, CO_2 fills pore spaces and fractures of the permeable formation and it buoyantly rises towards the caprock since the immiscible, supercritical CO_2 phase has a much lower density and viscosity than the liquid brine in the reservoir (Fig. 2.3). Over time, CO_2 can displace the insitu fluid in which it may dissolve or mix, or the CO_2 may react with host rocks and the minerals or even the combination of these processes can take place. Due to the corrosive character of CO_2, the assessment of CO_2-rock interactions and the determination of the mechanisms that can prevent the CO_2 from reaching the surface and causing leakage, are crucial issues.

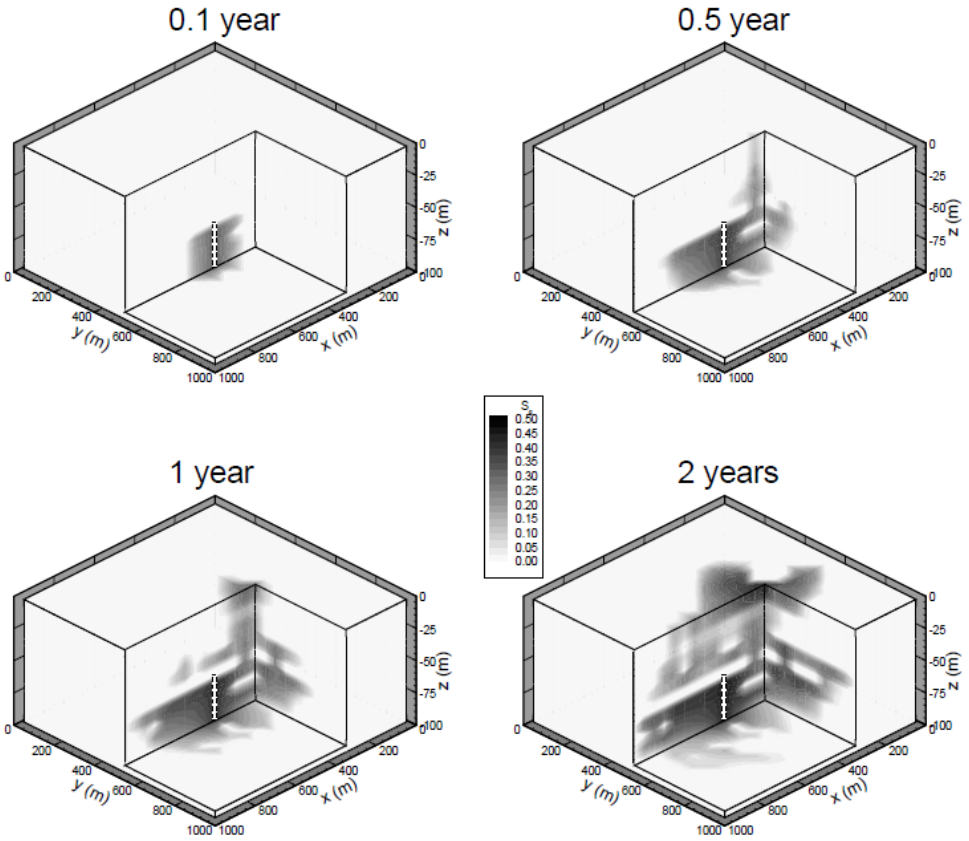

Figure 2.3: CO_2 distribution model after 0.1, 0.5, 1.0 and 2.0 years of injection (Hovorka et al., 2001).

2.2.1. Trapping Mechanisms

The success of geological storage depends on a combination of different trapping mechanisms. As hydrologic and chemical processes, trapping mechanisms can be divided into five categories: stratigraphic, structural, residual, solubility and mineral (IEA, 2008). These mechanisms take place based on the local geology and act together when there is more than one mechanism present. Their relative importance is expected to change over time as CO_2 migrates and interacts with the rocks and fluids (Fig. 2.4). Even though the process is very slow (may take place over thousands of years, depending on the reservoir characteristics), the most secure phase of CO_2 trapping is mineral trapping.

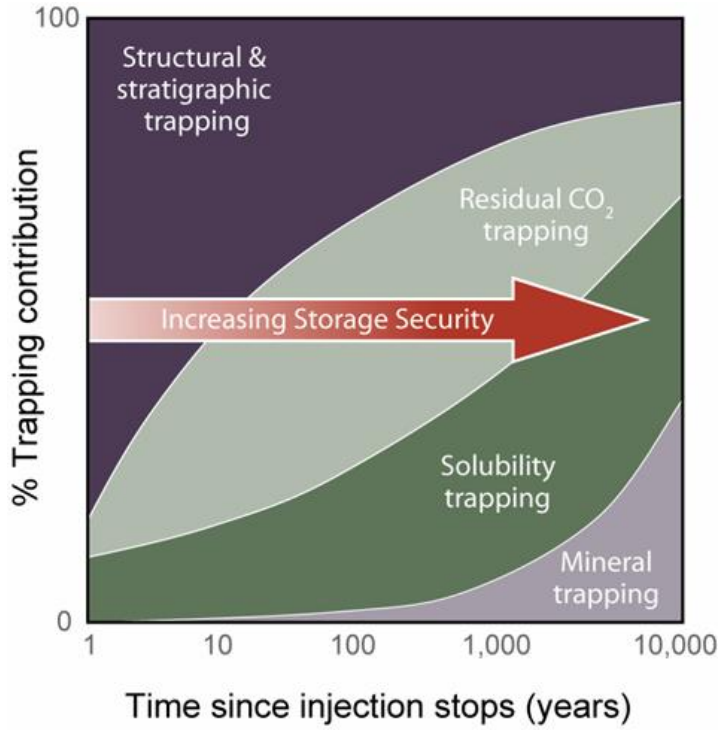

Figure 2.4: A general depiction of the development of trapping mechanisms over time (IPCC, 2005).

Stratigraphic trapping is formed by changes in rock type caused by variation in the geological setting (Fig. 2.5). When the supercritical CO_2 is injected, it is not dissolved in formation water immediately, and due to its supercritical state, CO_2 is less dense than the formation water and so it moves upwards until it reaches the top of the formation and is trapped by an impermeable layer of caprock (CO_2CRC, 2011). The caprock is comprised of clays, salt, shale or ultramafic rock types.

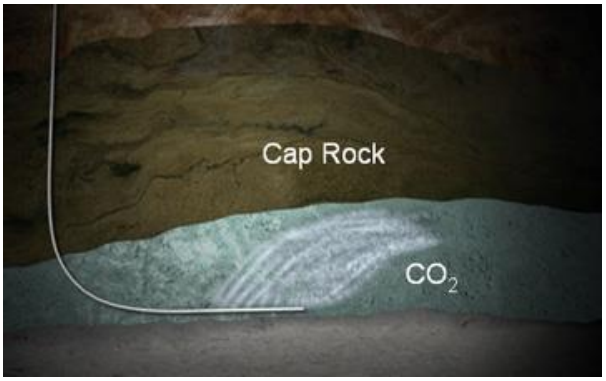

Figure 2.5: The injected CO_2 is trapped by the impermeable caprock (CCP, 2008).

Structural trapping is developed with the shift of impermeable rocks by a fault or fold in the geologic strata (Fig. 2.6) (IEA, 2008). These sealing faults (tilted blocks), anticline structures and unconformities have the potential to trap buoyant CO_2. Faults can act as permeability barriers in some circumstances and in others, as preferential pathways for fluid flow (Salvi et al., 1999).

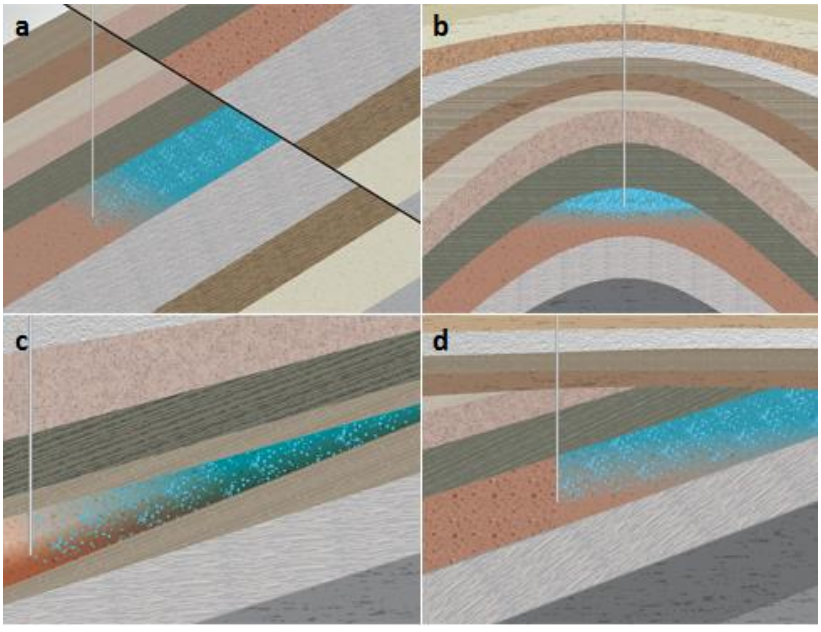

Figure 2.6: Examples for the structural trapping: a) fault trapping; b) anticline trapping; c) facies change trapping; d) unconformity trapping (CO_2CRC, 2011).

Residual trapping which usually begins after the injection stops, occurs with the trapping of CO_2 in the narrow pore spaces in the reservoir rock by the capillary pressure of water (the difference in pressure across the interface between two phases) so that it can no longer move upwards (Fig. 2.7). Eventually, this residually trapped CO_2 can dissolve into the formation water (CO_2CRC, 2011).

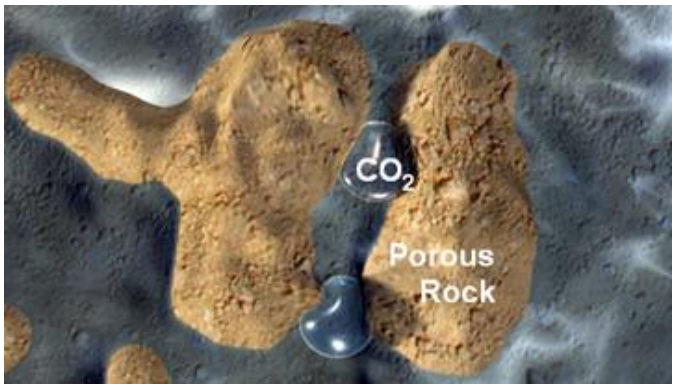

Figure 2.7: Residual trapping of CO_2 within the pores of a rock (CCP, 2008).

CO_2 in the subsurface can go through a series of geochemical interactions with the rock and formation water that will further enhance storage capacity and its security.

In *solubility (dissolution) trapping* (Fig. 2.8), when CO_2 dissolves in groundwater, its density increases, it becomes heavier than the surrounding water and begins to sink downwards. This allows the CO_2 to become more dispersed in the water, increasing the security of the mechanism and over time, the amount of CO_2 dissolved in the water can also increase (CO_2CRC, 2011). When CO_2 dissolves into the groundwater, firstly solubility trapping occurs. The solubility of CO_2 in water increases with increasing pressure and decreases with increasing temperature and increasing water salinity.

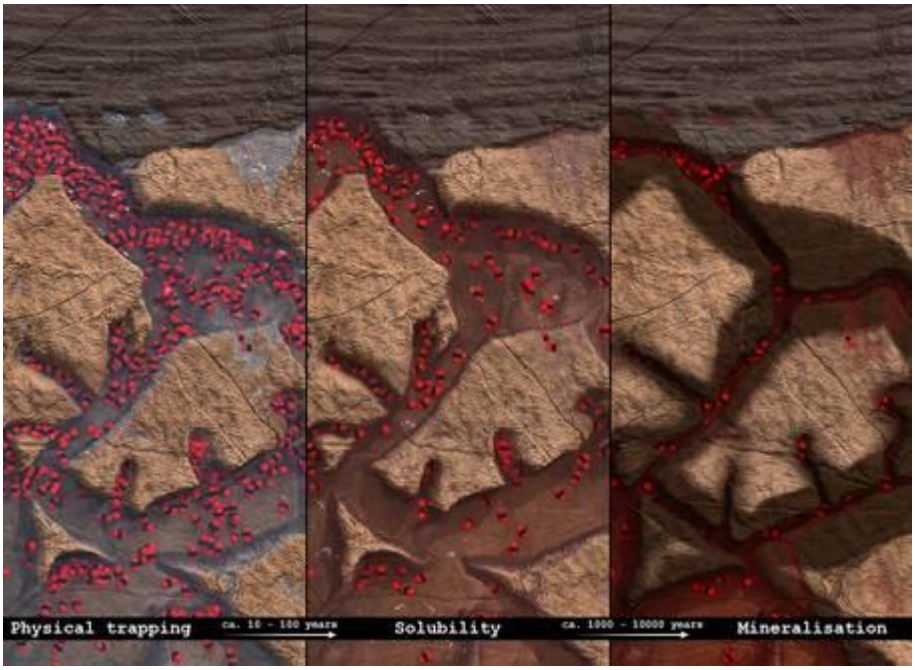

Figure 2.8: Following physical trapping mechanisms, geochemical trapping (solubility and mineral trapping) mechanisms can take place (Solomon, 2007).

Dissolution of CO_2 in the waters can be represented by the chemical reaction:

$$CO_2\ (g) + H_2O \leftrightarrow H_2CO_3 \leftrightarrow HCO_3^- + H^+ \leftrightarrow CO_3^{2-} + 2H^+$$

In the chemical reaction induced by CO_2 injection, initially CO_2 dissolves in water and the weak carbonic acid is formed. This is followed by rapid dissociation of carbonic acid to produce the bicarbonate ion, resulting in an immediate drop in pH and increasing the acidity. The dissolved bicarbonate species react with cations such as alkali earth metals (Ca, Mg, and Ba) or Fe^{2+} to precipitate carbonate minerals (e.g. calcite, magnesite or siderite) expected to confine CO_2.

Further addition of CO_2 to the system results in the increase of the partial pressure of CO_2 and consequently it causes the dissolution of carbonate minerals in the reservoir (Appelo & Postma, 2005).

Solubility trapping increases the acidity of the groundwater, and then dissolved CO_2 reacts directly or indirectly with minerals from the surrounding rocks, leading

to the precipitation of stable carbonate minerals (*mineral trapping*) (Fig. 2.8). The reaction to form these minerals takes place depending on the composition of the reservoir rock, the temperature and pressure, the chemical composition of the water, the water/rock contact area and the rate of fluid flow through the rock (CO_2CRC, 2011). Formation of carbonate minerals takes place from the continuous reaction of the bicarbonate ions with cations such as calcium, magnesium with the reaction:

$HCO_3^- + Ca^{2+} = CaCO_3(s) + H^+$ *(calcite)*

Gunter et al. (1993) states mineral trapping as the most permanent form of geological storage. Although this trapping mechanism is believed to be relatively slow, potentially taking a thousand years or longer, the permanence of storage, combined with the potentially large storage capacity of some geological settings makes this mechanism a desirable feature for long-term CO_2 storage.

Carbon geochemistry and stable isotopes with noble gas tracers also provide insight into the understanding of deep carbon cycle and, thus, the subsurface behaviour of CO_2 (Lollar & Ballentine, 2009). The analysis of the carbon isotopic signature of CO_2 helps determine the origins of samples and better understand CO_2 migration. Particularly, using the stable carbon isotopes, the CO_2 lost via dissolution process can be distinguished from the CO_2 lost through precipitation as carbonates. Noble gases provide information about the source of CO_2 in continental settings; moreover, they have also been used to observe the fate of geologically stored CO_2 and to calculate the volume of water in contact with oil reservoirs. In continental settings, the contributions of magmatic fluid to subsurface systems are identified with the examination of the $^3He/^4He$ ratios. $CO_2/^3He$ ratio is utilized in the identification of mantle-derived CO_2 from other sources and the changes in $CO_2/^3He$ provide a measure of the amount of CO_2 lost or gained.

2.2.2. Dedolomitization

Dedolomitization, which can be considered as the opposite reaction of dolomitization, is a special mechanism of mineral trapping process which occurs under certain conditions (Escorcia et al., 2013). It involves dolomite ($CaMg(CO_3)_2$) dissolution and calcite ($CaCO_3$) precipitation processes where Mg^{2+} is substituted by Ca^{2+} ion modifying the porosity and permeability of carbonate rocks.

In the study of Appelo and Postma (2005) it is stated that the groundwater in equilibrium with both calcite and dolomite has special properties represented by the following reaction:

$$Ca^{2+} + CaMg(CO_3)_2 \leftrightarrow 2\ CaCO_3 + Mg^{2+}$$

In this case of equilibrium, the $[Mg^{2+}]$ / $[Ca^{2+}]$ ratio becomes invariant at constant temperature and pressure. Simultaneous occurrence of calcite and dolomite equilibrium, if accompanied by the dissolution of gypsum or anhydrite (fuelling the necessary Ca^{2+} ions to the reaction), leads to the process of dedolomitization (Appelo and Postma, 2005).

Gypsum dissolution, as it increases Ca^{2+} concentration of the system, triggers calcite precipitation which causes the CO_3^{2-} concentration to decrease. As a result, the dissolution of dolomite is provoked, increasing Mg^{2+} concentration. The obtained net result is that the transformation of dolomite to calcite is induced by the dissolution of gypsum and waters with increased Mg^{2+}, and SO_4^{2-} concentrations are produced. It should also be noted that for each mole of dissolved dolomite, two moles of calcite are precipitated.

$$CaSO_4 + CaMg(CO_3)_2 = 2CaCO_3 + Mg^{2+} + SO_4^{2-}$$

Dedolomitization creates a quite different carbonate environment than calcite dissolution which is driven by CO_2 instead of the input of Ca^{2+} ions in dedolomitization (Romanak et al., 2010):

$$CO_2\ (aq) + H_2O + CaCO_3 \leftrightarrow Ca^{2+} + 2HCO_3^-$$

According to Auqué et al. (2009), dedolomitization is one of the most desired mechanisms due to the secure mineral trapping system (the calcitized dolomite may develop into a reservoir rock for a few hundred thousands of years) and the net increase in porosity. This increase is the result of the volume created by the dissolution of 1 mole of gypsum (74.7 cm^3/mole) or anhydrite (46 cm^3/mole) and 1 mole of dolomite (64.36 cm^3/mole) which is much larger than the volume filled by the precipitation of 2 mole of calcite (36.93 cm^3/mole), according to the stoichiometry in reaction. Nevertheless, the distribution of this porosity increase may not be homogeneous and decrease in porosity might occur at a local scale. This argument emphasizes the significance of a detailed mineralogical and geochemical characterization of the reservoirs which are considered for the CO_2 storage, to accurately predict the long term evolution of the system.

2.3. Monitoring the Site

Tracking the CO_2 migration in the subsurface and monitoring the system are essential to reduce the uncertainties, to maintain a safe storage and to give early warnings about the potential risks. Monitoring is required for variety of purposes (IPCC, 2005):

- Controlling the injection process, and measuring the well and caprock integrity, injection rates, wellhead and formation pressures.
- Verification of the injected CO_2 quantity and tracking the migration of CO_2 from the injection point.
- Optimization of the project efficiency, injection pressures and drilling of new injection wells.
- With suitable monitoring techniques (such as geochemical, biochemical and remote sensing procedures), making sure that the storage proceeds smoothly and CO_2 remains contained in the reservoir.
- Providing early warning in the case of any seepage or leakage that might require intervention.

- Observation of the ground movements and microseismicity in case of the potential small-scale movements caused by the pressure increase due to the injection.
- Building a reliable relationship with the society and sharing the necessary information regarding the safety of the storage site.

A wide range of monitoring techniques is available and can be applied for CO_2 storage projects. The applicability and sensitivity of these techniques are site-specific to some extent (IPCC, 2005). Proper monitoring techniques are selected according to the technical and geological characteristics of the site and the monitoring purposes (CO_2GeoNet, 2008). Before conducting an effective monitoring study, a baseline survey which shows the initial state of the site must be performed which provides a tool for the comparison for successive surveys.

In the case of CO_2 storage, the monitoring methods can be divided as direct and indirect monitoring (CO_2GeoNet, 2008). Direct CO_2 monitoring consists of the measurement and analysis of fluids from deep wells and gas concentrations taken from the soil or atmosphere, whereas geophysical surveys and the monitoring of pressure or pH changes in the groundwater are the indirect monitoring methods.

Both present and future storage projects require the monitoring of CO_2 migration in the sub-surface for the potential environmental impacts on groundwater, air quality and/or plant and animal life. Available methods include well testing and pressure monitoring, chemical analyses of water samples, chemical tracers, chemical sampling, surface and borehole seismic analysis, electromagnetic, and other geotechnical instruments (Fig. 2.9). Effects of CO_2 on atmosphere and ecosystems can be monitored by chemical instruments and the examination of the plant and animal life. Remote sensing, soil analyses and measurement of water quality are also suitable methods to detect the migration of CO_2 (IEA, 2008 and Shukla et al., 2010).

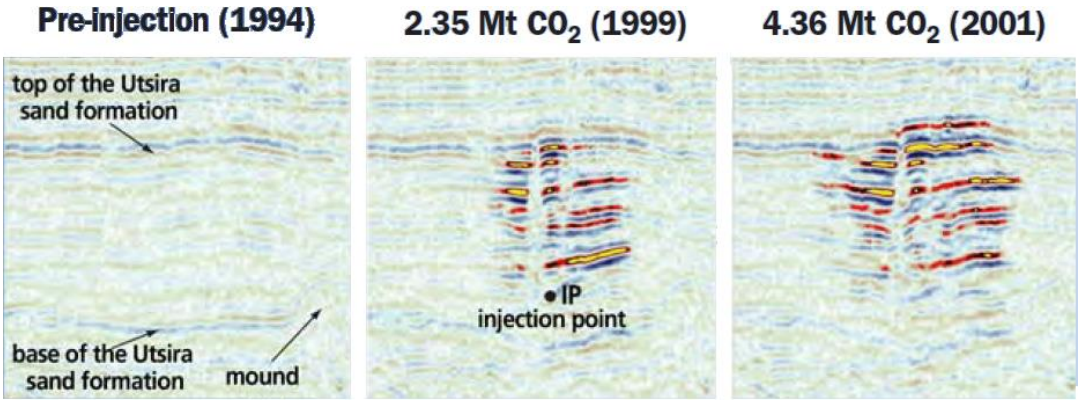

Figure 2.9: Monitoring the CO_2 plume at the Sleipner pilot with seismic imaging method [before injection (which began in 1996) and after injection] (CO2GeoNet, 2008).

Monitoring studies should continue even after the cease of the injection to be able to detect any CO_2 migration that might take place afterwards leading to potential leakage. The improvement and assessment of long-term monitoring and the development of new types of equipment are currently in progress (IEA, 2008).

2.4. Migration Mechanisms and Potential Impacts of CO_2 Leakage and Risk Assessment

CO_2 that is trapped by residual trapping, solubility trapping, or mineral trapping mechanisms is securely stored within the reservoir. However, CO_2 that is held by stratigraphic or structural trapping has the potential to move out of the reservoir through leakage pathways and escapes back to the atmosphere; which is the principal risk of geological storage. It may also create local risks to groundwater, to ecology and hence, to humans.

Potential leakage pathways develop due to the man-made (deep wells) or natural (fracture systems and faults) structures in general. These pathways are (a) fractures in caprocks, (b) faults, (c) poorly designed active and badly sealed abandoned wells (Fig. 2.10).

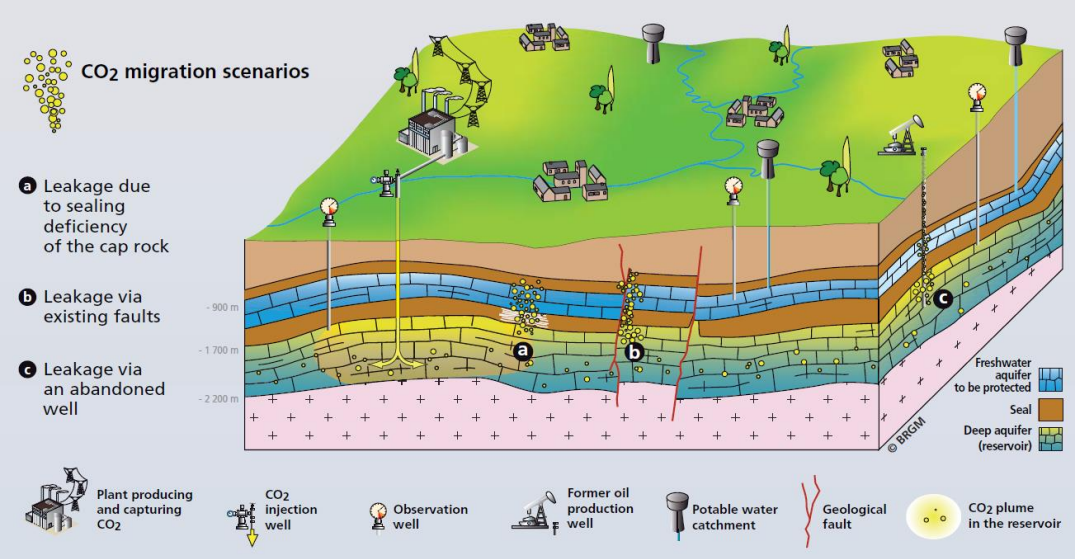

Figure 2.10: Potential leakage scenarios of CO_2 storage (CO2GeoNet, 2008).

In caprocks, the presence of potentially weak spots could provide leakage pathways due to the changes in pressure. The selection of suitable sites and the characterization of parameters of the reservoir (strength, lateral distribution and sealing properties of cap rocks) are critical factors for the early detection of such leakage. Permeable or reactivated faults of reservoirs may provide pathways for fluid ascension. However, detection and prediction of possible CO_2 migration pathways along faults is rather uncertain; therefore, faults need to receive special attention in monitoring. Both active and abandoned wells may form leakage pathways if improperly installed/sealed (failure of the cement for the abandoned wells) or if the materials of the wells are corroded. Due to technical improvements in well cementation and logging, properly sealed boreholes are often considered safer than the older ones, so that monitoring of older wells has to be taken into consideration in monitoring strategies (Rütters et al., 2013). Although the significant vulnerability is caused by the leaks from the abandoned wells, they can be sealed with heavy mud or cement.

In case of leakage, the occurrence of CO_2-rock interactions is likely, while it is considered highly unlikely that CO_2-rock interactions are capable of triggering

leakage paths. Nevertheless, if a leakage pathway is already in place, these interactions have potential to either enhance leakage via dissolution and shrinkage of clay minerals or restrict it through precipitation of fast reacting minerals (Gaus, 2010).

If leakage is detected in a site, it is expected that the leakage can be eliminated by reducing injection rate or reservoir pressures or by balancing pressure in different parts of the reservoir. The leaks can be safely dissipated and necessary repairing procedures can be performed or the escaped CO_2 can be collected and re-injected since the leakage will be a slow process. However, any dispersal into the atmosphere decreases the effectiveness of the storage (IEA, 2008).

As for the CO_2 impact on human health and environment; for humans, CO_2 is very dangerous at very high concentrations. In fact, CO_2 concentrations above 5000 ppm can cause death if exposed too long (CO_2GeoNet, 2008). Enclosed environments and topographical depressions have higher risks of increased CO_2 concentration since CO_2 is denser than air, it has the tendency to accumulate close to ground. On marine ecosystems, the main effect will be the local lowering of pH and its impact, and on terrestrial ecosystems the potential effects are death of some plants, potable aquifer contamination and rock dissolution resulting in the decrease of structural integrity due to the acidification of groundwater. Contamination of potable aquifers is one of the main concerns where the potable character of water is significantly modified with the geochemical reactions that may occur. The dissolution of leaking CO_2 acidifies the water, triggering metal mobilisation (Gaus, 2010). All these factors considered, it can be said that CO_2 leakage is dangerous for human and animal health and for ecosystem.

Risk assessment studies aim to the determination and quantification of the potential risks caused by the subsurface injection of CO_2 (IPCC, 2005). Most risk assessments include the usage of scenarios that identify, classify and describe possible future states of the storage site and events that may result in leakage of CO_2 or other risks. These scenarios are the main step for the development of risk

assessment models using all the relative components from the site with respect to the specified case. The assessment models help with the modification of the processes to remove excess risks and to determine and implement appropriate monitoring and intervention strategies to maintain the remaining risks. Natural analogue studies provide a strong base for understanding and identifying the health, safety and environmental risks that may emerge. Careful site selection, correct operation, extensive monitoring studies, performance and risk assessments, effective regulatory supervision and the implementation of remediation measures to eliminate or restrict the causes and impacts of leakage whenever necessary are some of the main procedures that will ensure the safety of the CO_2 storage (IPCC, 2005).

CHAPTER 3

GEOTHERMAL FIELDS IN TURKEY

Turkey is situated in the tectonically active Alpine–Himalayan belt and is constantly under the effect of the relative movement of the European and the Afro–Arabian plates, resulting in the formation of extensive volcanism as well as the presence of numerous grabens and active faults. These features induce the widespread geothermal activity in the form of hot springs, fumaroles, hydrothermal alterations and recent mineralizations. The hot springs in Turkey are distributed in parallel with the fault systems and the Tertiary–Quaternary volcanics (Fig 3.1). More than 600 hot springs are present in Turkey some of which have temperatures exceeding 100^{o}C that lead to the recognition of an important geothermal potential in Turkey (Söğüt et al., 2010). In fact, Turkey is the seventh richest country in the world and 1st in Europe with respect to geothermal energy potential (Dagistan, 2007). In regard to this potential, extensive geothermal exploration and investigations have been implemented by the General Directorate of the Turkish Mineral Research and Exploration (MTA) since the 1960s. Balçova-İzmir (1962) and Kızıldere-Denizli (1968) are some of the examples for the earliest fields discovered. According to the MTA report of geothermal energy studies, a total of 190 geothermal fields have been discovered by MTA and the number of drilled wells is 506 with the total depth of 252,515 m (MTA, 2011).

The highest geothermal energy potential in Turkey is associated with the western Anatolian region and, as a result, most of the geothermal energy studies are focused on this region. The estimated reservoir temperature using geothermometry applications is as high as about 250^{o}C (Mutlu and Güleç, 1998) which is also

confirmed by the bottom hole temperatures measured in Kızıldere and Germencik fields. Mutlu and Güleç (1998) and Güleç et al. (2002) suggest that the extensional tectonics of western Anatolia provide a deep-seated heat source (associated with asthenospheric upwelling) and a deep circulation of waters along the faults of the widespread graben system.

The northern Anatolian region is bounded to the south by the dextral North Anatolian Fault along which most of the geothermal fields are situated. The geothermometry applications yield reservoir temperature estimates around 110 °C (Mutlu and Güleç, 1998). This relatively low geothermal energy potential in the North Anatolian region is attributed to the lack of a regional heat source and the restriction of local magmatic activities which are limited to pull-apart basins (Mutlu and Güleç, 1998; Güleç et al., 2002).

The eastern Anatolian region, on the other hand, undergoes contemporary compression. Despite the availability of a potential heat source at depth and recently active volcanoes, the relatively moderate geothermal energy potential of this region can be attributed to the lack of well-developed fault systems and consequently, the deficiency of deep hydrothermal circulation (Mutlu & Güleç, 1998).

The utilization fields of geothermal energy in Turkey include domestic heating, greenhouse heating, industrial processes, heat pumps, spas and thermal resorts for balneological purposes, and electricity generation. Presently operating geothermal power plants of Turkey are in Denizli-Kızıldere, Aydın-Germencik, Çanakkale-Tuzla, Aydın-Salavatlı, İzmir-Seferihisar and Aydın-Bozköy-Çamur fields (MTA, 2011). In addition, there are more fields in development which are suitable for electricity production.

Figure 3.1: Distribution of geothermal areas and hot-springs in Turkey in relation to the major tectonic and volcanic features (from MTA, 2012). The selected fields for this study are indicated by black circles.

Given that the hydrogeochemical data used in thesis study are from the fields located in western, eastern and northern Anatolia, the geologic characteristics of geothermal fields in these regions are further explained in the following sections.

3.1. Western Anatolia

Western Anatolia is a valuable region in terms of geothermal energy. The grabens in this region host the main and the most important geothermal fields which comprise approximately 70% of the total geothermal energy potential in Turkey (Yılmazer, 2009).

Western Anatolia comprises two major paleotectonic units, the Sakarya Continent to the north and the Menderes-Taurus platform to the south (Figure 3.2A), which are separated from each other by the İzmir-Ankara Suture representing a branch of the Neo-Tethys (Şengör, 1984). The Sakarya Continent is composed of a basement made up of Paleozoic to Triassic aged metamorphic rocks of Kazdağ Massif and Karakaya Complex (amphibolites, gneisses, schists, phyllites, marbles, metaperiodites, metabasites); this basement is overlain by Tertiary clastics and

carbonates (Bingöl, 1969; Bingöl et al., 1973; Bozkurt and Mittwede, 2001). The Menderes-Taurus platform consists of a basement comprised by a gneissic-migmatitic core surrounded by a schist and marble envelope (Dürr, 1975; Şengör et al., 1984), known as the Menderes Massif metamorphics; these metamorphics are overlain by Upper Cretaceous ophiolitic mélange (Şengör & Yılmaz, 1981) and Neogene terrestrial sediments. Both the Sakarya Continent and the Menderes Massif seem to have been largely affected by magmatic activities characterized by widespread volcanic products and granitic intrusions of Neogene-Quaternary age.

As regard to the neotectonic setting, western part of Turkey is one of the most seismically active and rapidly deforming regions in the world. In this region, the most distinguished neotectonic features are the approximately E–W-trending grabens with their intervening horsts and related active normal faults. These grabens are the products of N-S extension prevailing in the region since about the late Miocene (Dewey and Şengör, 1979; Şengör et al., 1985; Bozkurt, 2003) in response to the westward escape of the Anatolian plate in between the North Anatolian and the East Anatolian Fault Zones which formed as a consequence of Arabian-Anatolian collision along the Bitlis-Zagros Suture Zone (Fig. 3.2B). The largest and best developed of these grabens comprise the Edremit, Bakırçay, Kütahya, Simav, Gediz, Küçük Menderes, Büyük Menderes, and Gökova grabens (Fig. 3.2C).

The studies conducted for the distribution of the geothermal fields with respect to the major grabens reveal that in general, the high-enthalpy fields are bound to the grabens in the south, while the grabens at the north include the relatively low-enthalpy fields (Şimşek & Güleç, 1994). From south to north, the geothermal systems comprise Kızıldere-Denizli, Tekkehamam-Denizli, Salavatlı-Aydın, and Germencik-Aydın geothermal systems within the Büyük Menderes Graben; Balçova-İzmir and Seferihisar-İzmir near the Çubukludağ Graben; Salihli-Manisa within the Gediz Graben; Ömer-Gecek within Afyon Graben; Sındırgı-Balıkesir and Simav-Kütahya within the Simav Graben; Emet-Kütahya within Kütahya

Graben; Dikili-İzmir and Balıkesir area near Bakırçay (Bergama) Graben, and Tuzla-Çanakkale and Edremit-Balıkesir fields within Edremit Graben (Fig 3.2C).

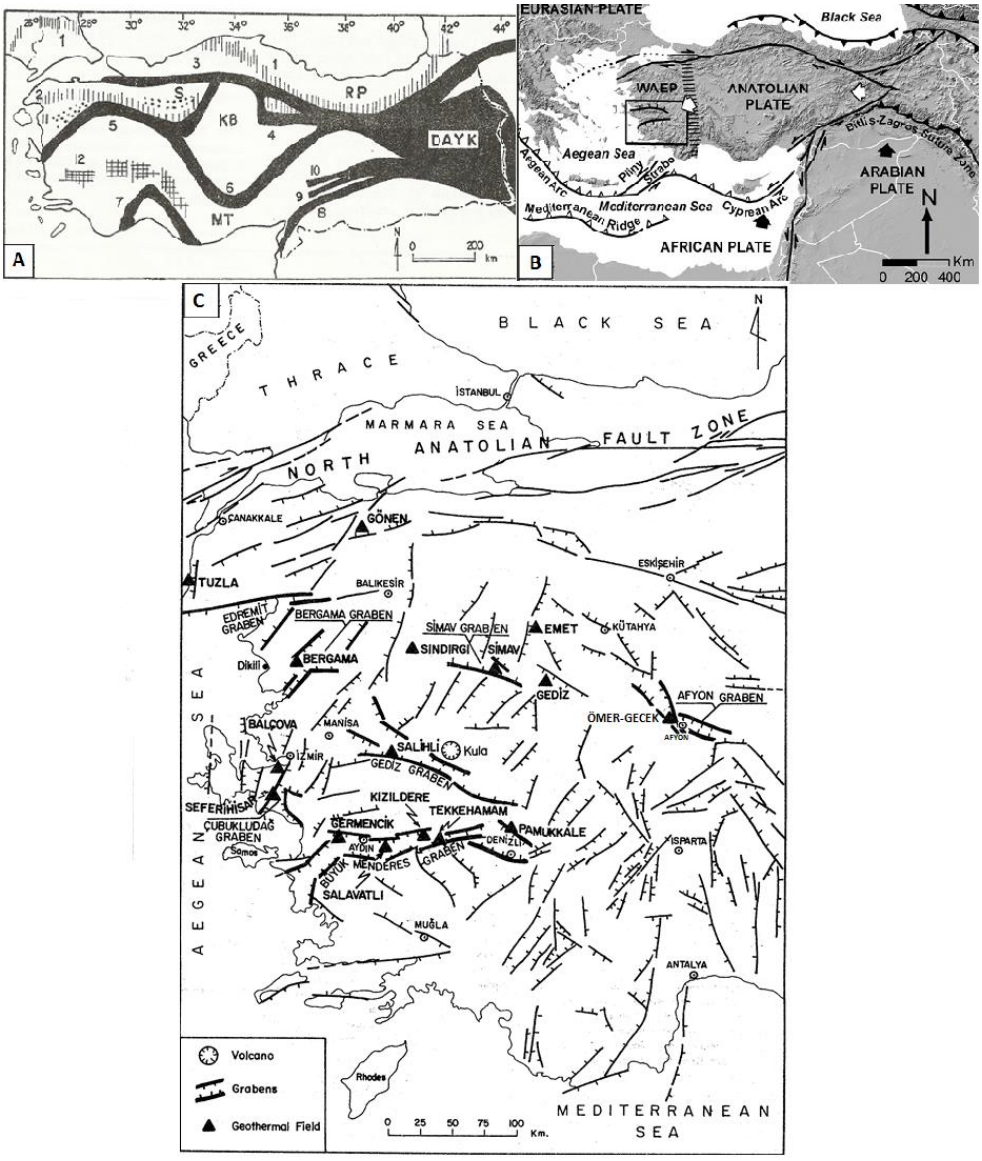

Figure 3.2: A) Paleotectonic units and suture zones of Turkey (from Şengör, 1984). RP:Rhodope-Pontide Fragment, KB:Kırşehir Block, S:Sakarya Continent, MT:Menderes-Taurus Block, DAYK:East Anatolian Accretionary Complex, 1-Main-Paleo-Tethys Suture, 2-Karakaya Suture, 3-Intra Pontide Suture, 4-Erzincan Suture, 5-İzmir-Ankara Suture, 6-Inner Tauride Suture, 7-Antalya Suture, 8-Asurid Suture, 9-Çüngüş Suture, 10-Maden Suture. B) Neotectonic structures of Aegean and Eastern Mediterranean regions (from Bozkurt, 2001) (WAEP: Western Anatolian Extensional Province). C) Geothermal fields of Western Anatolia (Şimşek & Güleç, 1994).

In the following section, the main geological features of the primary geothermal systems of western Anatolia are reviewed. The fields are grouped according to the associated grabens as previously mentioned. The data compiled from drilling studies is summarized in Table 3.1.

Table 3.1: Drilling data on the primary geothermal systems in western Anatolia

Graben	Geothermal System	No. of drilled wells	Max drilled depth (m)	Max measured Temp.(°C)	Reservoir rocks	Cap rocks	References
Büyük Menderes Graben	Kızıldere (Denizli)	21	2261	242	Pliocene limestone, Paleozoic to Mesozoic Menderes Massif marble, schist, and quartzite	Pliocene alternating sandstone, conglomerate, claystone	Şimşek, 2003; Şimşek et al., 2005; Tarcan, 2005; MTA, 2005
	Tekkehamam (Denizli)	2	2001	168	Pliocene limestone, Paleozoic to Mesozoic Menderes Massif marble, schist, and quartzite	Pliocene alternating sandstone, conglomerate, claystone	Gökgöz, 1998; MTA, 2005; Karakuş & Şimşek, 2013
	Salavatlı (Aydın)	2	1510	172	Paleozoic to Mesozoic Menderes Massif marble, quartzite, and mica shists	Pliocene alternating sandstone, conglomerate, claystone	Özgür, 2003; Tarcan, 2005; MTA, 2005; Karamanderesi, 2013
	Germencik (Aydın)	9	2398	232	Miocene sandstone, conglomerate, Paleozoic to Mesozoic Menderes Massif marble, schist and quartzite	Pliocene alternating sandstone, conglomerate, claystone, siltstone	Tarcan, 2005; MTA, 2005; Karakuş & Şimşek, 2013
Çubukludağ Graben	Balçova (İzmir)	31	1100	140	Bornova melange chert, limestone, serpentinite and mafic submarine volcanics	Neogene interbedded conglomerate, sandstone, claystone, mudstone, marl and limestone	Şimşek & Güleç 1994; Tarcan, 2005; MTA, 2005; Tarcan et al., 2009
	Seferihisar (İzmir)	6	2009.5	153	Bornova melange chert, limestone, serpentinite and mafic submarine volcanics	Neogene interbedded conglomerate, sandstone, claystone, mudstone, marl and limestone	Tarcan & Ünsal, 2003; MTA, 2005
Gediz Graben	Salihli (Manisa)	20	1189.1	168	Paleozoic to Mesozoic Menderes Massif marble, schist, gneiss and quartzite	Neogene intercalated claystone, sandstone, conglomerate and siltstone	Tarcan, 2005; MTA, 2005; Özen, 2012
Afyon Graben	Ömer-Gecek (Afyon)	25	905	98	Neogene limestones, conglomerates, Paleozoic schist and marble	Neogene sandy clay, silt, marl, tuffs and clayey limestone	Mutlu, 1998; MTA, 2005
Simav Graben	Sındırgı (Balikesir)	1	987	106	Neogene dacite and tuff, Upper Cretaceous serpentine and recrystallized limestone	Neogene conglomerate, sandstone, siltstone and marl	MTA, 2005; Aksoy et al., 2009
	Simav (Kütahya)	15	958	162.4	Neogene Naşa basalts; Mesozoic limestone, sandstone, conglomerate of Kırkbudak fm; Paleozoic to Mesozoic Simav marble, schist,	Neogene rocks of claystone, sandstone and conglomerate	Gemici & Tarcan, 2002; MTA, 2005
Kütahya Graben	Emet (Kütahya)	4	325	49	Paleozoic to Mesozoic Menderes Massif gneiss, schist, phyllites and marble	Neogene alternating conglomerate, sandstone and limestone	Gemici et al., 2004; MTA, 2005
Bakırçay Graben	Dikili (İzmir)	11	1500	131.5	Late Miocene-Pliocene fracture zones in Yuntdağ volcanic-I consist of altered andesite	Pliocene mudstone, siltstone, limestone, sandstone and conglomerate of Soma fm	Özen et al., 2005; MTA, 2005; Karahan, 2013

Table 3.1 (cont'd): Drilling data on the primary geothermal systems in western Anatolia

Graben	Geothermal System	No. of drilled wells	Max drilled depth (m)	Max measured Temp.(°C)	Reservoir rocks	Cap rocks	References
Bakırçay Graben	Gönen (Balıkesir)	17	800	80	Paleozoic to early Mesozoic gneiss, schist, marble, granodiorite and crystallized limestone	Upper Miocene-Pliocene conglomerate, sandstone, marl, claystone, clayey limestone	MTA, 2005; Mutlu, 2007; Mutlu & Kılıç, 2009
Edremit Graben	Tuzla (Çanakkale)	14	1020	174	Lower Miocene rhyolitic tuffs, ignimbrites, latitic and rhyolitic lavas; Paleozoic schist, crystallized limestone and granodiorite	Miocene tuffitic claystone, conglomerates and sandstone	Tarcan, 2005; MTA, 2005; Baba et al., 2009
	Edremit (Balıkesir)	22	496	62	Permeable agglomerate and conglomerate units; Plio-Quaternary unconsolidated sandstone, mudstone and conglomerate	Ballıca Formation of siltstone, marl, conglomerate, sandstone, clayey limestone; Plio-Quaternary sediments	MTA, 2005; Avşar et al., 2013

Büyük Menderes Graben: Kızıldere, Tekkehamam, Salavatlı, Germencik

Regarding the energy potential, the most important fields are the ones related with the Büyük Menderes Graben (BMG) in the south. BMG which is represented by a great number of hot springs is an E-W trending graben structure, approximately 175 km long and 10-20 km wide, bounded by active normal faults. The prominent geothermal fields of BMG include Kızıldere, Tekkehamam, Salavatlı and Germencik (Fig. 3.3).

The Kızıldere geothermal field is located 40 km west of the city of Denizli, in the eastern section of the BMG, and it is the first acknowledged high-temperature geothermal field in Turkey. Tekkehamam field is also located at the eastern segment, while Salavatlı geothermal field is in the middle, and Germencik is in the western part of the BMG.

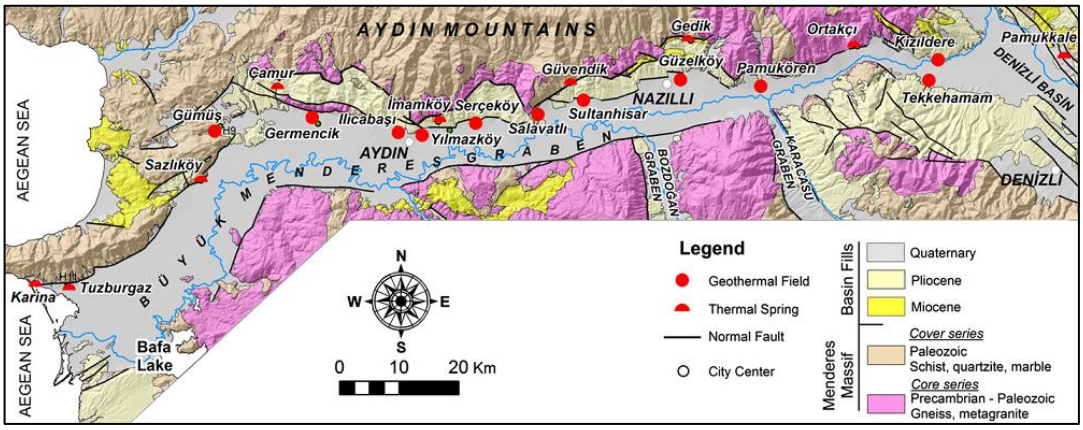

Figure 3.3: General geologic map and location of important geothermal fields of BMG (Karakuş & Şimşek, 2013).

The basement of these fields is composed of Menderes Massif metamorphics consisting of gneisses, schists, and an alternation of quartzites, micaschists and marbles known as the İğdecik Formation. This formation is overlain by fluvial and lacustrine Pliocene sediments, that are divided into four lithologic units, from bottom to top: the Kızılburun Formation, a 200-m thick formation of alternating red and brown conglomerates, sandstones, shales and lignite layers; the Sazak Formation, comprising intercalated gray limestones, marls and siltstones, 100–250m in thickness; the Kolonkaya Formation, made up of yellowish green marls, siltstones and sandstones, 350–500m in thickness, and, finally, the Tosunlar Formation, composed of alternating units of poorly-consolidated conglomerates, sandstones and mudstones with fossiliferous clay units, about 500m in thickness (Şimşek et al., 2005). These units are unconformably overlain by Quaternary alluvium. In Kızıldere field, Sazak formation, İğdecik formation and deep-seated gneisses and quartzites are the three main reservoirs (Şimşek et al., 2005), whereas Germencik field has two reservoirs, quartz schists, gneisses and marbles of Menderes Massif comprise the first reservoir, Neogene aged sandstones and conglomerates form the secondary reservoir. Clay-bearing sedimentary levels of Neogene age act as cap rock of the system (Filiz et al., 2000).

Çubukludağ Graben: Seferihisar and Balçova

The Seferihisar geothermal field is situated 40 km SW of İzmir close to the Aegean Sea within the Çubukludağ graben. Balçova geothermal field is located to the NE of the Seferihisar field and it is approximately 10 km SW of İzmir (Fig. 3.4).

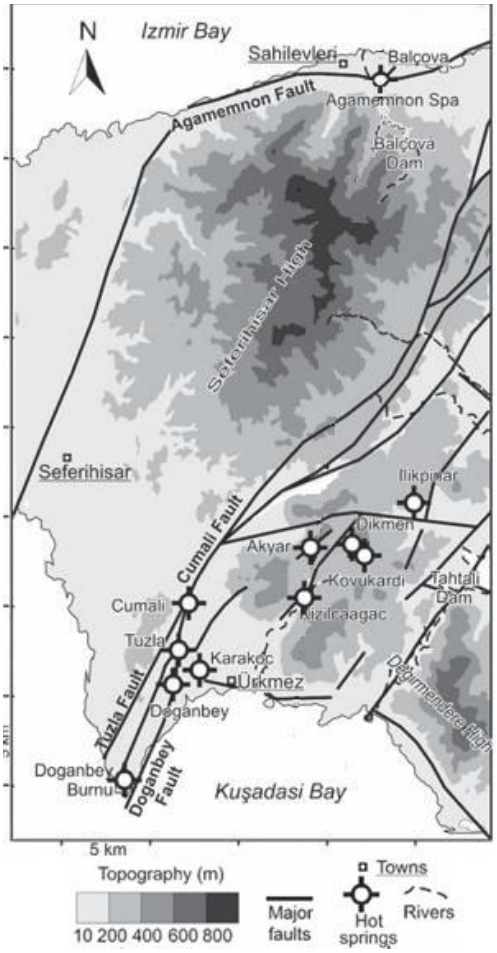

Figure 3.4: The Seferihisar–Balçova Geothermal system (Magri et al., 2010 and the references therein)

The stratigraphic series of the Seferihisar and Balçova areas consist of Paleozoic metamorphic rocks of the Menderes Massif as basement which is overlain by the Upper Cretaceous to Paleocene Bornova mélange (İzmir flysch) consisting of interbedded conglomerate, sandstone-shale, limestone lenses, limestones and

serpentinite bodies, mafic volcanics, chert and their complexes. These units are covered by Neogene terrestrial sediments of interbedded conglomerate, sandstone, claystone, mudstone, and marl and limestone lenses. Quaternary alluvium overlies all the lithologies. Fractured mafic submarine volcanics and highly permeable limestone and serpentinite bodies of the Bornova mélange are the reservoir rocks, while relatively impermeable clay-rich zones and sandstone, shale levels of the Neogene sediments act as the system cap rock (Tarcan & Gemici, 2003; Tarcan et al., 2009).

Gediz Graben: Salihli

Gediz Graben which is the second largest graben of western Anatolia after BMG, is 150 km long and up to 40 km wide. The geothermal fields of Salihli are located in the southern part of the Gediz Graben and approximately 48 km SE of Manisa (Fig. 3.5).

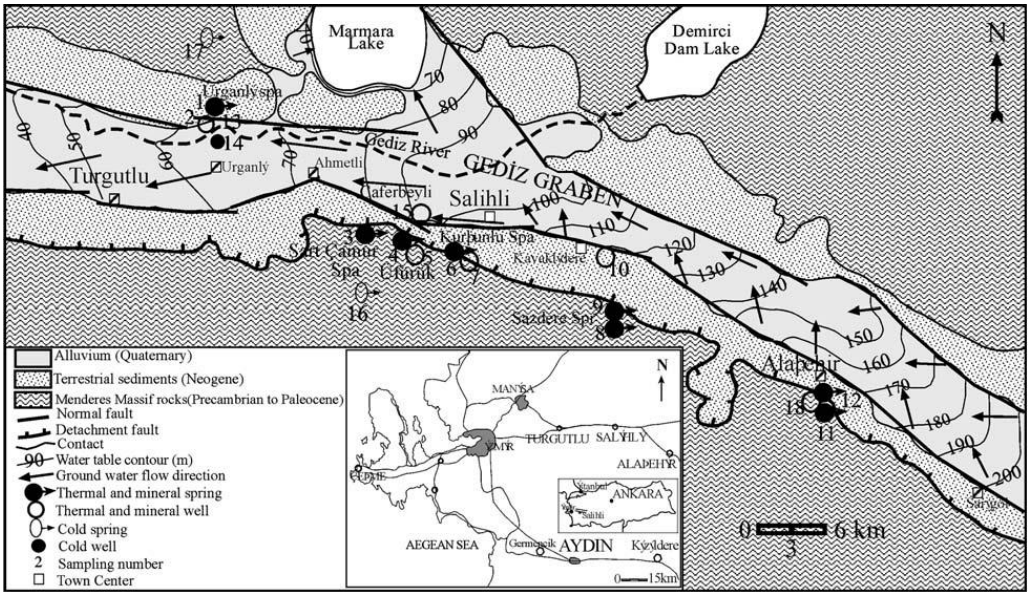

Figure 3.5: Simplified hydrogeological map of the Gediz Graben (Tarcan, 2005 and the references therein).

The Salihli geothermal fields are divided into four main groups from west to east as Caferbeyli, Sart-Çamur, Üfürük and Kurşunlu. The stratigraphic sequence of the area starts with the Paleozoic metamorphics of the Menderes Massif as the basement. The Neogene terrestrial sediments, which are called as Acıdere, Göbekli and Asartepe including poorly cemented clayey levels, have very low permeability as a whole. The oldest sedimentary unit, Acıdere formation consists of fine grained calcareous mudstones, siltstones, sandstones and pebbly sandstones. The Göbekli formation covers a vast area in the region and is dominated by intercalated sandstone, pebbly sandstone, conglomerate beds and mudstones. The Asartepe formation consists of poorly compacted alluvial-fan deposits that comprise mainly conglomerates with intercalated sandstone. The older units are overlain unconformably by Quaternary travertines and alluvium (Tarcan et al., 2000; Özen et al., 2012). The metamorphics of the Menderes Massif act as aquifer for both cold ground waters and thermal waters. The clayey levels of the Neogene terrestrial sediments act as cap rocks for the geothermal systems.

Afyon Graben: Ömer-Gecek

In Afyon area a total of four geothermal fields are present: Ömer–Gecek, Gazlıgöl, Sandıklı, and Heybeli-Karaburun. Ömer-Gecek field is a distinguished area with its many hot springs and it is located 15 km northwest of the city of Afyon (Fig. 3.6). Most of the hot springs are concentrated in three sites: the Uyuz Bath, Ömer Bath, and Gecek Bath.

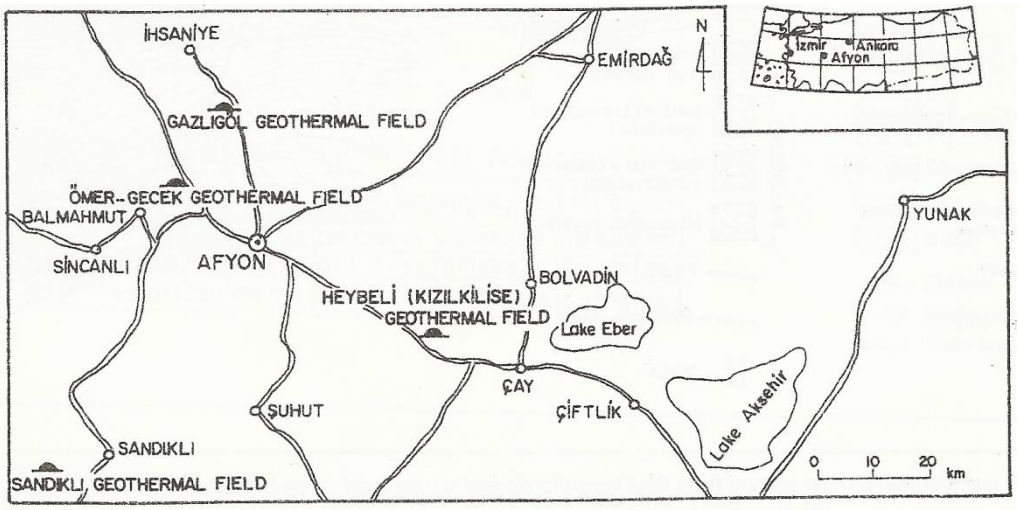

Figure 3.6: Location map of the geothermal fields in Afyon, Turkey (Şimşek & Güleç, 1994).

The oldest unit in the Ömer-Gecek field is the metamorphic rocks of Paleozoic age. In a general sequence, they are observed from bottom to top as: (1) muscovite-biotite-calc-quartz schist; (2) marble; and (3) albite-chlorite-muscovite-sericite schist. Meta-conglomerate and meta-sandstones are also present as big lenses and bands in the schists. Neogene deposits comprised of conglomerate-sandstone, clayey limestone-sandstone, and volcanic glass-trachyandesitic tuff unconformably overlie the Paleozoic basement. As a result of the volcanic activity, tuffs, agglomerates, and lava flows of andesitic, trachytic, trachyandesitic and basaltic compositions are intercalated with the Neogene sediments. Quaternary deposits of travertine and alluvium are the youngest sediments observed in the area. Neogene limestone, silicified limestone, and Paleozoic schist and marbles are the most likely reservoir rocks of the field. Sandy clay, silt, marl and tuffs of Neogene age are the main cap rocks (Mutlu, 1998).

Simav Graben: Sındırgı, Simav

Sındırgı geothermal field is 25 km east of Balıkesir-Sındırgı town and it is located on the western segment of Simav graben. Simav geothermal field, which includes

thermal waters of Eynal, Çitgöl and Naşa, is located in the central part of the Simav graben approximately 4 km north of Simav town (Fig. 3.7).

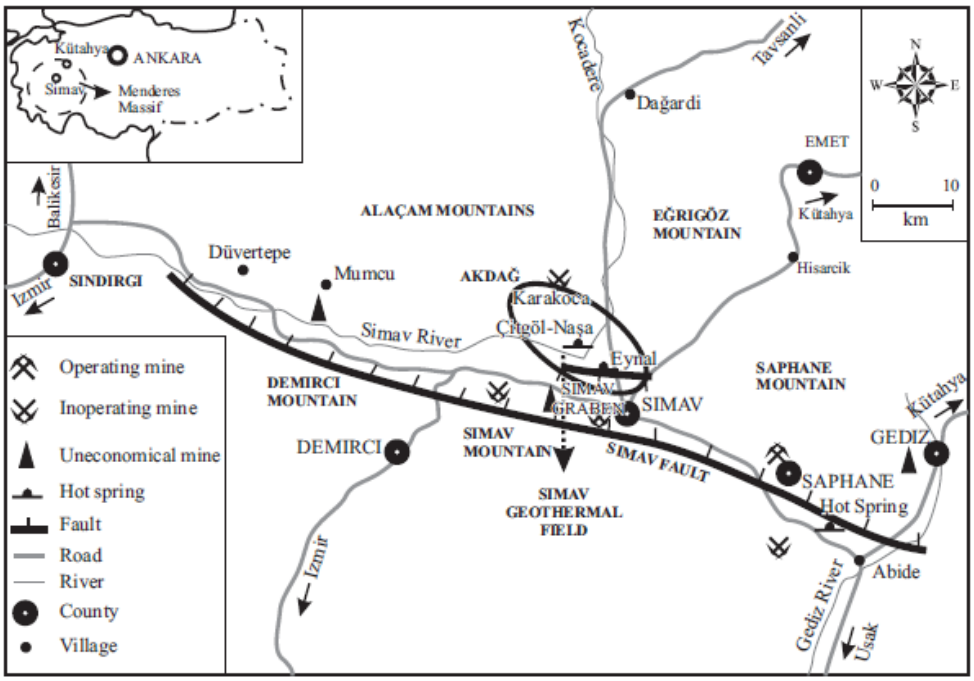

Figure 3.7: Location map of Simav geothermal area, Turkey (Palabıyık & Serpen, 2008 and the references therein)

The basement of Sındırgı geothermal field is formed by the complex of Upper Cretaceous serpentinite, radiolarite and limestone. This unit is unconformably overlain by Neogene sediments (conglomerate, sandstone, siltstone and marl) and mafic volcanics (dacite and tuff) (Aksoy et al., 2009). There are two different reservoir rocks in the field. First one is the mafic volcanic series which are close to the surface, and the other one is Upper Cretaceous recrystallized limestones. Ophiolitic units around the area and Neogene sediments form thick cap rocks of the field.

On the other hand, the basement of Simav geothermal field is the Paleozoic Simav metamorphics which consist of quartzite, quartz-muscovite schist, mica-schist,

calcschist and recrystallized limestone (marble). This unit is overlain unconformably by Mesozoic Kırkbudak formation (conglomerate, sandstone, siltstone and limestone). These rocks are covered by Cenozoic Toklargözü formation and Eynal formation made up of coarse clastic rocks The Paleocene Eğrigöz granite cuts the metamorphics and Kırkbudak formation. The Naşa basalts are the youngest volcanic rocks. Main reservoir rocks of the field are calcschist and recrystallized limestone levels of Kırkbudak formation; the Naşa basalts comprise the potential (secondary) reservoir rocks. Impermeable Neogene rocks, such as claystone, sandstone and conglomerate, cap the Simav geothermal system (Gemici & Tarcan, 2002; MTA, 2005).

Kütahya Graben: Emet

Emet geothermal field is located in the N-S trending Hisarcık-Emet basin, close to Kütahya graben (Fig. 3.8).

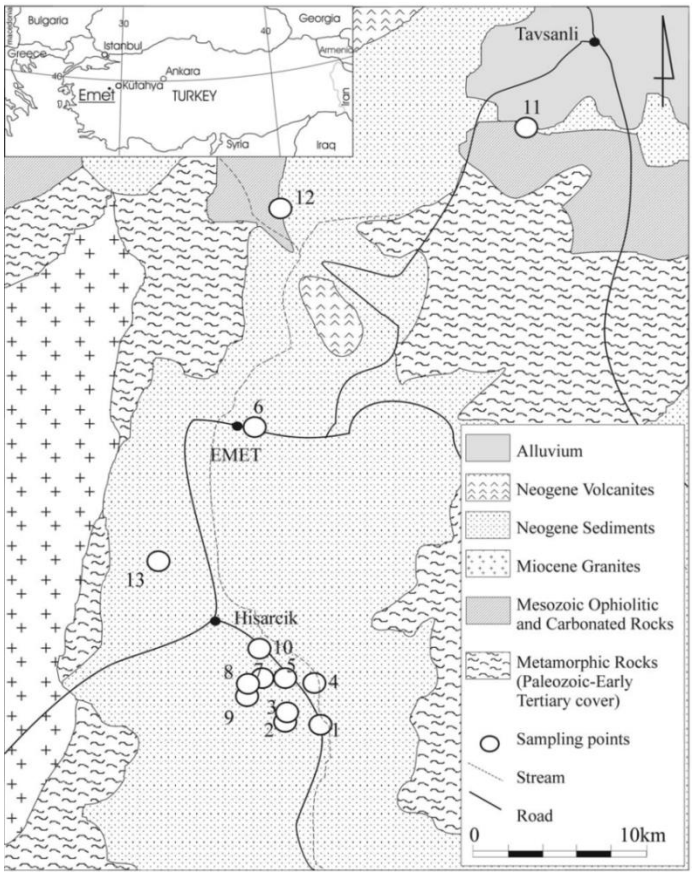

Figure 3.8: Geological map of Emet geothermal field (Gemici et al., 2004 and the references therein).

Menderes Massif metamorphic rocks constitute the principle basement rocks of Emet geothermal field. Paleocene Eğrigöz granite cuts the metamorphic rocks. Neogene lacustrine sediments (Kızılbük formation) in the Emet area consist, from bottom to top, of: basal conglomerate and sandstone, alternating thin-bedded limestone with lenses of marl and tuff, and a red unit that is composed of conglomerate, sandstone, clay, tuff, marl, limestone, coal and gypsum bands. A borate bearing unit of clay with marl, limestone and tuff intercalations (Hisarcık and Emet formations) and capping basalts overlies the red unit. The youngest features are the Quaternary deposits of travertine and alluvium. Investigations show that there are two reservoirs for the thermal waters; Paleozoic metamorphic rocks and Neogene terrestrial rocks (Gemici et al., 2004; MTA, 2005).

Bakırçay Graben: Dikili, Balıkesir

Thermal and mineral waters of Dikili town are located 100 km far from İzmir on the western segment of Bakırçay graben. On the basis of locality, geothermal systems of this area can be divided into three groups: (1) Dikili, (2) Kaynarca and (3) Kocaoba geothermal systems. Located near the eastern part of Bakırçay graben, Balıkesir is one of the largest geothermal provinces in Turkey. There are eight geothermal fields in the Balıkesir region; these are Gönen, Manyas, Pamukçu, Bigadiç, Sındırgı, Edremit, Balya and Susurluk geothermal fields (Fig. 3.9).

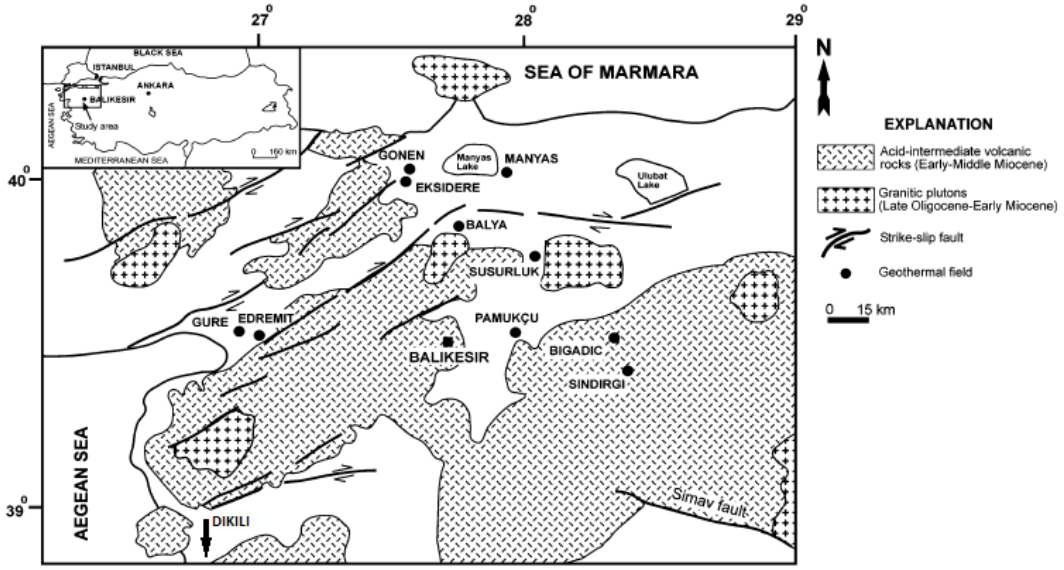

Figure 3.9: Geological map of the Balıkesir region showing the geothermal areas (from Mutlu & Kılıç, 2009).

In the Dikili area, the basement is comprised of Tertiary granodiorite of Kozak Massif. Neogene Yuntdağı volcanics, clayey limestone - marl - siltstone - mudstone - sandstone - conglomerate intercalations of Soma formation, Dededağı basalts and Quaternary alluvium are the cover units of the granodioritic basement. The composition of Yuntdağı volcanics is andesite, dacite and rhyolite. Due to the well-developed fracture systems of these volcanics, they act as reservoir rocks,

whereas mudstones and siltstones in Soma formation act as cap rocks for the system (Özen et al., 2005; MTA, 2005; Karahan, 2013).

In the Balıkesir area, metamorphic rocks consisting of gneiss, schist, marble and ophiolites of Paleozoic to early Mesozoic age and a mélange association of upper Cretaceous age form the basement. In the area, there are also several granitic plutons with ages ranging from Oligocene to middle Miocene. All these magmatic rocks are covered by Neogene sediments comprised of conglomerate, sandstone, marl, claystone and clayey limestone. The youngest unit is the Quaternary alluvium. The reservoir rocks in geothermal fields of the Balıkesir area are gneiss, marble, granodiorite and recrystallized limestone of Paleozoic to early Mesozoic age. The upper Miocene-Pliocene sediments such as conglomerate, sandstone, marl, claystone, form the cap rock of the systems (MTA, 2005; Genç 1998 in Mutlu, 2007).

Edremit Graben: Tuzla, Edremit

Tuzla geothermal field is located in northwestern Turkey, 80 km SW of Çanakkale and 5 km from the Aegean Sea. Due to the effect of seawater, the thermal water of Tuzla has extremely high dissolved salt content. Edremit geothermal field which is 87 km W of Balıkesir, is located on the eastern segment of Edremit graben. (Fig. 3.10).

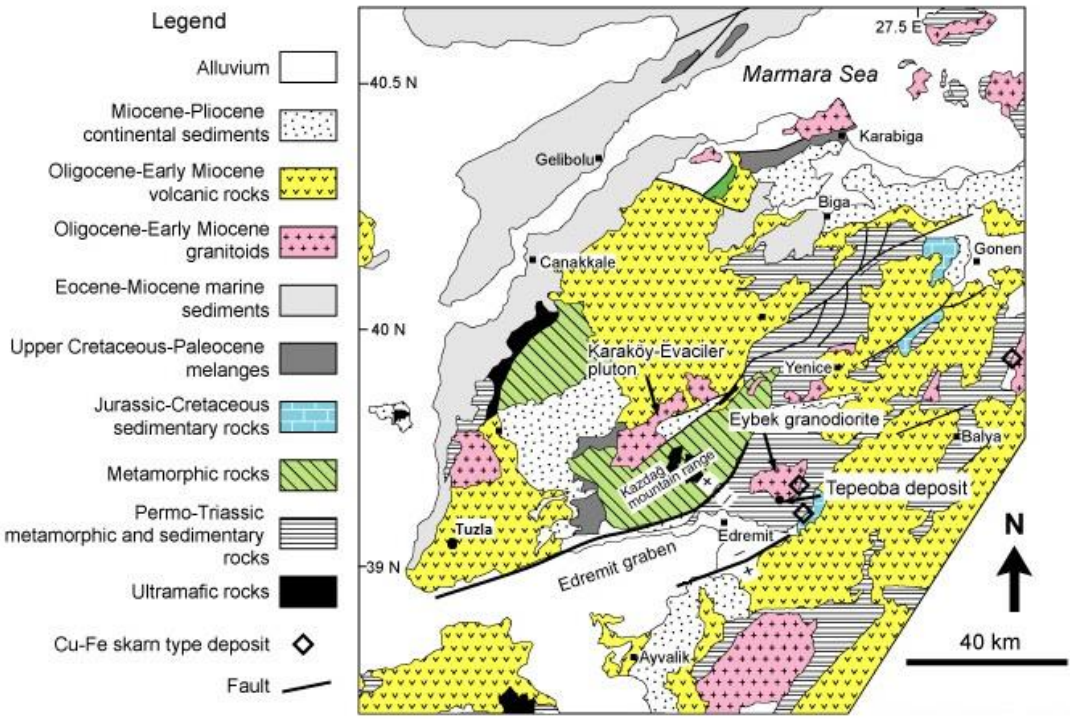

Figure 3.10: Geological map of the Biga Peninsula (Okay & Satır, 2000).

The basement of the Tuzla geothermal field consists of Paleozoic metamorphic rocks that are schist and recrystallized limestone. The metamorphic basement is intruded by a large granodioritic pluton, named as Kestanbol pluton. These units are overlain by Mesozoic conglomerate, sandstone, marl and limestone-sandstone which are in turn overlain by Miocene rhyolitic tuffs, ignimbrites, latitic and rhyolitic lavas. Different type of lavas and recrystallized limestone of metamorphic basement comprise the reservoir rocks, whereas tuffitic claystone, conglomerates and sandstones on the top of these units act as cap rock for the system (Gevrek et al., 1984-1985; MTA, 2005).

The basement of Edremit geothermal field is made up of metamorphic rocks (schists, gneisses, amphibolites, metadunites, migmatites, and marbles) of the Kazdağ Massif. The basement is overlain by spilitic basalts, radiolarites and clastics of Karakaya Formation which are also overlain by the sandy limestones of Bilecik Formation. These units are intruded by the Eybek Granodiorite. The Plio-

Quaternary sediments of unconsolidated sandstone, mudstone and conglomerate form the youngest units in the field. Two aquifers are present in the field: a deeper confined aquifer and a shallower unconfined aquifer. The shallower aquifer is comprised of Quaternary and Plio-Quaternary loosely cemented, unconsolidated sandstone, mudstone and conglomerate units. This shallow aquifer overlies the Ballıca Formation of siltstone–marl–conglomerate–sandstone–clayey limestone which is impermeable and acts as a cap rock for the deeper confined aquifer. The deeper aquifer is composed of agglomerate and conglomerate units which are permeable (Avşar et al., 2013).

3.2. Eastern Anatolia

Eastern Anatolia has a rather moderate geothermal potential resulting from the lack of deep fault systems which prevent deep hydrothermal circulation of waters, despite the widespread Neogene-Quaternary volcanism which provide a sufficient heat source in the region (Mutlu & Güleç, 1998).

The geologic framework of eastern Anatolia has been characterized by the collision between the Arabian and the Anatolian plates in middle Miocene. The tectonic regime in the region seems to have changed from compressional–contractional in middle Miocene-early Pliocene to compressional–extensional (tectonic escape) until present (Koçyiğit et al., 2001). By the ongoing convergence between the Arabian and the Eurasian plates, the Anatolian Plate is squeezed out with a westward motion along the East and North Anatolian faults. Five different tectonic blocks are recognised in Eastern Anatolia: i) the Eastern Rhodope–Pontide fragment (granulite facies rocks), ii) northwestern Iranian fragment (magmatic–migmatitic lithologies covered in most parts by collision-related volcanics), iii) Eastern Anatolian Accretionary Complex, EAAC (ophiolitic mélange with flysch units), iv) Bitlis–Pötürge Massif (gneisses, schists, quartzites and marbles), and v) the Arabian foreland (Keskin, 2007) (Fig. 3.11).

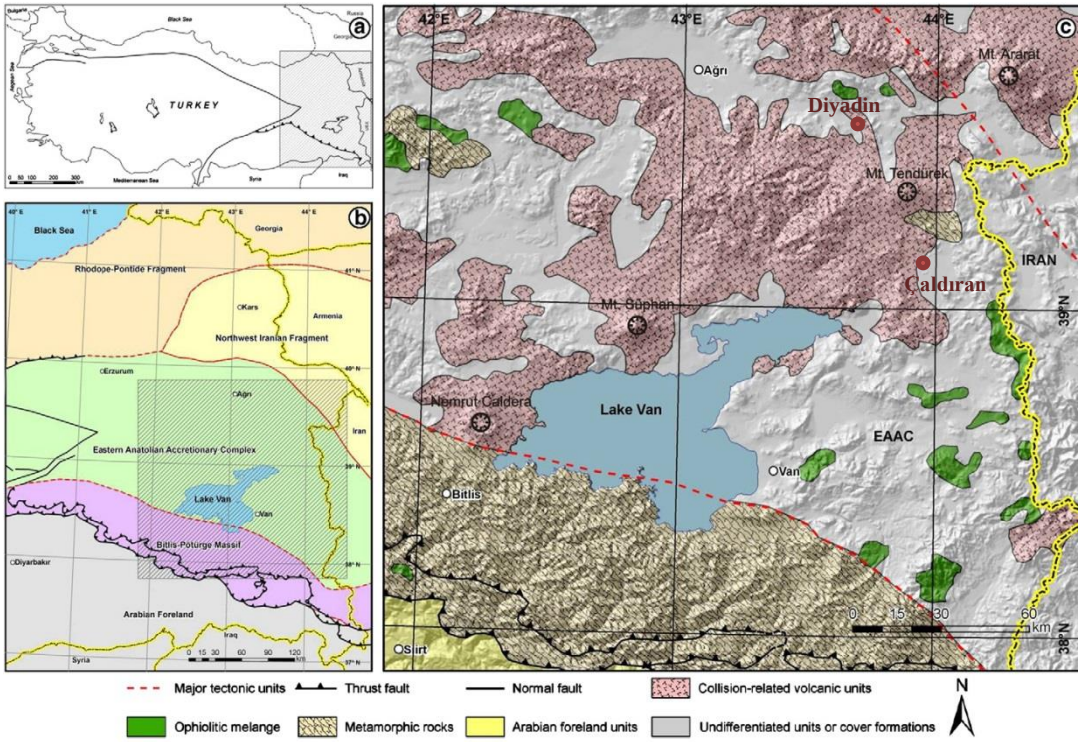

Figure 3.11: Maps showing a) the location, b) major tectonic units and c) geology of eastern Anatolia. (from Keskin, 2007 in Mutlu et al., 2012).

Following the middle Miocene collision of the Arabian and Anatolian plates, intense volcanic activity seems to have initiated and generated lava flows and pyroclastics of variable composition (from basalts to rhyolites) which cover the basement units. This activity has given rise to the formation of several stratovolcanoes aligned in a NE–SW direction (e.g. Ararat, Tendürek, Süphan, and Nemrut) aging from 2.5 to <0.01Ma (Yılmaz et al., 1998; Özdemir et al., 2006; Özdemir, 2011) (Fig. 3.11). Among them, Nemrut volcano on the southwest coast of Lake Van is reported to be historically active where the latest gas and ash eruptions took place in 1692 (Karakhanian et al., 2002).

The important geothermal areas of the region are concentrated around the young volcanoes (e.g., Diyadin-Ağrı, Çaldıran-Van, Nemrut-Bitlis areas) (Mutlu and Gulec, 1998; Mutlu et al., 2012). The drilling data relevant to Diyadin and Çaldıran geothermal fields are given in Table 3.2.

Table 3.2: Drilling data on the primary geothermal systems in eastern Anatolia

Geothermal System	No. of drilled wells	Max drilled depth (m)	Max measured Temp.(°C)	Reservoir rocks	Cap rocks	References
Diyadin (Ağrı)	6	215.1	78	Paleozoic marbles, gneiss, schists and lacustrine limestones	Pliocene-Quaternary schists, altered tuffs and ignimbrites	Pasvanoğlu & Güler, 2010; Mutlu et al., 2013
Çaldıran (Van)	1	573	83	Paleozoic to Mesozoic metamorphic rocks of serpentinized peridotite, gabbro, volcanic deposits, red limestone and sandy limestone	Plio-Quaternary andesite, basalt, tuff, ignimbrite, pyroclastic rocks; Eocene-Miocene sediments of sandstone, sandy limestone, marl, shale and mudstone	Aydın et al., 2013

Diyadin Geothermal Field

Diyadin geothermal field is located at southeast of Ağrı (Fig. 3.12) and it is a tectonic depression where many hot and cold springs are present.

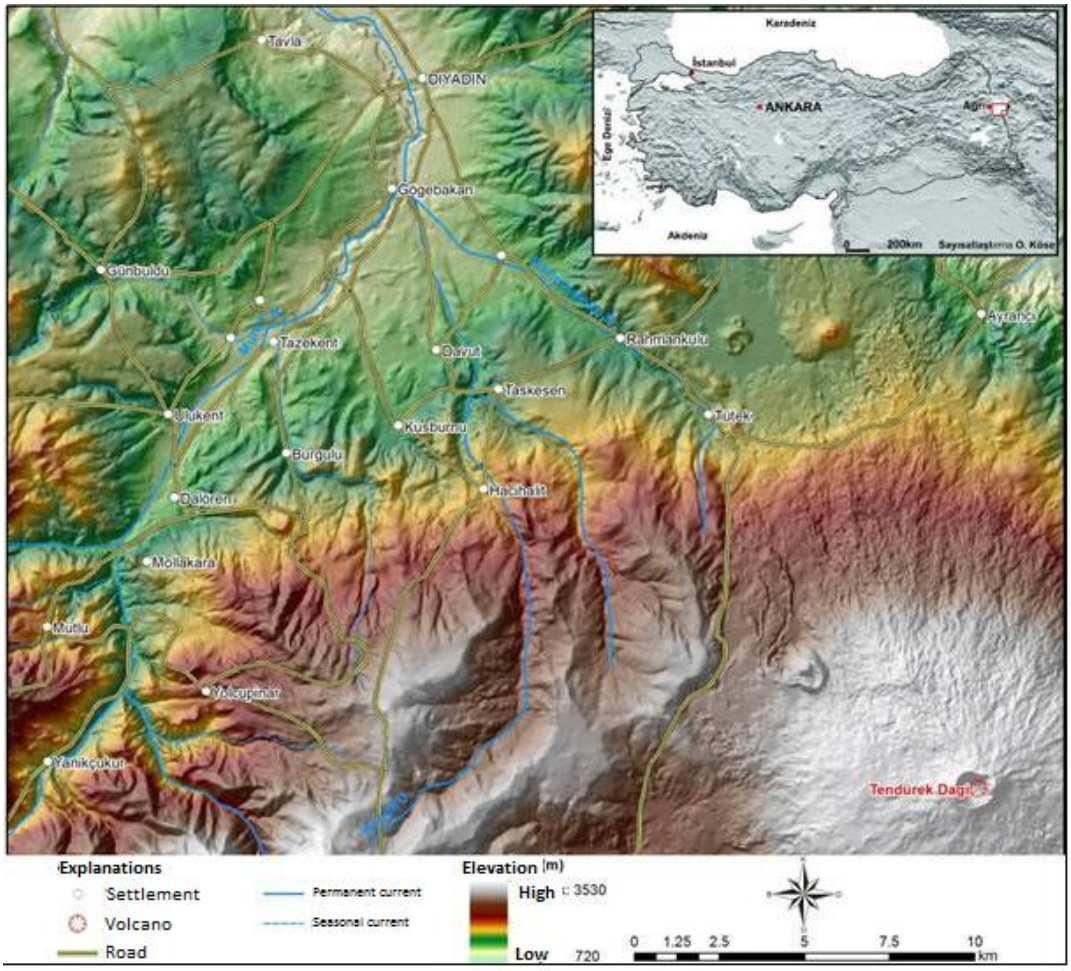

Figure 3.12: Location map of Diyadin geothermal field (Mutlu et al., 2013).

The basement of Diyadin field consists of marble, gneiss, schist and quartzite of Paleozoic-Mesozoic age. Above this unit, upper Cretaceous ophiolitic rocks (serpentinized peridotite, gabbro, volcanic deposits, red limestone and sandy limestones) are observed. These units are overlain by sediments of Miocene to Pliocene age made up of sandstone, sandy limestone, marl, micritic limestone, shale, claystone, mudstone and evaporates. Pliocene-Quaternary andesite, basalt, tuff, ignimbrite, lava flow and pyroclastic rocks which are named as Tendürek Volcanics, cover all the units. At the top, Quaternary alluvium and travertine are present (Mutlu et al., 2013). Paleozoic marbles, gneiss, schists are the main reservoir rocks whereas the lacustrine limestones form the secondary reservoir

rocks due to their relatively high secondary porosity and permeability. Pliocene-Quaternary schists and altered tuffs and ignimbrites comprise the cap rocks (Pasvanoğlu, 2013).

Çaldıran Geothermal Field

The geothermal springs in the Çaldıran plain are situated at northeast of Lake Van (Fig. 3.13).

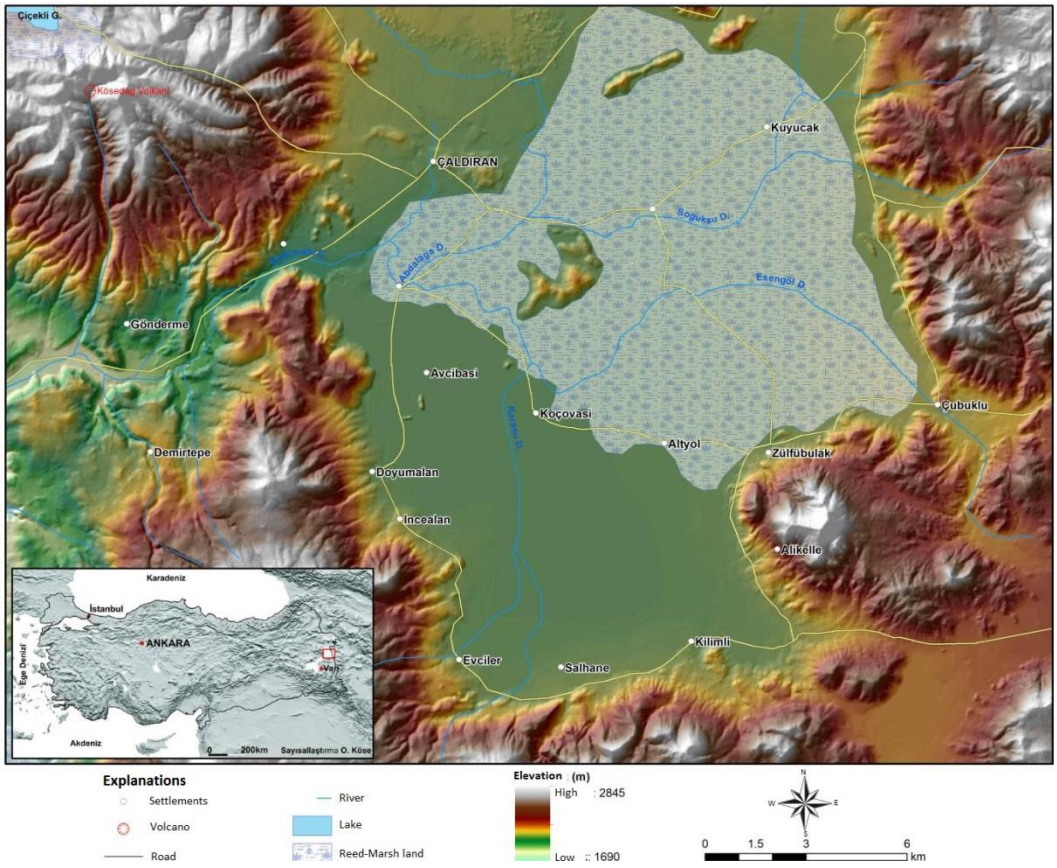

Figure 3.13: Location map of Çaldıran geothermal field (Aydın et al., 2013).

Paleozoic metamorphics and upper Cretaceous ophiolitic mélange (also called Kemertepe Complex) which consists of serpentinized peridotite, gabbro, volcanic deposits, red limestone and sandy limestone blocks, form the basement of the area.

Sediments of Eocene-Miocene age (mainly carbonates, evaporates) overlie the mélange. These sediments include sandstone, sandy limestone, marl, micritic limestone, neritic limestone, shale, claystone and mudstone. Above these units, Pliocene-Quaternary andesite, basalt, tuff, ignimbrite, lava flow and pyroclastic rocks (Tendürek Volcanics) are observed. Quaternary alluvium covers all the units. Reservoir rocks of Çaldıran geothermal field are comprised of Paleozoic-Mesozoic metamorphic rocks and the cap rocks are made up of Plio-Quaternary volcanic rocks and Eocene-Miocene sediments (Aydın et al., 2013).

3.3. Northern Anatolia

The important geothermal areas of northern Anatolia are situated along one of the major neotectonic structures (seismically active zones) of Turkey, North Anatolian Fault Zone (NAFZ). The geothermal activity is concentrated especially in the western and central-western segments of the zone associated with the tectonic activity along the NAFZ. As previously mentioned, this region has the lowest geothermal energy potential in Turkey, mainly due to restriction of the heat source (young magmatic activities) to pull-apart basins (Mutlu & Güleç, 1998). The major geothermal fields located along the NAFZ are from west to east: Yalova, Efteni, Mudurnu, Seben, Bolu, Kurşunlu, Hamamözü, Gözlek, and Reşadiye (Fig. 3.14).

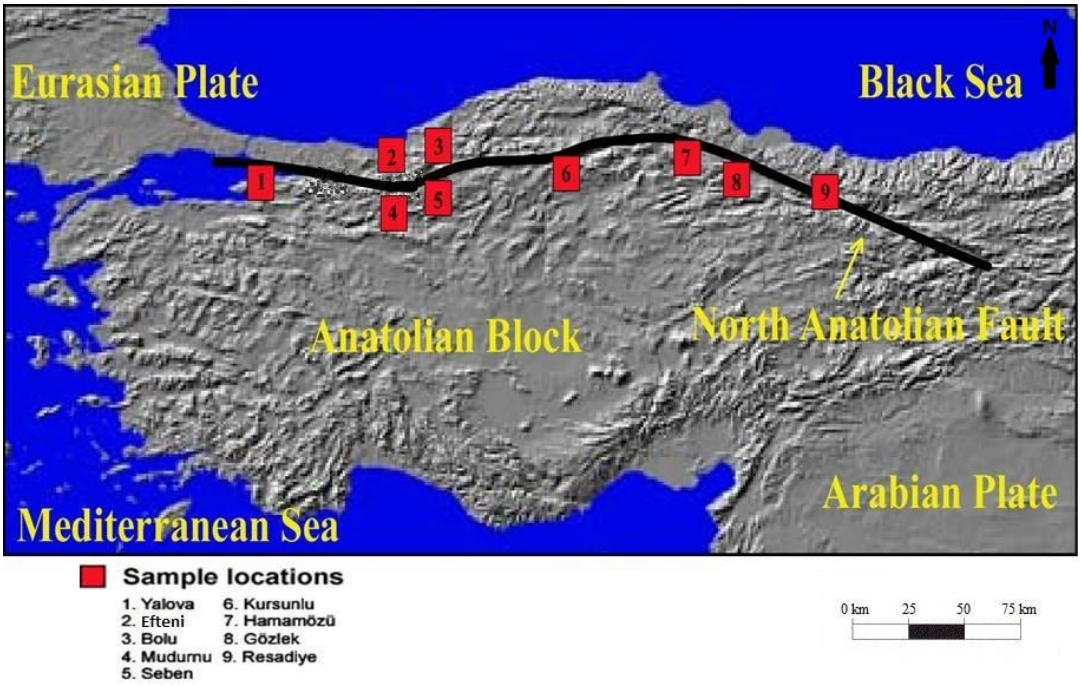

Figure 3.14: Location map of the sampled geothermal fields along the NAFZ (Güleç et al., 2006)

Paleozoic metamorphics composed of schists and marbles form the basement rocks of the geothermal areas along NAFZ. Upper Jurassic-lower Cretaceous limestones and upper Cretaceous flysch comprised of intercalations of limestone, conglomerate, marl, sandstone, claystone and siltstone, unconformably overlie this metamorphic basement. Intercalated with, or overlying, the upper Cretaceous flysch, there are upper Cretaceous to Miocene basaltic-andesitic lava flows, tuffs and agglomerates. Neogene clastics and lacustrine limestones overlie these lithologies (Şahinci, 1970; Canik, 1972; Koçak, 1974; Özcan and Ünay, 1978; Erzenoğlu, 1989; MTA, 2005). The youngest units in the region are the Plio-Quaternary fluviatile deposits, and in the eastern-central segment of the NAFZ these deposits are associated with Plio-Quaternary volcanics which have rather small exposures (Tatar et al., 1995).

The drilling data relevant to the geothermal fields along the NAFZ are summarized in Table 3.3.

Table 3.3: Drilling data on the primary geothermal systems along the NAFZ

Geothermal System	No. of drilled wells	Max drilled depth (m)	Max measured Temp.(°C)	Reservoir rocks	Cap rocks	References
Yalova	1	673.5	40	Tertiary volcanics (particularly Eocene andesites)	Neogene clastics and limestones; impermeable clayey levels of the flysch facies	MTA, 2005; Süer et al, 2008
Efteni (Düzce)	-	-	43.6 (hot spring)	Mesozoic limestones	Neogene clastics and limestones; impermeable clayey levels of the flysch facies	MTA, 2005; Süer et al, 2008
Mudurnu (Bolu)	2	125	39.8	Mesozoic limestones	Neogene clastics and limestones; impermeable clayey levels of the flysch facies	MTA, 2005; Süer et al, 2008
Seben (Bolu)	1	2200	90	Mesozoic limestones	Neogene marl, sandstones and limestones; impermeable clayey levels of the flysch facies	Canik & Pasvanoğlu, 2003; MTA, 2005; Süer et al, 2008; Yılmazdemir, 2011
Bolu	3	758.5	43	Upper Cretaceous limestones and sandstones	Neogene clastics and limestones; impermeable clayey levels of the flysch facies	MTA, 2005; Süer et al, 2008
Kurşunlu (Çankırı)	3	680	54	Tertiary volcanics	Neogene clastics and limestones; impermeable clayey levels of the flysch facies	MTA, 2005; Süer et al, 2008
Hamamözü (Amasya)	1	500	42.5	Mesozoic limestones; secondary permeability zones of schists	Neogene clastics and limestones; impermeable clayey levels of the flysch facies	MTA, 2005; Süer et al, 2008
Gözlek (Amasya)	3	530.3	40.5	Mesozoic limestones	Neogene clastics and limestones; impermeable clayey levels of the flysch facies	MTA, 2005; Süer et al, 2008
Reşadiye (Tokat)	1	238.9	46.5	Mesozoic limestones	Neogene clastics and limestones; impermeable clayey levels of the flysch facies	MTA, 2005; Süer et al, 2008

The primary reservoir rocks of the geothermal fields located along the NAFZ (except Yalova and Kurşunlu) are Mesozoic limestones. Tertiary volcanics constitute the reservoir rocks of Yalova and Kurşunlu (Koçak, 1974; MTA, 2005). The cap rocks of these systems are composed of impermeable clayey levels of the flysch facies and the Neogene deposits.

CHAPTER 4

HYDROGEOCHEMICAL CHARACTERIZATION OF GEOTHERMAL FIELDS: DATA COMPILATION

In most of the geothermal fields in Turkey, Na–Ca–HCO_3 type waters are the major water types except that Na–Cl type waters are typical for the coastal areas of western Anatolia and for a few inland areas of western and central Anatolia where deep water circulation exists. The discharge temperature of the springs ranges up to 100^{o}C, and the bottom-hole temperatures in drilled wells up to 242^{o}C. Western Anatolian fields that have the highest geothermal energy potential in Turkey, are associated with the western Anatolian extensional tectonics which provide a regional, deep-seated heat source (asthenospheric upwelling) and a widespread graben system allowing deep circulation of waters (Mutlu & Güleç, 1998).

In this chapter, the chemical compositions of thermal waters in Turkey that are compiled from previous studies are presented and their hydrogeochemical characteristics are reviewed. From the viewpoint of CO_2 storage, to investigate the geothermal fields as natural analogues, several fields are selected for detailed hydrogeochemical characterization. The selection is based on:

a) The available and reliable hydrogeochemical data with sufficient parameters,

b) The available isotope and gas geochemistry data (although these data are not used in the geochemical modelling in this study, the availability of these data is also taken into account in order to compare the conclusions derived from previous studies to those of present study),

c) Most recent publications (articles not reports).

4.1. Western Anatolia

Among the geothermal fields of western Anatolia, Kızıldere, Tekkehamam, Germencik, Balçova, Salihli, Sındırgı, Simav, Emet, Dikili, Balıkesir, and Edremit fields are selected for the hydrogeochemical investigation. The data relevant to the chemical and isotopic compositions of the geothermal fluids from the geothermal fields of western Anatolia are given in Table A.1 and A.2, respectively.

4.1.1. Kızıldere, Tekkehamam and Germencik Geothermal Fields

Chemical composition of Kızıldere, Tekkehamam and Germencik geothermal systems are compiled from Şimşek et al. (2005), Gökgöz (1998), Filiz at al. (2000), respectively (Table A.1). Isotope compositions are taken from Karakuş and Şimşek (2013) and Mutlu et al. (2008) (Table A.2).

Thermal occurrences in these fields can be grouped into three as, i) Na-HCO_3 type Kızıldere, ii) Na-SO_4 type Tekkehamam and iii) Na-HCO_3-Cl type Germencik waters (Fig. 4.1) The bicarbonate nature of the Kızıldere waters are attributed by Şimşek et al. (2005) to a long time interaction of the waters with the carbonate levels of the metamorphic basement. The SO_4-rich nature of Tekkehamam waters are stated by Gökgöz (1998) to be due to oxidation of H_2S gas escaping from magma, and/or dissolution of minerals like gypsum. The Cl-rich character of the Germencik waters, on the other hand, is attributed (by Mutlu and Güleç, 2008) to the presence of connate fossil waters at depth. The stable oxygen- and hydrogen-isotope compositions points to an essentially meteoric origin for the thermal waters in the fields of Büyük Menderes Graben (BMG) as the data points on $\delta^{18}O$ vs. δD diagram (Fig. 4.2) plot in the vicinity of the Global and/or Local Meteoric Water Lines. Additionally, however, the effects of water-rock interaction and mixing are also recognized, particularly in the Germencik field. In this respect, the reservoir seems to be recharged mainly by meteoric waters penetrating to depths along the major fault zones. These waters after being heated at depth, ascend through the major faults bounding the graben, and flow towards the centre of the graben where

they mix with colder groundwater (Şimşek, 1985, 2005). The studies on the controls of He-CO_2 systematics (Mutlu et al., 2008) reveal that water samples are significantly affected by degassing in the hydrothermal system and/or have experienced CO_2 loss via calcite precipitation (Fig. 4.3).

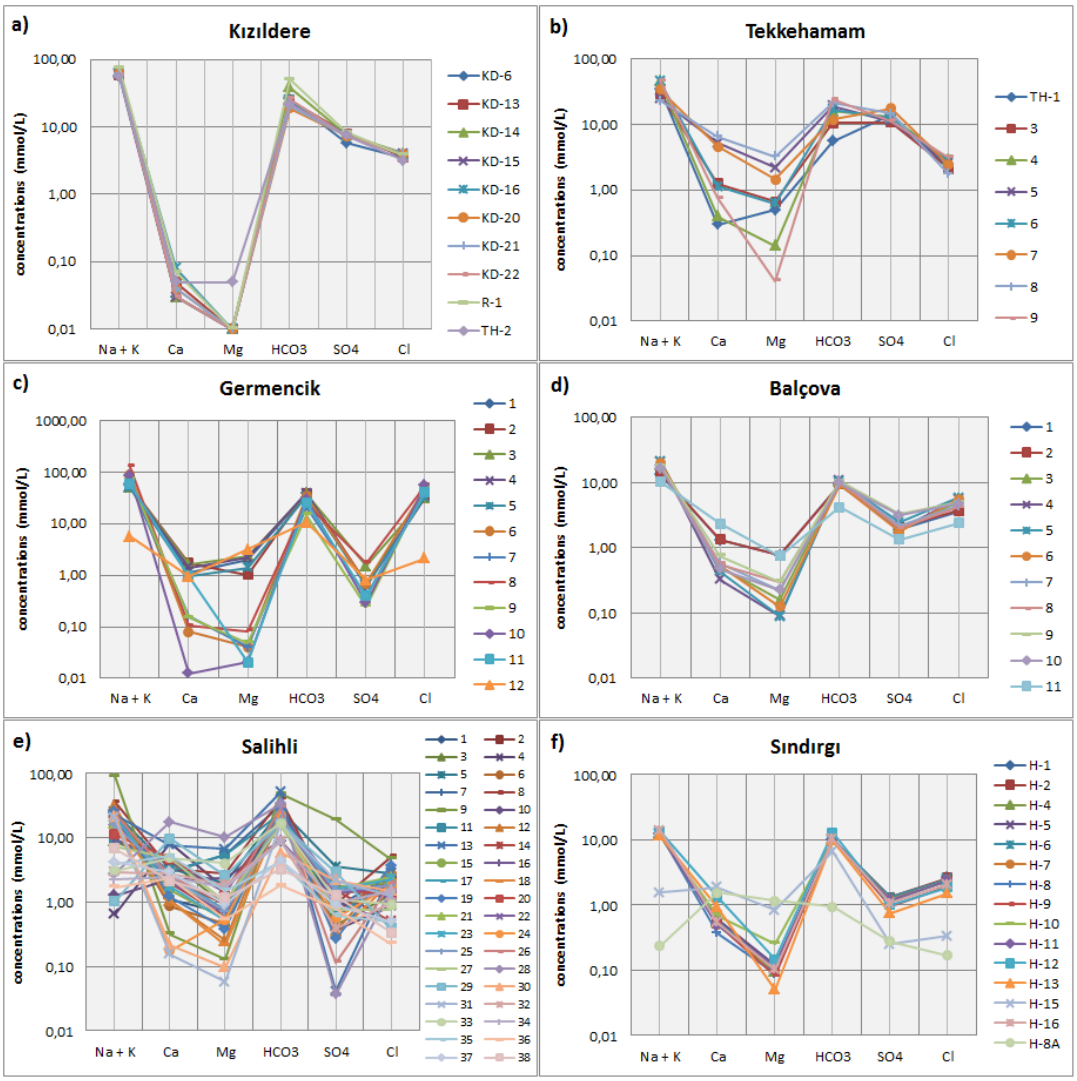

Figure 4.1: Schoeller diagrams of the geothermal fields of western Anatolia a) Kızıldere, b) Tekkehamam, c) Germencik, d) Balçova, e) Salihli, f) Sındırgı.

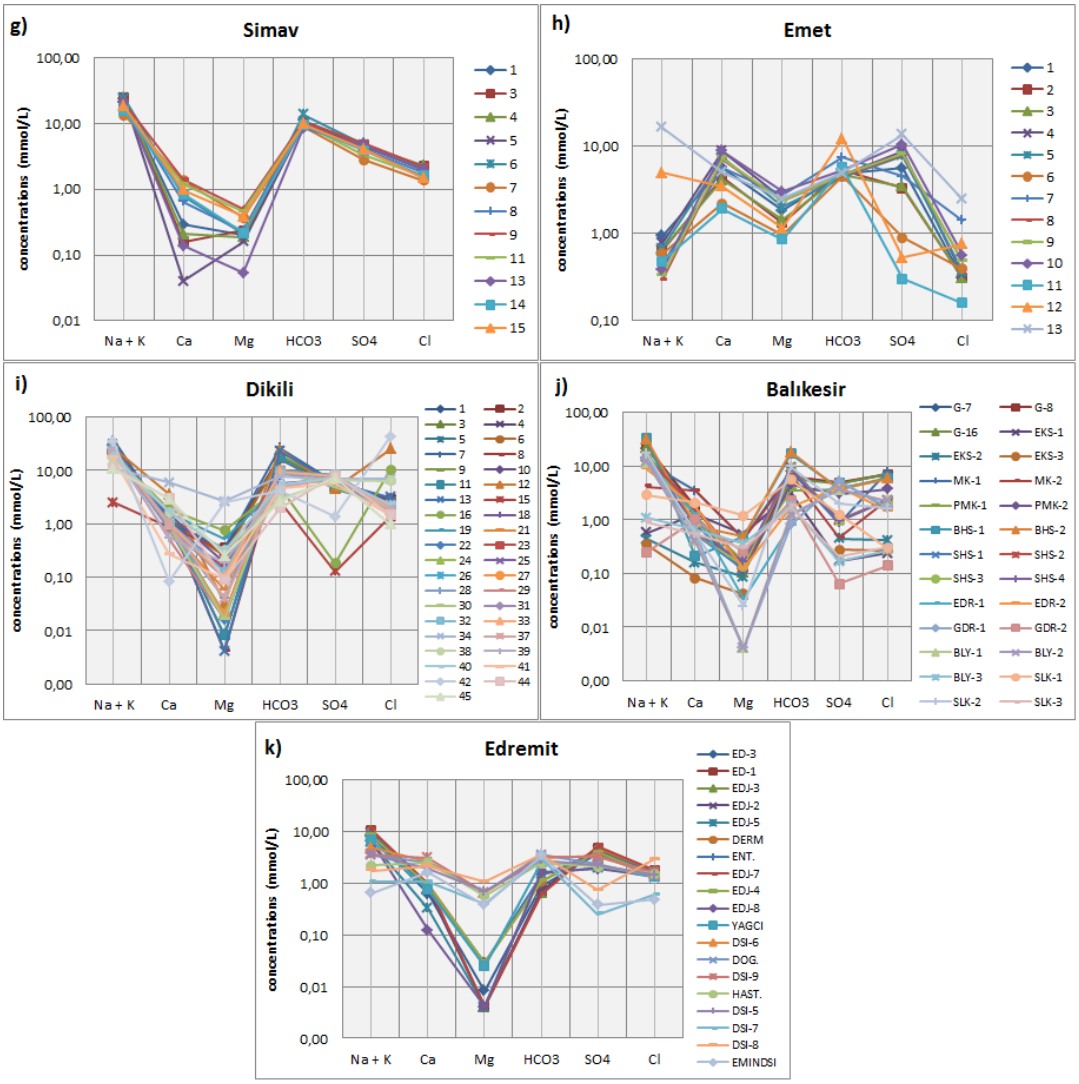

Figure 4.1 (cont'd): Schoeller diagrams of the geothermal fields of western Anatolia g) Simav, h) Emet, i) Dikili, j) Balıkesir, k) Edremit.

4.1.2. Balçova Geothermal Field

Chemical composition of Balçova geothermal system is compiled from Tarcan et al. (2009); isotope data are from Mutlu et al. (2008) (Table A.1 and A.2). The chemistry of thermal waters is dominated by Na and HCO_3 (Fig 4.1). Na-rich nature of thermal waters is attributed (Tarcan et al., 2009) to rock dissolution and ion exchange reactions in deep aquifers at high temperatures.

$\delta^{18}O$ and δD values indicate a meteoric origin for Balçova waters (B-101 in Table 4.2 and Fig. 4.2). However, since the area is close to shore, the relatively high $\delta^{18}O$ and δD values (compared to the fields of BMG) are probably due to the effects of sea water influx into the host aquifer; this is also supported by the high Na and relatively high Cl contents of waters (Mutlu et al., 2008). He-CO_2 systematics seems to be controlled mainly by CO_2 loss via calcite precipitation (Fig. 4.3).

4.1.3. Salihli Geothermal Field

The concentration of the constituents in thermal waters from Salihli geothermal field are compiled from Tarcan et al. (2005) and Özen et al. (2012) (Table A.1). The waters are dominantly Na-HCO_3 type except in Sart and Üfürük where waters are Na-Ca-HCO_3 and Ca-Mg-HCO_3 types, respectively (Fig 4.1).

Oxygen- and hydrogen-isotope compositions (Fig.4.2 and Table A.2) point to the effects of water-rock interaction and evaporation of waters of metoric origin (Özen et al., 2012).

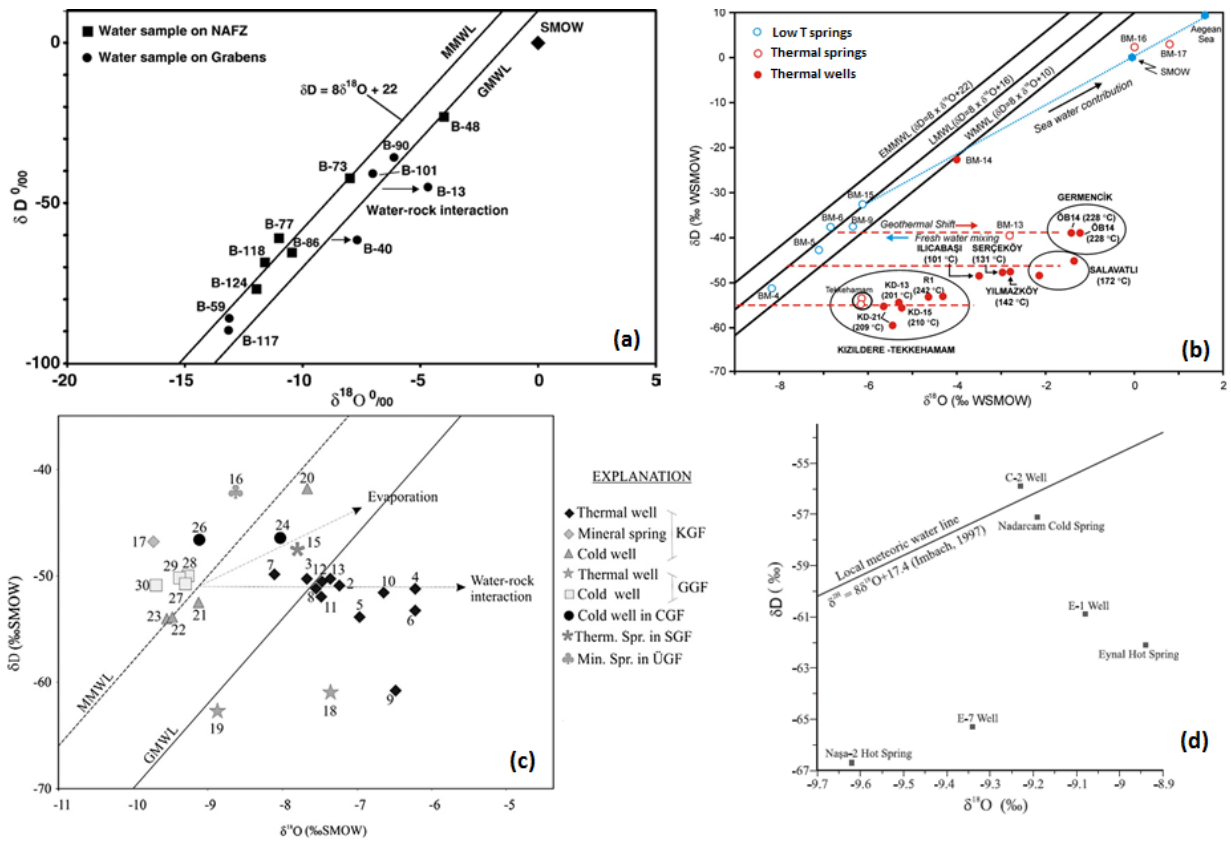

Figure 4.2: $\delta^{18}O$–δD diagrams for the western Anatolian waters. MMWL: Mediterranean Meteoric Water Line ($\delta D=8\ \delta^{18}O+22$; Gat and Carmi, 1970); GMWL: Global Meteoric Water Line ($\delta D=8\ \delta^{18}O+10$). (a) western Anatolian waters (from Mutlu et al., 2008), (b) waters in the BMG (from Karakuş & Şimşek), 2013, (c) waters in Salihli field KGF: Kurşunlu geothermal field, CGF: Caferbeyli geothermal field, GGF: greenhouse geothermal field (from Özen et al., 2012), (d) waters in Simav field (from Palabıyık & Serpen, 2008). Sample numbers are given in Table A.2.

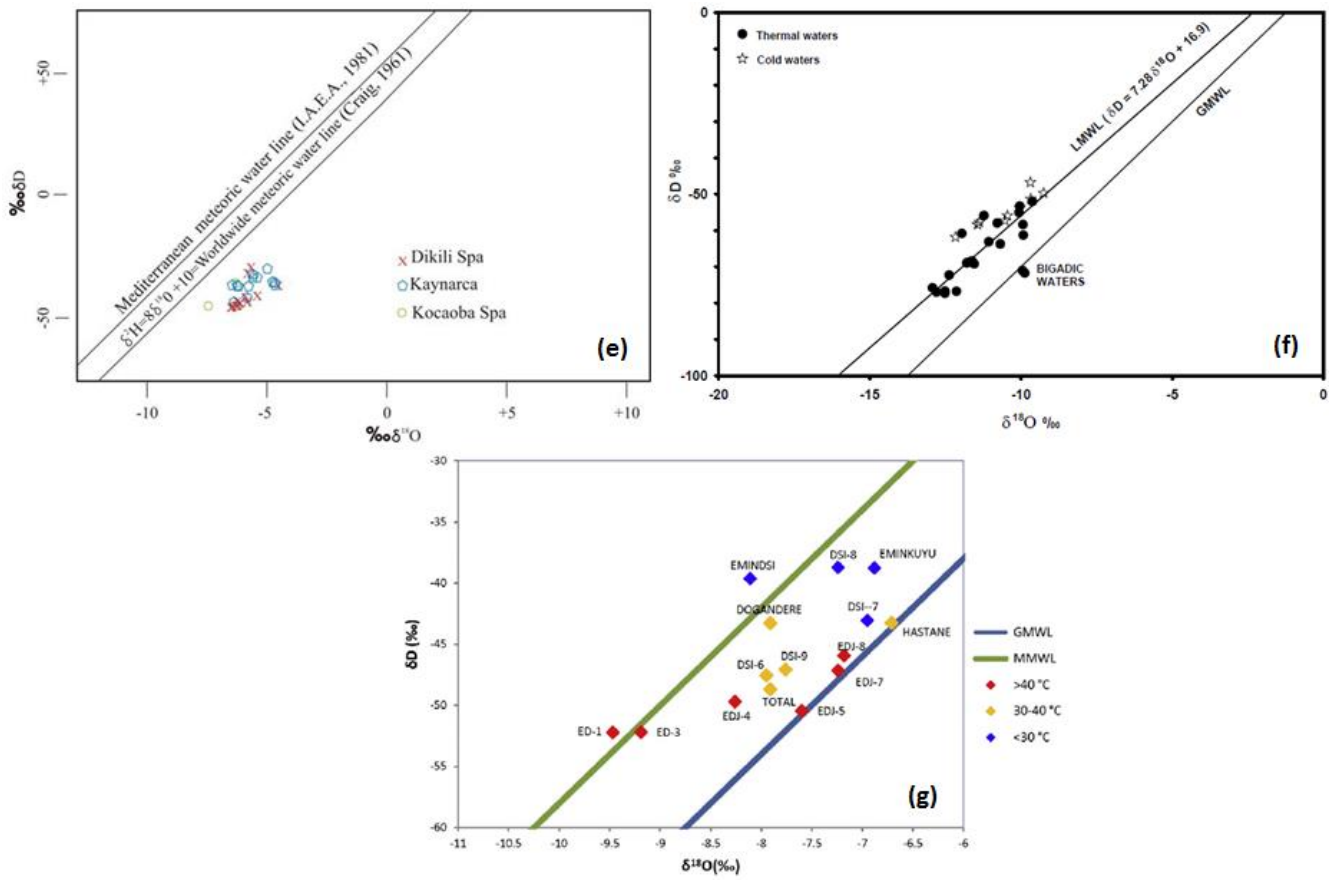

Figure 4.2 (cont'd): $\delta^{18}O$–δD diagrams for the western Anatolian waters. MMWL: Mediterranean Meteoric Water Line ($\delta D=8\ \delta^{18}O+22$; Gat and Carmi, 1970); GMWL: Global Meteoric Water Line ($\delta D=8\ \delta^{18}O+10$). (e) waters in Dikili field (from Özen et al., 2005), (f) waters in the Balıkesir region (from Mutlu, 2007), (g) waters in Edremit field (from Avşar et al., 2013). Sample numbers are given in Table A.2.

4.1.4. Sındırgı Geothermal Field

The geochemical analyses of Sındırgı (Hisaralan) geothermal field are taken from Aksoy et al. (2009) and the isotope data are from Mutlu et al. (2008) (Table A.1 and Table A.2). The thermal waters in the field are of Na-HCO_3 character (Fig. 4.1).

Dominance of HCO_3 content in thermal waters indicates dissolution of carbonate minerals and connection to the limestone reservoir rocks. On the other hand, long interaction time between thermal waters and reservoir rocks results in the exchange of Na ion in ophiolitic rocks such as clay and serpentine, with Ca and Mg, making Na the major cation of the system (Aksoy, Demirkıran, & Şimşek, 2009). The $\delta^{18}O$–δD composition of Sındırgı (Hisaralan) sample (B-118) plot on local Mediterranean Meteoric Water Line (MMWL) (Fig. 4.2) pointing to meteoric origin. When the isotopic data of Sındırgı field is compared to the data of other fields in western Anatolia, it can be seen that $\delta^{18}O$ values do not show any enrichment (i.e. shift from MMWL). This means that Sındırgı waters have less circulation time and a lower temperature with respect to other fields. Combined He-CO_2 systematics suggest the effect of degassing and calcite precipitation in the deep hydrothermal system in Sındırgı (sample no. B-118 in Fig. 4.3) (Mutlu et al., 2008).

4.1.5. Simav Geothermal Field

Data on the chemical properties of Simav geothermal field are obtained from the study of Gemici & Tarcan (2002) (Table A.1). The thermal waters are $NaHCO_3$ in nature (Fig. 4.1). Although the dominant anion in waters is bicarbonate, sulphate concentration in Simav field is distinctly higher than those of other fields in western Anatolia. According to Palabıyık and Serpen (2008), the high SO_4 levels are due to the presence of alunite mineral in the vicinity (Şaphane area) which is a product of hydrothermal alteration of tuffs.

The isotope compositions ($\delta^{18}O$ and δD) suggest meteoric origin (Fig. 4.2 and Table A.2) and Palabıyık and Serpen (2008) state that through the Simav fault which penetrates very deep, the heat at depth is transferred with naturally convecting meteoric waters in the metamorphic crust. In addition, it is observed that the water is enriched in ^{18}O pointing to the existence of long time fluid-rock interaction in the system at depth and/or boiling due to the high temperature in the reservoir.

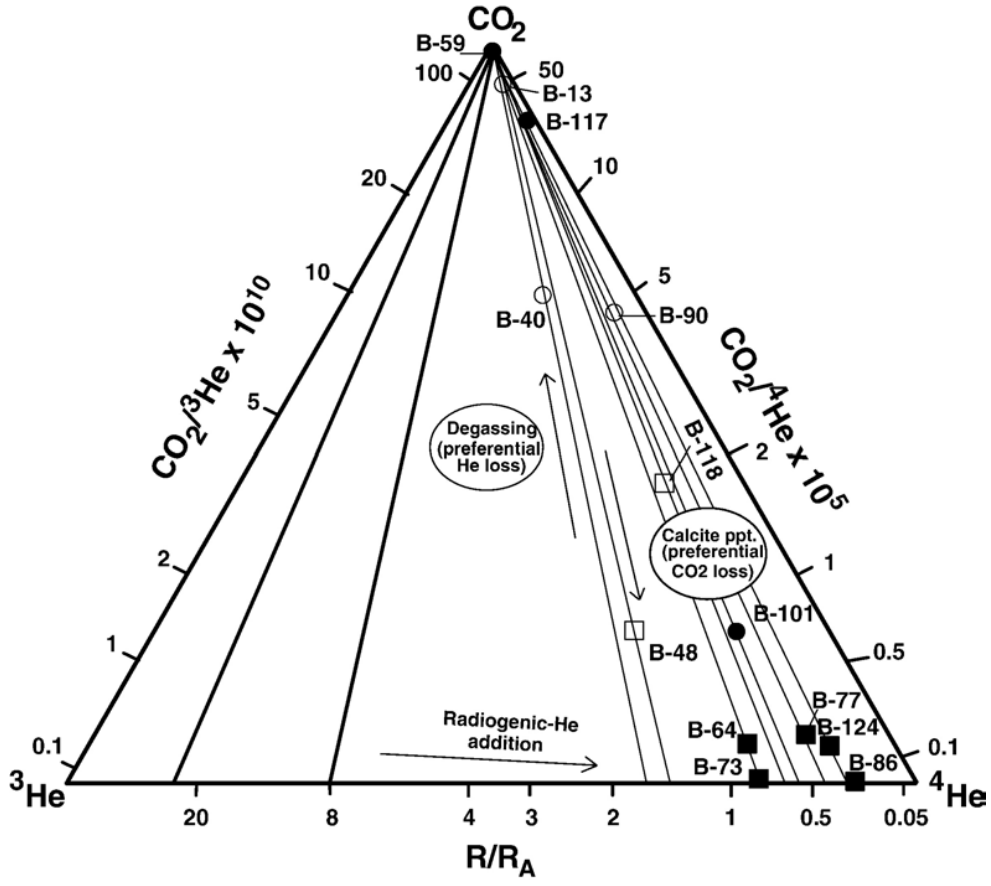

Figure 4.3: CO_2–^3He–^4He ternary diagram for the western Anatolian fluids. Bold solid lines represent mixtures between mantle-He (8 and 30 R_A) and pure CO_2. Light solid lines indicate various mixtures between CO_2 and helium yielding observed C–He systematics of the samples. Arrows show the effects of degassing, calcite precipitation and radiogenic-He addition (symbols as in Fig. 4.2 and empty circles and squares represent gas samples on grabens and gas samples on NAFZ, respectively. Sample numbers are given in Table A.2.

4.1.6. Emet Geothermal Field

Waters of Emet geothermal field are analysed by Gemici et al. (2004) and the results are tabulated in Table A.1. With respect to their chemical composition, the waters can be categorized into three different groups:

1) Ca-Mg-SO_4-HCO_3 type waters (samples 1, 2, 3, 4, 5, 6, 7, 8, 9 and 10).

2) Ca-Mg-HCO_3 type waters (samples 11 and 12).

3) Na-Ca-SO_4 (sample 13).

The dominancy of calcium in most of the samples suggests the dissolution of carbonate (limestone and dolomite) reservoir rocks. The dominancy of SO_4 as anion of the thermal waters, on the other hand, reflects the dissolution of gypsum layers in the Kızılbük formation below the Emet borate deposits. Gemici et al. (2004) suggest that in water-rock interaction, dissolution of $CaSO_4$ is an important process. As $CaSO_4$ dissolves the SO_4/HCO_3 ratio increases, which results in the shift of the type of water from HCO_3-dominant to SO_4-dominant.

4.1.7. Dikili Geothermal Field

For the geochemical characterization of the waters of Dikili geothermal field, the relevant data are taken from the study of Özen et al. (2005) (Table A.1). The chemistry of the waters in the area show similarities and the water types in Dikili Spa, Kaynarca and Kocaoba are Na-HCO_3-SO_4, Na-SO_4-HCO_3, Na-Ca-SO_4, respectively. The high concentrations of Na and HCO_3 ions in the waters are attributed by Özen et al. (2005) to a combination of mixing with cold groundwater, water rock interaction and ion exchange reactions in the aquifers.

In addition to the chemical analyses of waters in Dikili area, Özen et al. (2005) also conducted isotope studies which suggest that thermal waters in the geothermal fields are of meteoric origin and show slight $\delta^{18}O$ enrichment (Fig. 4.2 and Table A.2). The recharged meteoric water is heated at depth and ascends to the surface

along the faults. Hydrogeochemical assessment points to a potential mixing process of thermal waters with cold water before and/or after heating at depth.

4.1.8. Balıkesir Thermal Waters

The results of chemical analyses of waters from the Balıkesir region are taken from Mutlu (2007) (Table A.1). Included in this group, Gönen, Pamukçu, Edremit and Balya waters are Na-SO_4 type, whereas Bigadiç and Sındırgı waters are characterized by Na-HCO_3 enrichment. The Ekşidere thermal water is of Ca-HCO_3 character, and the Manyas and Susurluk fields are represented by Na-Ca-HCO_3 type waters. Low chloride concentrations in hot waters may suggest shallow water circulation in most of the geothermal fields. On the other hand, relatively high levels of sulphate concentration in these waters may be generated from the oxidation of metallic sulphides or escape of H_2S from a deep hot-water system.

The isotope studies (Mutlu, 2007) (Table A.2, Fig. 4.2) show that except for the Bigadiç waters, most of the Balıkesir waters point to a common meteoric origin on the Local Meteoric Water Line (LMWL). Different position of the Bigadiç thermal waters with an ^{18}O shift is explained with water-rock interaction process as a consequence, $\delta^{18}O$ content of these waters is increased. In fact, some other thermal waters (e.g. G-7, G-8, G-16, PMK-1, PMK-2, MK-1) with slight ^{18}O shifts might have also undergone oxygen exchange reactions. Isotope composition of inorganic carbon in the Gönen, Susurluk, Bigadiç, Sındırgı and one of the Manyas waters (-4.8 to +0.7 ‰) (Mutlu, 2007) closely resembles marine limestones which are represented with $\delta^{13}C$ values of about -3 to +3‰ (Clark & Fritz, 1997). Mutlu (2007) states that the relatively high temperatures of the Bigadiç, Sındırgı, Gönen and Susurluk thermal waters might have induced carbonate dissolution process resulting in carbon isotope compositions similar to marine limestones. On the other hand, it can be observed in He-CO_2 systematics (Fig. 4.3) that some waters in Balıkesir fields (sample B-124 from Gönen and B-77 from Manyas, Table A.2) are mainly affected by degassing in the hydrothermal system and/or have experienced CO_2 loss via calcite precipitation (Mutlu et al., 2008).

4.1.9. Edremit Geothermal Field

Chemical composition of Edremit geothermal system is taken from Avşar et al. (2013) (Table A.1 and A.2). The hydrogeochemical facies of the waters are defined by the dominant cation–anion pair which indicates that waters >40°C are of "Na − SO_4" type, waters <30°C are of "Ca − HCO_3" type and those with temperatures between 30 and 40 °C are "Ca − SO_4" type.

All water samples from Edremit field plot in between Mediterranean Meteoric Water Line (MMWL) and Global Meteoric Water Line (GMWL) (Fig. 4.2), suggesting a common meteoric source for the waters. Chemical compositions and isotopic studies in Avşar et al. (2013) indicate that "mixing" and "water–rock interaction" are potential subsurface processes.

4.2. Eastern Anatolia

Diyadin and Çaldıran geothermal fields of eastern Anatolia are studied for the hydrogeochemical investigation. The data relevant to the chemical composition of the geothermal fluids from these fields are given in Table A.3. Table A.4 gives the isotopic composition of samples from all over the eastern Anatolian region including those from the Diyadin and Çaldıran geothermal fields.

4.2.1. Diyadin Geothermal Field

Chemical and isotope compositions of Diyadin geothermal system are acquired from Mutlu et al. (2013) and Mutlu et al. (2012), respectively (Table A.3 and Table A.4). The hydrogeochemical characteristics of Diyadin field are Na-HCO_3 type for thermal waters (TUN, KOP, KUS, TAZ, MLK, DIB) while Ca-HCO_3 type for cold waters (Fig. 4.4). Although all the waters in the field are HCO_3 – dominated, some of the samples with high temperatures (MLK, KOP, KUS, TUN) have relatively high amount of Cl, indicating that these waters have longer water-rock interaction times and/or deep circulation. In addition, BUR and EBU waters are characterized by relatively high SO_4 contents accompanied by low pH values.

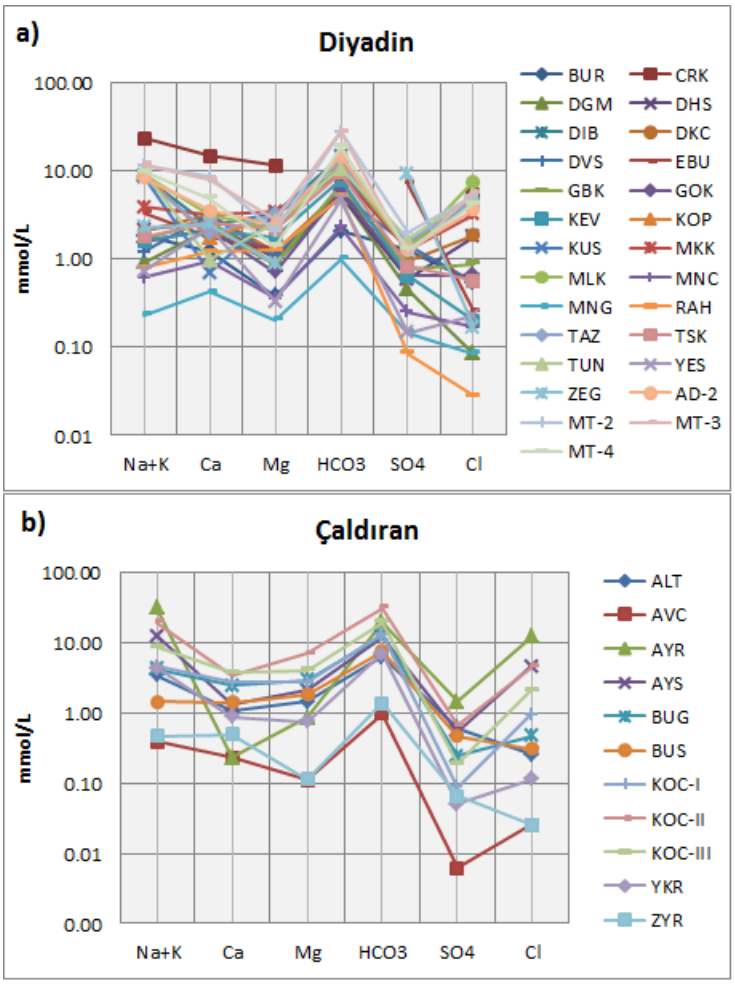

Figure 4.4: Schoeller diagrams of the geothermal fields of eastern Anatolia a) Diyadin, b) Çaldıran

The isotope composition of the eastern Anatolian thermal waters is depicted in terms of $\delta^{18}O$–δD diagram in Fig. 4.5. As can be seen from Fig. 4.5 most waters plot close to the Global Meteoric Water Line (GMWL), pointing to a meteoric origin. Waters in the northeast and eastern parts of the region (samples CAY, DYD, DVT, AYR, HAD, CAM-1, CAM-2), including Diyadin samples (DYD, DVT), plot off the (global and local) meteoric water lines indicating the effect of water–rock interaction process and evaporation and/or phase separation on their isotopic compositions (Mutlu et al., 2012).

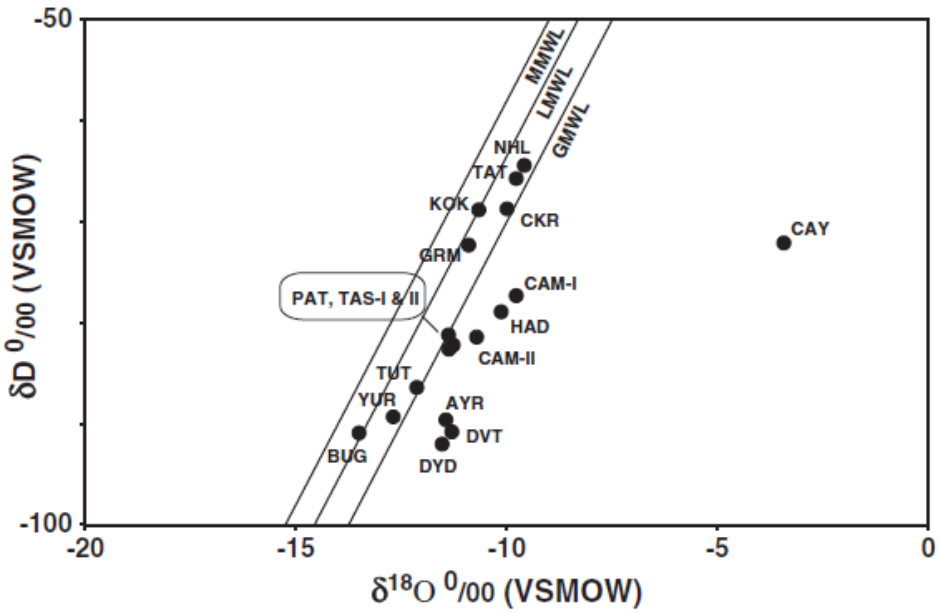

Figure 4.5: $\delta^{18}O$–δD diagram for the eastern Anatolian thermal waters. MMWL: Mediterranean Meteoric Water Line ($\delta D=8\ \delta^{18}O+22$); LMWL: Local Meteoric Water Line ($\delta D=8\ \delta^{18}O+16.5$); GMWL: Global MeteoricWater Line ($\delta D=8\ \delta^{18}O+10$) (Mutlu et al., 2012). Sample numbers are given in Table A.2.

The He-CO_2 systematics (Fig. 4.6) of Diyadin (samples DYD and DVT) which have high $CO_2/^3He$ values indicate that these waters have undergone hydrothermal degassing while the sample CKR is most likely affected by mixing processes. $\delta^{13}C$ (CO_2) values suggest derivation from marine limestone (or slab carbonate) rather than an organic sedimentary source (Mutlu et al., 2012).

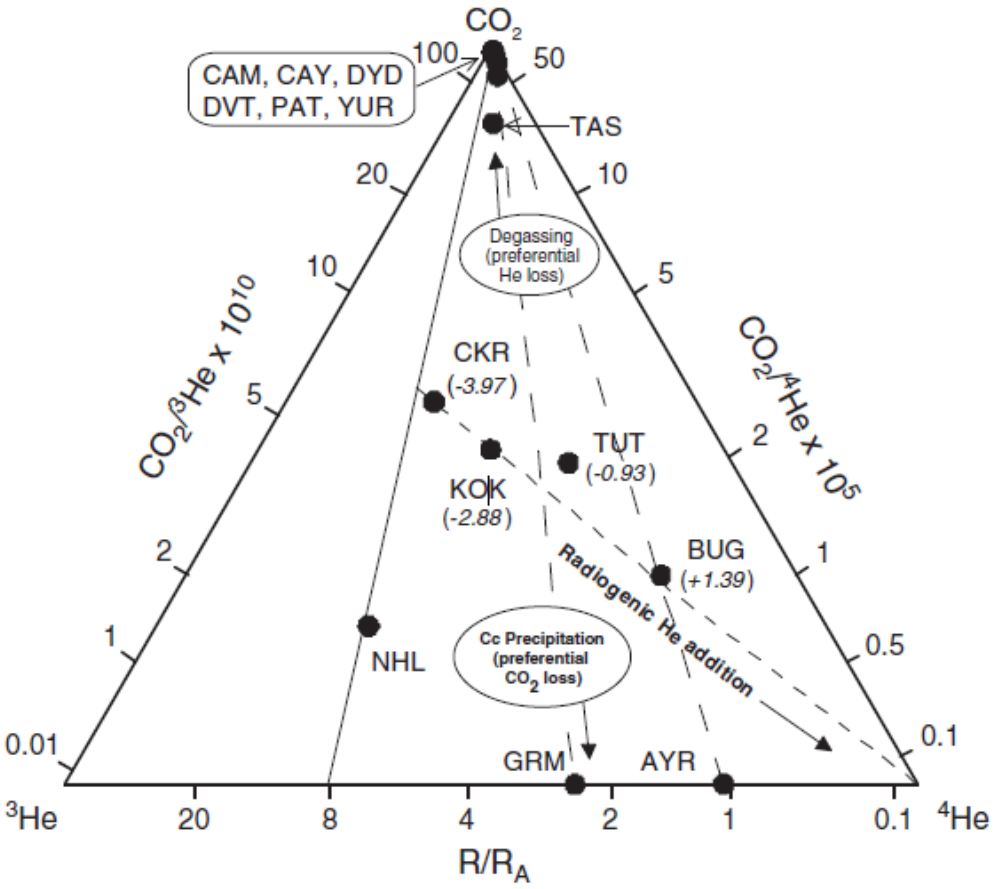

Figure 4.6: CO_2–^3He–^4He ternary diagram for the eastern Anatolian fluids. Bold solid line represents mixture between mantle-He (8 and 30 R_A) and pure CO_2. Numbers in parenthesis are $\delta^{13}C$ values. Short dashed line indicates addition of radiogenic helium (~0.05 RA); long dashed lines represent CO_2 loss relative to helium (Mutlu et al., 2012). Sample numbers are given in Table A.4.

4.2.2. Çaldıran Geothermal Field

Chemical composition of Çaldıran geothermal system is compiled from Aydın et al. (2013); isotope data are from Mutlu et al. (2012) (Table A.3 and A.4). The water samples of ALT, AYR, AYS, KOC-II, KOC-III and YKR are Na-HCO_3 type, and the samples of AVC, BUG, BUS, KOC-I, KOC-III and ZYR are Ca-Mg-HCO_3 type waters (Fig. 4.4). It can be observed that HCO_3 is the major anion of the field. On the other hand, the major cation is Na in AYR and KOC-II thermal waters whereas in BUG, Mg-Ca are the major cations. This may indicate that waters in

Çaldıran geothermal field may originate from aquifers with different lithologies (Aydın et al., 2013).

The O- and H-isotope composition of Çaldıran waters in Fig. 4.5 are represented by samples AYR and BUG. BUG plots on the local meteoric water line, while AYR plots off the meteoric water lines indicating the effect of water–rock interaction process and evaporation and/or phase separation.

With respect to the He-CO_2 systematics (Fig. 4.6), one of the samples from Çaldıran field (BUG) fall on a mixing line between mantle- and crustal-components; the other sample, AYR, has extremely low $CO_2/^3He$ value suggesting either the effect of degassing (where the sample represents the first formed gas) or calcite precipitation (Mutlu et al., 2012). $\delta^{13}C$ (CO_2) values, like those of Diyadin samples, point to a marine limestone (or slab carbonate) source for carbon, rather than an organic sedimentary source (Mutlu et al., 2012).

4.3. Northern Anatolia

The geochemical analyses of the geothermal fields along the North Anatolian Fault Zone (NAFZ) are taken from Süer et al. (2008) and the isotope data are from Süer et al. (2008) and de Leeuw et al. (2010) (Table A.5 and Table A.6). In these articles, the compositions are determined for a total of 3-sampling periods in three years of monitoring and in this thesis study, the average values are used in the calculations. The sampled fields are Yalova, Efteni, Mudurnu, Seben, Bolu, Kurşunlu, Hamamözü, Gözlek, and Reşadiye. Most of the thermal waters in these fields are Na-HCO_3 type (Efteni, Seben, Gözlek, Reşadiye and Kurşunlu samples), apart from the Ca-HCO_3 type Bolu and Mudurnu, and the Na-SO_4 type Yalova samples (Fig. 4.7). Hamamözü has a mixed character while the cold waters in this field are Ca and/or Mg-HCO_3 type. The hydrogeochemical facies of these waters (HCO_3-type) are most likely the result of the dissolution of the limestones that comprise the reservoir rock. The dominancy of Na, as cation, can be associated with the ion exchange reactions taking place with the overlying sediments. The SO_4 type character of Yalova waters is attributed to either the dissolution of evaporites

containing gypsum, or the oxidation of sulphide-bearing minerals (Süer et al., 2008).

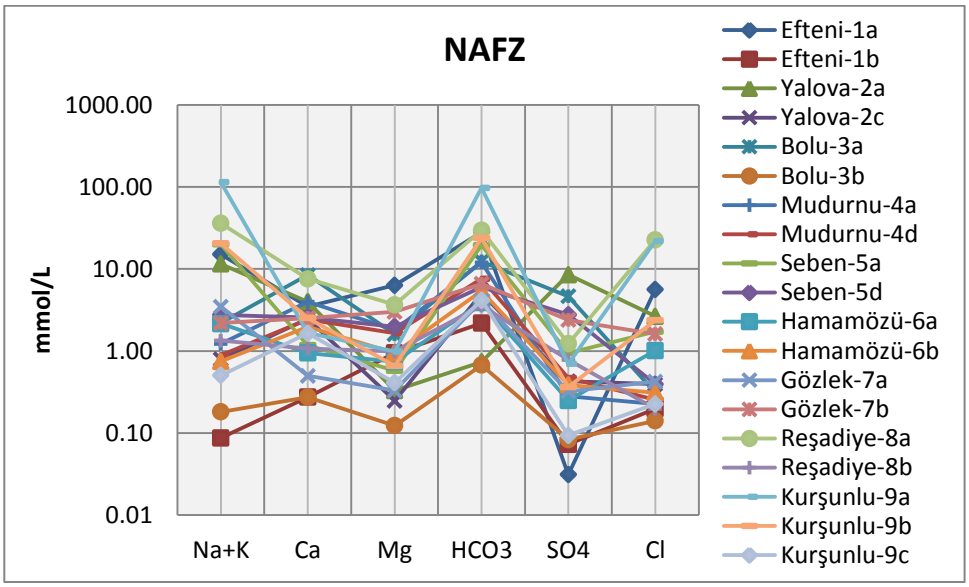

Figure 4.7: Schoeller diagrams of the geothermal fields along the NAFZ

The stable isotope compositions which are plotted in the $\delta^{18}O$ vs. δD diagram (Fig. 4.8) reveal that both hot and cold waters have a meteoric origin. Only the sample from Kurşunlu field (sample no. 9a) plots off the line with a relatively high $\delta^{18}O$ value, suggesting that water-rock exchange, and/or calcite scaling might be effective for that area (Süer et al., 2008).

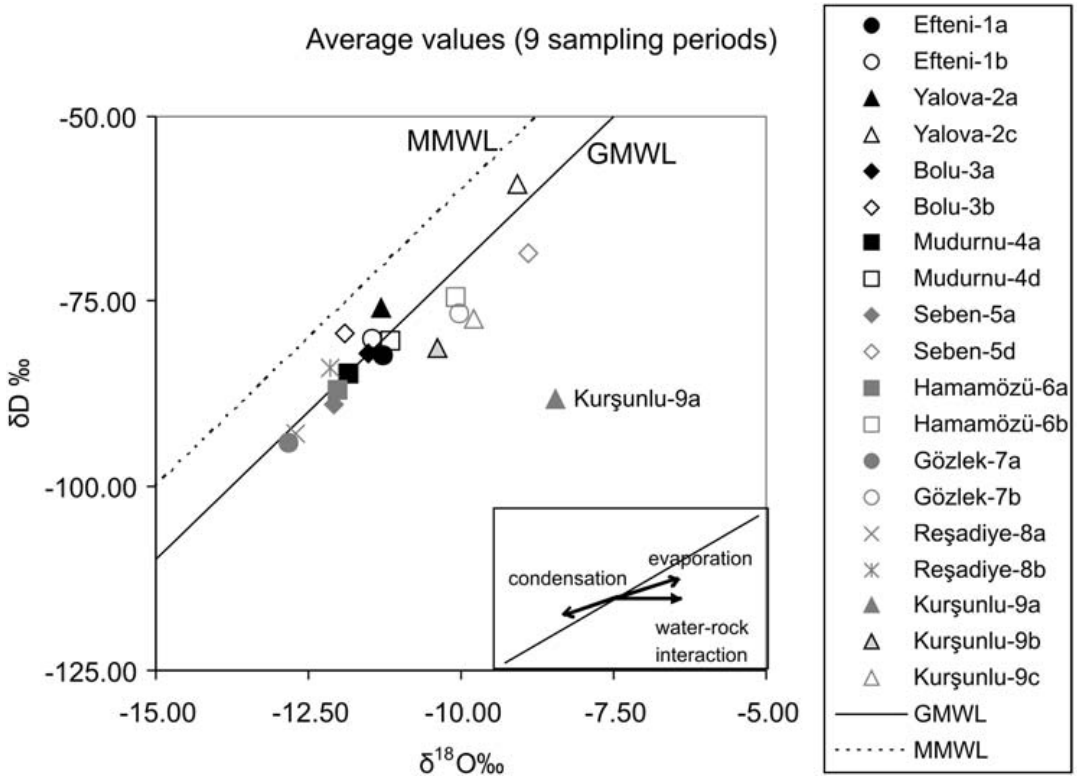

Figure 4.8: $\delta^{18}O$ vs. δD diagram of the sampled waters (data represent the average of nine sampling periods, GMWL: Global Meteoric Water Line (Craig, 1961), MMWL: Mediterranean Meteoric Water Line (Gat and Carmi, 1970) in Süer et al. (2008).

The He-CO_2 systematics of these fields seem to be under the effect of volatile degassing (phase separation) from the hydrothermal waters (de Leeuw et al., 2010) (Fig. 4.9).

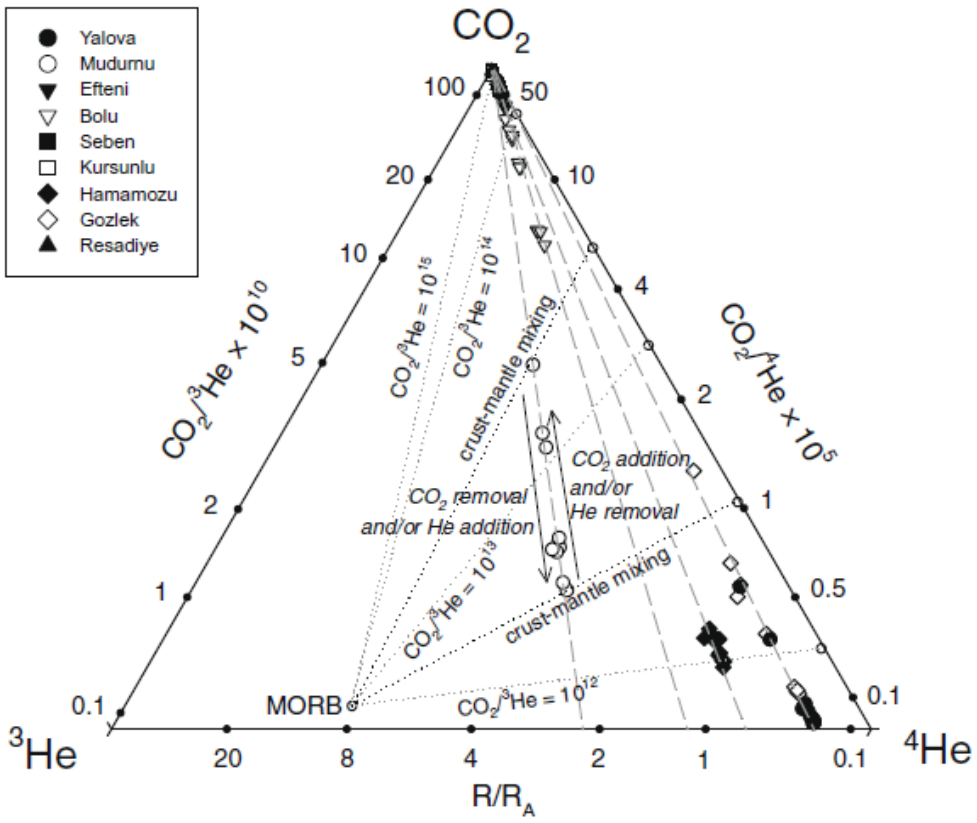

Figure 4.9: Ternary plot of CO_2–^3He–^4He for the geothermal fields along the NAFZ. Samples have been affected by two processes: (1) mixing between mantle-derived ($8R_A$, $CO_2/^3He = 2 \times 10^9$) and crustal ($0.02R_A$, $CO_2/^3He = 10^{10}$–10^{15}) volatiles, and (2) subsequent elemental fractionation between CO_2 and He. The first process is indicated by dotted lines connecting the MORB point to crustal values with $CO_2/^3He$ ratios ranging from 10^{12} to 10^{15}. Each sample location is characterized by its own specific $^3He/^4He$ ratio, resulting from the first process (volatile mixing). The second process is displayed with dashed lines that point towards/away from the CO_2 apex. All samples of the same location show variable CO_2/He ratios, and lie on the same elemental fractionation line, which is the result of phase separation (de Leeuw et al. 2010).

CHAPTER 5

HYDROGEOCHEMICAL MODELLING: PROCESSES CONTROLLING THE GEOCHEMICAL BEHAVIOUR OF THE SYSTEMS

For a successful storage of CO_2, the potential site must be evaluated thoroughly before the application of the technology. The important parameters to achieve this aim are understanding the geomechanical properties of both the reservoir and the cap-rock, as well as the geochemical reactions that take place within the system. It is crucial to comprehend how a reservoir will react to the injection of CO_2 from a geochemical point of view, such as the migration path of the gas and the water-rock interactions. With the initiation of the injection, the short-term interactions take place between the injected gas and well material, while longer-term interactions occur between the gas and the host rock and/or the cap-rock (i.e. trapping mechanisms that are explained in Chapter 2). To be able to interpret these interactions and to monitor the impact of the injection, long-term geochemical modelling is very important.

In this thesis study, various geothermal fields from western, eastern and northern Anatolia are utilized as natural analogues of CO_2 storage sites. Each field has its own characteristics; therefore, to make an efficient prediction of the potential mechanisms in the system, various geochemical approaches are undertaken. These approaches include the geochemical characterization of the system, speciation-solubility calculations, estimation of the relative contribution of carbonate and sulphate minerals to the carbon budget of the hydrothermal system, and other modelling types related to mass-balance calculations (e.g. inverse modelling, dedolomitization modelling) depending on the behaviour of the field.

For geochemical characterization of groundwaters, electrical conductivity (EC) is used as a tracer of the hydrogeochemical evolution of the system as EC is related to the amount of dissolved constituents and the temperature of water. Typically EC correlates well with TDS (Total Dissolved Solids); with increasing depth and time of circulation, water dissolves more minerals from the rocks it comes into contact with and therefore, EC increases. The geochemical characterization is essential to predict and interpret the potential mechanisms in the system by the observation of the evolution of elemental compositions.

Speciation–solubility relations are based on saturation index calculations. The saturation index (SI) is a useful quantity for the determination of whether water is saturated (in equilibrium), undersaturated, or oversaturated with respect to a particular mineral. SI values are calculated using the chemical activities of the dissolved ions of the mineral (ion activity product, IAP) and their solubility product (K_{sp}) with the equation: $SI = \log (IAP/K_{sp})$. If the result is negative ($SI < 0$) the mineral is dissolved, if positive ($SI > 0$) it is precipitated, and if zero ($SI = 0$) then the water and mineral are at chemical equilibrium. Speciation–solubility calculations are performed with the assistance of the *PHREEQC* code (Parkhurst & Appelo, 1999) and using the thermodynamic database *llnl.dat* (Lawrence Livermore National Laboratory database) distributed with the code. The reason for choosing this database over others is that it contains more mineral species and allows calculation of equilibrium conditions at a wider range of temperatures between 0-300 °C (Soong et al., 2003). The necessary inputs to the *PHREEQC* program for the speciation - solubility calculations are; temperature, pH and concentrations of dissolved elements for each sample. The Saturation Index (SI) calculations were carried out for Anhydrite, Gypsum, Aragonite, Calcite, Dolomite, and Magnesite minerals which are the major phases involved in water-rock interactions within the carbonate system. A graph is prepared with the SI of these minerals against the major anion of the related field.

Given the fact that calcium is the major common ion in the processes controlling the geothermal systems related to the trapping mechanisms, to understand the

general model of the systems, the examination of the evolution of dissolved calcium concentrations with the increasing interaction between thermal waters and minerals is crucial. In this regard, for estimation of the relative contribution of carbonate minerals' dissolution to the total dissolved calcium, the amount of calcium derived from dissolution of $CaSO_4$ minerals (gypsum or anhydrite) (as inferred from total dissolved sulphate), is subtracted from the total dissolved calcium concentrations. This procedure has been previously applied by Auqué et al. (2009) to a Spanish thermal system (the Alhama–Jaraba complex) and stands from the fact that when $CaSO_4$ dissolves, the concentration of both Ca and SO_4 increases at a one-to-one ratio.

Mass-balance calculations (inverse modelling) have also been performed with the help of *PHREEQC* code. This modelling allows the determination of the direction and magnitude of mass transfers accompanied by the potential geochemical reactions taking place between two hydraulically-connected points of a system. As inputs of modelling, the compositions assigned to initial and final solutions are those of water samples likely to represent, respectively, the least evolved (lowest EC) and the most evolved (highest EC) waters of the geothermal fields. Another parameter for inverse modelling is the determination of the mineral phases of the system to be considered as sources and sinks.

A geochemical modelling that is previously implemented by Romanak et al. (2010) using the *PHREEQC* code is dedolomitization modelling for a study of the Dockum aquifer in SACROC oil field, Texas. In this thesis study, dedolomitization modelling is performed for the geothermal fields that show indications for dedolomitization. For the modelling, a high HCO_3^- - low Ca^{2+} water sample from each of the corresponding field is used as the input for *PHREEQC*.

The geochemical approaches mentioned above have led to the recognition of three distinctive groups of geothermal fields in regard to the possible trapping mechanisms in the systems (Table 5.1).

Table 5.1: Comparison of three different groups of geothermal fields in Turkey, determined for this study

Region	Geothermal Field	*SO_4	*HCO_3	*Ca	*Mg	**Gypsum/ Anhydrite	**Calcite/ Aragonite	**Dolomite	**Magnesite	***Ca (corrected)	Groups
Western Anatolia	Kizildere	-	+	-	-	diss.	ppt	ppt	ppt	neg	Group 1
	Germencik	+	+	-	-	diss.	ppt	ppt	ppt	neg	
	Balcova	+	+	-	-	diss.	ppt	ppt	ppt	neg	
	Simav	+	+	-	const	diss.	dom. ppt	ppt	dom. ppt	neg	
	Edremit	+	-	(slight) -	(slight) -	diss.	both	both	dom.diss.	neg	Group 2
	Balikesir	+	+	(slight) +	(slight) -	diss.	equil.	dom. ppt	dom.diss.	neg	
	Dikili	const	+	-	+	diss.	dom. ppt	dom. ppt	dom.diss.	neg	
	Sindirgi	+	+	-	-	diss.	dom. ppt	dom. ppt	dom.diss.	neg	
	Emet	+	-	+	+	diss.	dom. ppt	ppt	dom.diss.	neg	
	Salihli	+	+	+	+	diss.	dom. ppt	dom. ppt	both	neg	
	Tekkehamam	+	(slight) -	-	-	diss.	dom. ppt	ppt	both	neg	
Eastern Anatolia	Caldiran	+	+	+	+	diss.	dom.diss.	dom.diss.	dom.diss.	neg	Group 3
	Diyadin	(slight) +	+	const	+	diss.	dom.diss.	dom.diss.	dom.diss.	neg	
Northern Anatolia	NAFZ	+	+	+	+	diss.	both	dom. ppt	dom.diss.	neg	

*: represent major anions-cations (having an active role in CO_2 trapping mechanisms) showing positive (+), negative (-) or constant (const.) trends with increasing EC as a measure of hydrogeochemical evolution

**: diss: dissolution, ppt: precipitation, dom: dominantly, equil: in equilibrium

***: neg: negative, indicating corrected Ca trends against domiant anion of the system (see text for further explanation)

5.1. Mineral Trapping: Group I Type Geothermal Fields

Group I consists of geothermal fields located in Kızıldere, Germencik, Balçova, and Simav. The hydrogeochemical characteristics and saturation index calculations of the fields in this group all indicate that mineral trapping due to the precipitation of carbonate minerals might be the dominant mechanism in this system. In addition to these studies, mass-balance calculations are performed for the verification of the determined mechanism.

5.1.1. Hydrogeochemical Characteristics

The hydrochemistry of the water samples taken from the fields of Group I is tabulated in Appendix-Table A.1. The variations in the concentrations of the major ions (Na, Ca, Mg, HCO_3, SO_4, and Cl) vs. electrical conductivity (EC) are displayed in Fig. 5.1.

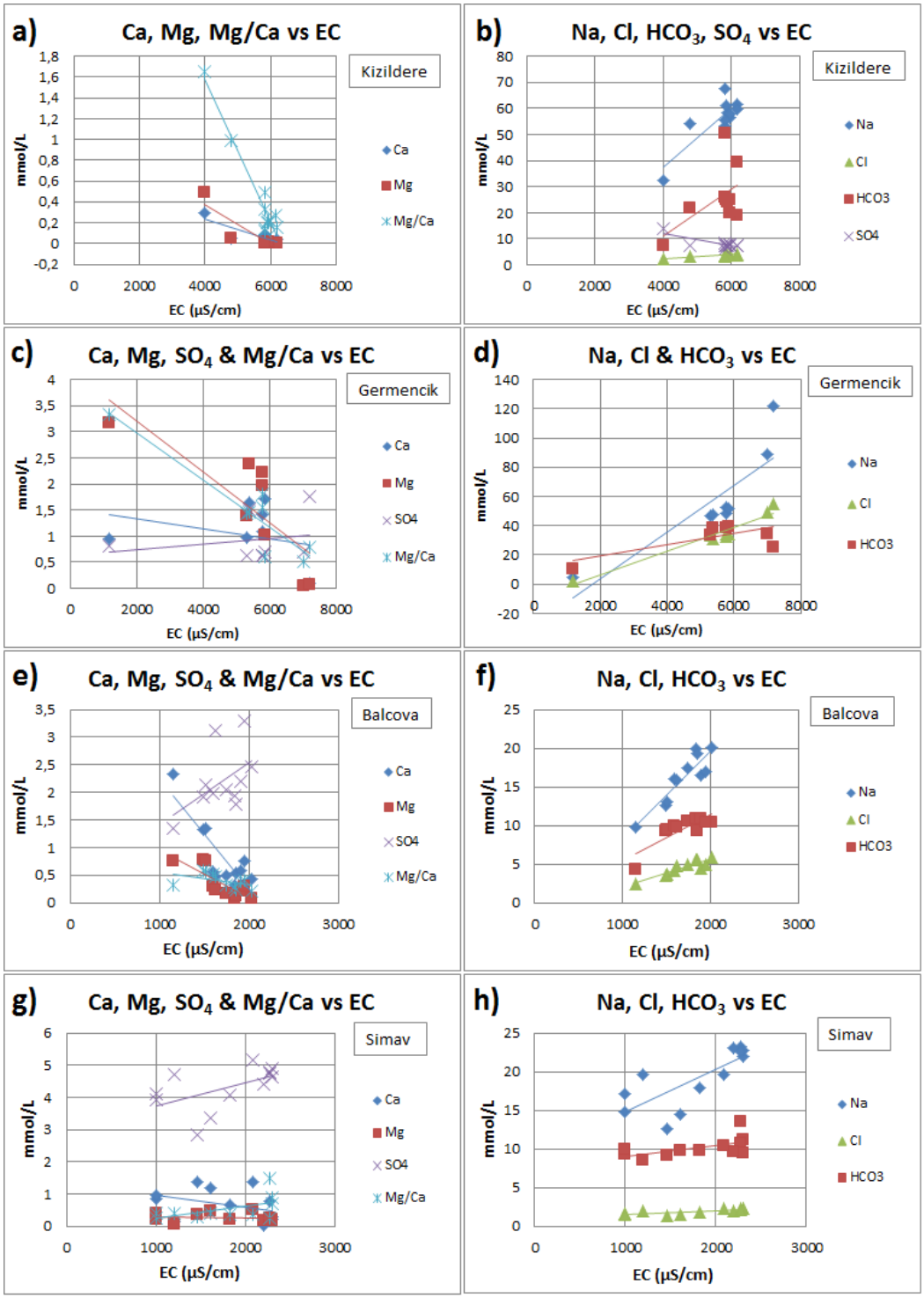

Figure 5.1: Concentration vs EC diagrams for geothermal fields of Kızıldere (a, b), Germencik (c, d), Balçova (e, f) and Simav (g, h).

The fields in Group I have similar geochemical variations characterized by decreasing Ca and Mg, while increasing Na, Cl and HCO_3 contents with increasing EC of the solutions. The SO_4 concentrations also have an increasing trend except for Kızıldere field. Mg/Ca ratio appears to have a negative trend in all fields apart from Simav. With respect to these observations (decreasing Ca and Mg with increasing EC, i.e. with progressive hydrogeochemical evolution), precipitation of Ca and Mg-bearing minerals can be anticipated in the hydrothermal system. Moreover, in Germencik, Balçova and Simav, the increasing SO_4 points to the dissolution of sulphate minerals. To strengthen these predictions, speciation – solubility calculations are carried out.

5.1.2. Speciation – Solubility Calculations

Saturation index (SI) calculations are performed for Anhydrite, Gypsum, Aragonite, Calcite, Dolomite, and Magnesite minerals for each field of Group I utilizing the *PHREEQC* code; the results are presented in Table 5.2, along with the calculated CO_2 partial pressure, and are depicted in terms of SI vs. major anion plots in Fig. 5.2.

Table 5.2: Summary of results from speciation - solubility calculations of Group I fields (spr: spring)

Geothermal Field	Sample	T(°C)	pH	log pCO_2	Saturation Index (SI)					
					Aragonite	Calcite	Dolomite	Magnesite	Gypsum	Anhydrite
Kizildere	KD-6	196	8.97	-1.56	0.88	1.03	3.22	1.22	-3.47	-2.34
	KD-13	195	8.89	-1.50	1.08	1.23	3.24	1.04	-3.04	-1.92
	KD-14	207	8.96	-1.27	0.93	1.09	3.35	1.32	-3.49	-2.30
	KD-15	205	8.82	-1.35	0.90	1.05	2.99	0.99	-3.15	-1.98
	KD-16	211	8.94	-1.40	1.37	1.52	3.59	1.13	-2.82	-1.61
	KD-20	201	8.92	-1.59	1.01	1.16	3.11	0.99	-3.05	-1.90
	KD-21	202	9.02	-1.67	1.03	1.18	3.23	1.10	-3.14	-1.99
	KD-22	202	9.3	-1.87	0.92	1.08	3.44	1.40	-3.62	-2.46
	R-1	242	8.8	-0.60	1.46	1.62	3.78	1.30	-2.93	-1.43
	TH-2	171	9.4	-2.38	1.00	1.15	4.14	1.96	-3.54	-2.57
Germencik	1	60	7.01	-0.54	0.53	0.67	2.95	0.84	-2.54	-2.40
	2	60	6.66	-0.23	0.35	0.49	2.10	0.17	-2.26	-2.11
	3	50	6.9	-0.51	0.46	0.60	2.66	0.57	-1.99	-1.94
	4	70	6.63	-0.15	0.34	0.49	2.54	0.66	-2.39	-2.16
	5	60	7.6	-1.14	1.03	1.17	3.87	1.26	-2.58	-2.44
	6	200	8.5	-0.93	1.29	1.44	4.57	2.17	-3.74	-2.59
	7	200	8.5	-1.12	1.58	1.74	4.84	2.15	-3.43	-2.28
	9	231	8.7	-1.20	1.73	1.89	5.31	2.54	-3.47	-2.15
	11	221	6.05	0.38	0.13	0.28	-0.15	-1.34	-1.29	-0.03
	12	17	7	-1.35	-0.49	-0.35	0.97	-0.36	-2.18	-2.44
Balcova	DHDNS	114	7.25	-0.96	1.06	1.21	3.40	0.98	-1.44	-0.85
	DHDNR	116	6.99	-0.72	0.80	0.95	2.83	0.68	-1.36	-0.77
	GEWR	138	6.33	-0.15	-0.29	-0.14	0.22	-0.77	-1.53	-0.78
	BD-2	129	7.77	-1.27	1.08	1.23	3.12	0.73	-2.00	-1.30
	BD-4	138	8.01	-1.45	1.42	1.56	3.63	0.94	-1.81	-1.06
	BD-5	117	7.84	-1.49	1.21	1.35	3.37	0.82	-1.88	-1.27
	B-4	86	7.38	-1.21	0.58	0.72	2.27	0.23	-1.83	-1.47
	B-5	105	7.07	-0.83	0.43	0.57	2.07	0.26	-1.77	-1.26
	B-10	92	7.05	-0.89	0.36	0.50	1.78	-0.02	-1.55	-1.14
	B-II	92	7.85	-1.66	0.93	1.07	3.05	0.68	-1.81	-1.40
	B-13	120	7.48	-1.49	1.33	1.47	3.72	1.06	-1.30	-0.67
Simav	1 (EJ-1)	163	8.74	-1.96	1.64	1.79	4.73	1.88	-2.09	-1.17
	3 (E6)	160	8.84	-2.11	1.39	1.54	4.64	2.04	-2.44	-1.54
	4 (E8)	150	9.2	-2.66	1.50	1.64	4.86	2.12	-2.59	-1.75
	5 (Eynal Spa Spr)	78	9.2	-3.20	0.45	0.60	3.34	1.39	-3.32	-3.02
	6 (E4)	98	7.07	-0.76	0.52	0.66	1.86	-0.07	-1.41	-0.95
	7 (Çitgöl well)	140	7.31	-0.84	1.33	1.48	3.36	0.76	-1.07	-0.30
	8 (Çitgöl well)	162	7.91	-1.19	1.64	1.79	3.99	1.15	-1.27	-0.36
	9 (Çitgöl Spr)	51	6.84	-0.99	-0.13	0.01	0.76	-0.74	-1.28	-1.21
	11 (Naşa well)	90	7.03	-0.91	0.50	0.64	2.04	0.10	-1.34	-0.95
	13 (Eynal Spr)	60	8.2	-2.30	0.28	0.42	1.62	-0.24	-2.30	-2.16
	14 (Çitgöl Spr)	83	7	-0.95	0.21	0.36	1.28	-0.41	-1.44	-1.10
	15 (Naşa Spr)	64	6.6	-0.74	-0.41	-0.26	0.26	-0.89	-1.44	-1.26

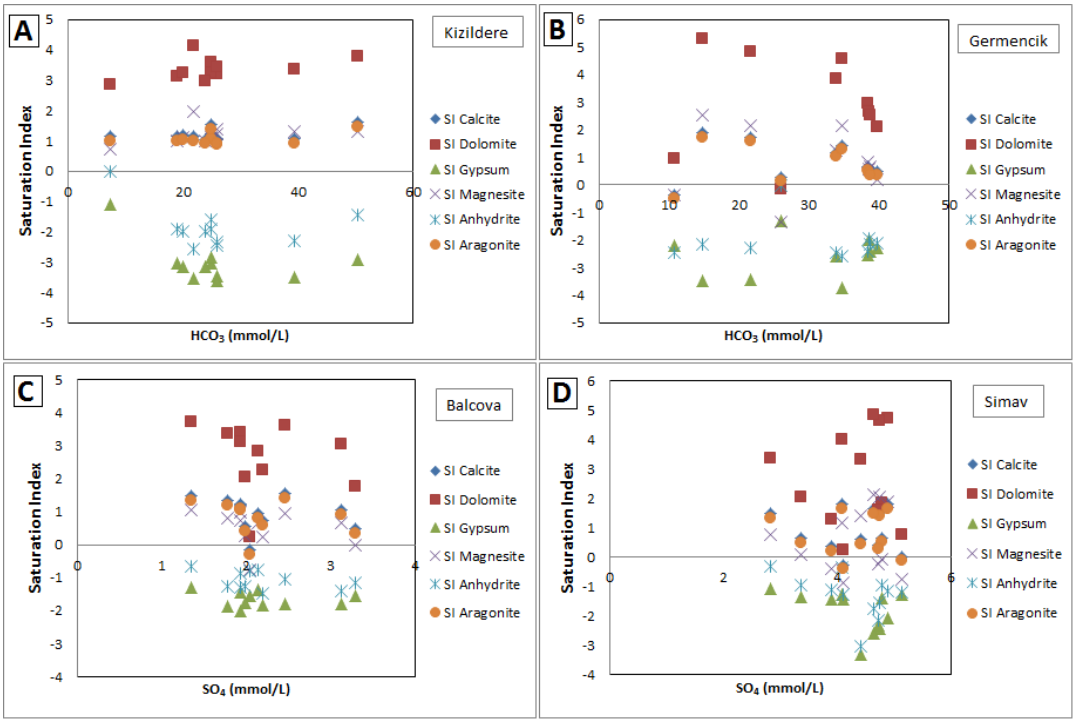

Figure 5.2: Evolution of saturation indices in the thermal waters of Kızıldere (A), Germencik (B), Balçova (C) and Simav (D) vs dominant anion concentrations

Speciation - solubility index calculations reveal that majority of waters are oversaturated with respect to carbonate minerals dolomite and magnesite, close to equilibrium or slightly oversaturated with respect to aragonite and calcite, and undersaturated with respect to sulphate minerals anhydrite and gypsum (Table 5.2, Fig. 5.2). In Simav, waters with relatively low pH are undersaturated with respect to carbonate minerals aragonite, calcite and magnesite (Fig. 5.2D). Undersaturation indicates the possibility of dissolution, and oversaturation points to the possibility of precipitation of the minerals. In this respect, anhydrite and gypsum dissolution and aragonite, calcite, dolomite and magnesite precipitation is expected in the geothermal system of these fields.

The SI results support the observations that were made regarding the hydrogeochemical character of the waters. Therefore, the depletion of Ca and Mg concentrations is attributed to the carbonate minerals' (aragonite, calcite, dolomite

and magnesite) precipitation, whereas the enrichment in SO_4 concentration suggests dissolution of sulphate minerals (anhydrite, gypsum).

For an assessment of possible relative contribution of carbonate minerals' dissolution to the total dissolved calcium, the amount of calcium derived from dissolution of $CaSO_4$ minerals (gypsum or anhydrite) (as inferred from total dissolved sulphate), is subtracted from the total dissolved calcium concentrations. The (corrected) Ca concentration estimated via this calculation is also shown in Fig. 5.3. As seen in Fig. 5.3, corrected Ca concentrations correlate negatively with SO_4. The negative trend of corrected Ca with SO_4 can be attributed to calcite and/or aragonite precipitation in parallel with gypsum and/or anhydrite dissolution. Moreover, the negative correlation between Mg and SO_4 in Balcova and Simav waters points to potential dolomite and/or magnesite precipitation in these fields along with calcite and aragonite.

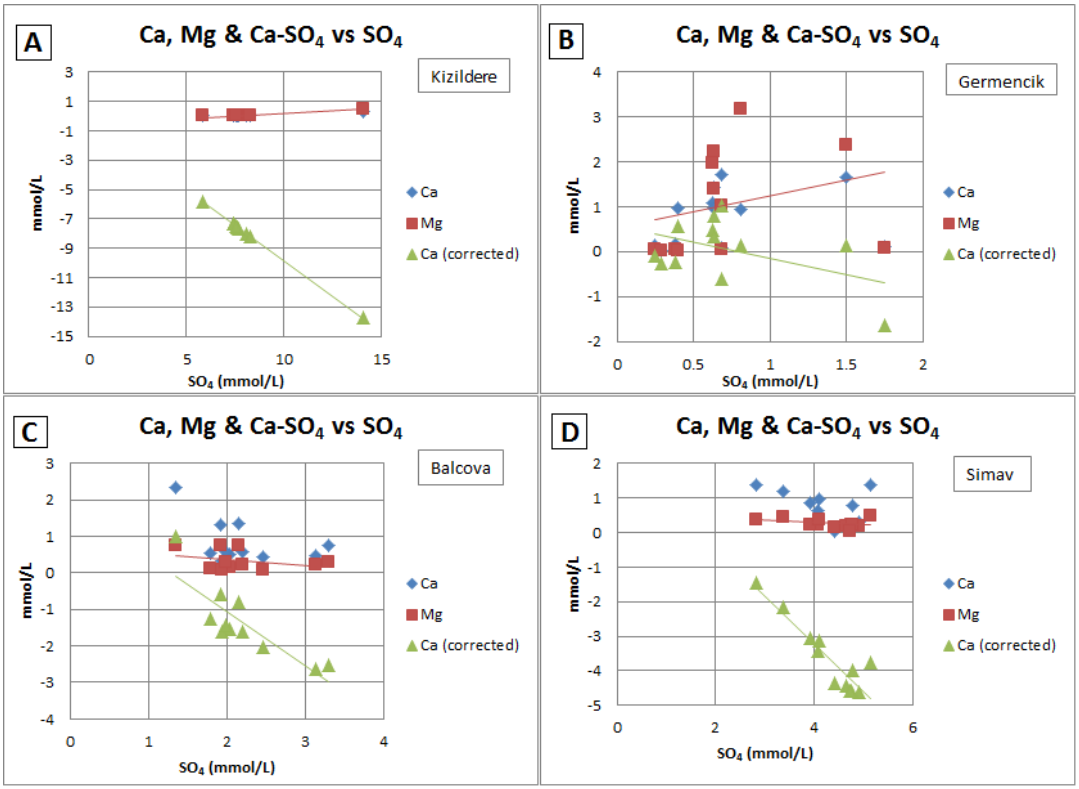

Figure 5.3: Evolution of analytic and corrected calcium concentrations and magnesium concentrations vs. total sulphate concentrations in the thermal waters of Kızıldere (A), Germencik (B), Balçova (C) and Simav (D) (see text for further explanation)

5.1.3. Mass-Balance Calculations

The investigation of hydrogeochemical patterns combined with speciation-solubility calculations lead to the identification of carbonate precipitation as the major (potential) mechanism for the trapping of CO_2 in the geothermal fields of Group I.

For a further verification of the validity of this process, mass-balance calculations (inverse modelling) have also been performed with the help of *PHREEQC* code. The least evolved (lowest EC) and the most evolved (highest EC) water samples of the geothermal fields are assigned to initial and final solutions, respectively. Furthermore, among the least and most evolved water samples, the ones with

relatively lower pH are selected in order to be able to reduce the potential degassing effects from the surface and to better represent the conditions at depth. Another parameter for inverse modelling is the determination of the mineral phases of the system to be considered as sources and sinks. The minerals that are used in saturation index calculations (such as gypsum, calcite, dolomite) are chosen for the modelling in which the dissolution of gypsum is imposed. Taking the mentioned inputs into account, mass-balance calculations are applied to Group I geothermal fields, and the results are presented in Table 5.3.

Table 5.3: Summary of results from mass-balance calculations of Group I geothermal fields

	Field	Initial Solution*	Final Solution*	Calcite mole transfer**	Dolomite mole transfer**
Mass-Balance Calculations	Kizildere	R-1	KD-13	-0.0202	-0.0001
	Germencik	3	2	1.437	-1.367
	Balcova	B-13	B-10	-0.208	-0.108
	Simav	15	1	-0.892	-0.190

*Sample numbers are given in Table A.1

**Negative mass transfer corresponds to precipitation and positive to dissolution.

Given that in mass-balance calculations, negative mass transfer values correspond to precipitation and positive values to dissolution, the results of Group I are consistent with the determined processes of dolomite ± calcite precipitation for the fields. The positive value obtained for calcite in Germencik can be inferred from the saturation index results of calcite that are close to equilibrium in Table 5.2, Fig. 5.2. Furthermore, the negative Mg/Ca ratio observed in EC diagrams of Kızıldere, Germencik and Balçova (Fig 5.1) imply that dolomite precipitation is more effective in those fields compared to calcite precipitation.

When all modelling results are considered, it is evident that in geothermal fields of Group I which includes Kızıldere, Germencik, Balçova and Simav, the precipitation of carbonate minerals is most likely the dominant mechanism in these

systems which lead to mineral trapping of CO_2 in carbonate minerals. This conclusion is also supported by the presence of scaling problem in these fields and the He-CO_2 systematics (Fig. 4.3) as reported by previous studies (Mutlu et al., 2008).

5.2. Solubility ± Mineral Trapping: Group II Type Geothermal Fields

Edremit, Balıkesir, Dikili, Sındırgı, Emet, Salihli and Tekkehamam comprise the geothermal fields of Group II. The hydrogeochemical characterization and saturation index calculations of the fields in this group point to the potential of solubility ± mineral trapping. The existence of dedolomitization seems also possible for some of the fields. Furthermore, mass-balance calculations and additional (dedolomitization) modelling are carried out for a proper interpretation of the mechanisms dominating the geothermal fields.

5.2.1. Hydrogeochemical Characteristics

The tabulated hydrochemistry of the water samples collected from the fields of Group II is given in Appendix-Table A.1. The variations in the concentrations of the major ions (Na, Ca, Mg, HCO_3, SO_4, and Cl) vs. electrical conductivity (EC) are illustrated in Fig. 5.4.

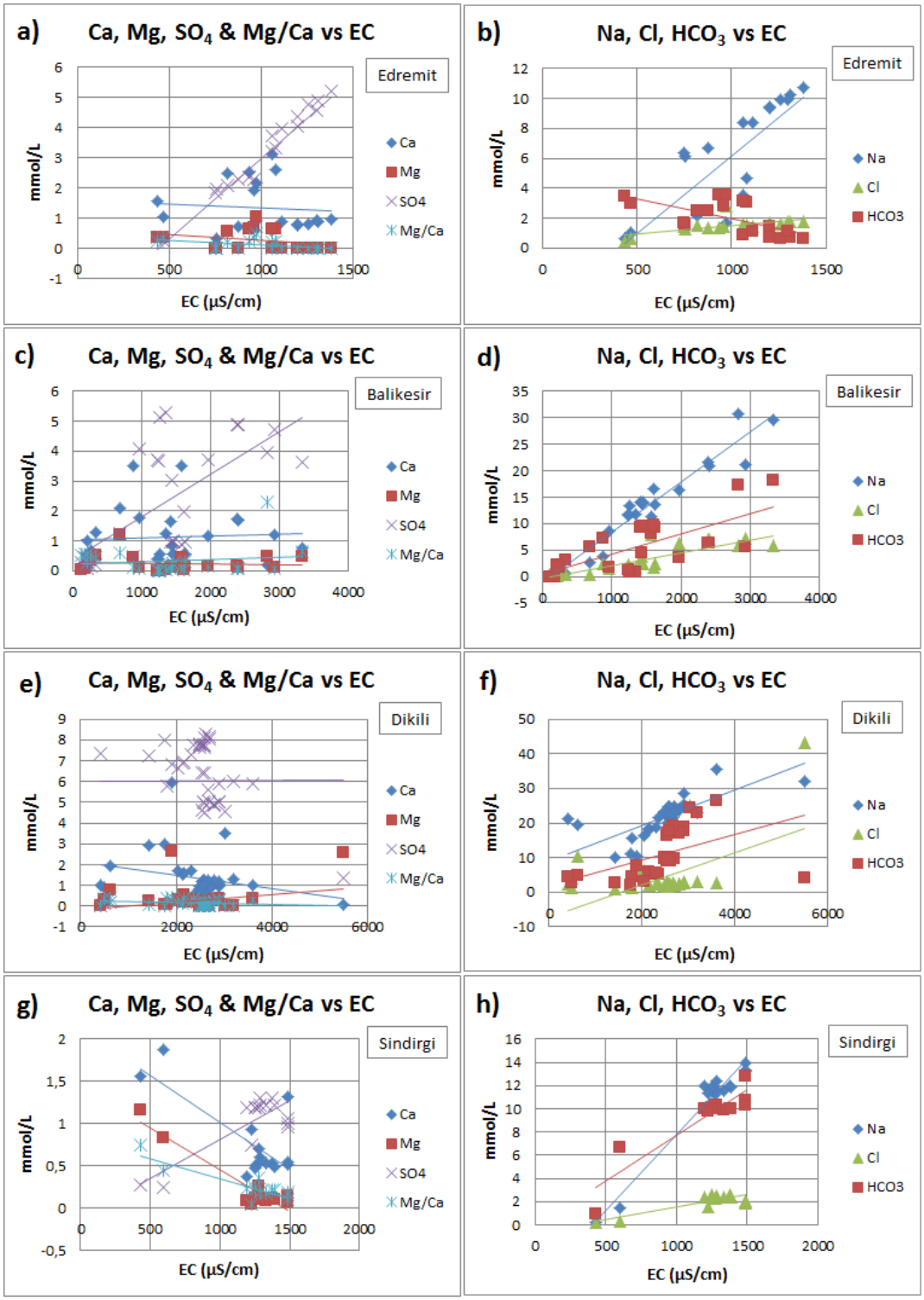

Figure 5.4: Concentration vs EC diagrams for geothermal fields of Edremit (a, b), Balikesir (c, d), Dikili (e, f) and Sindirgi (g, h).

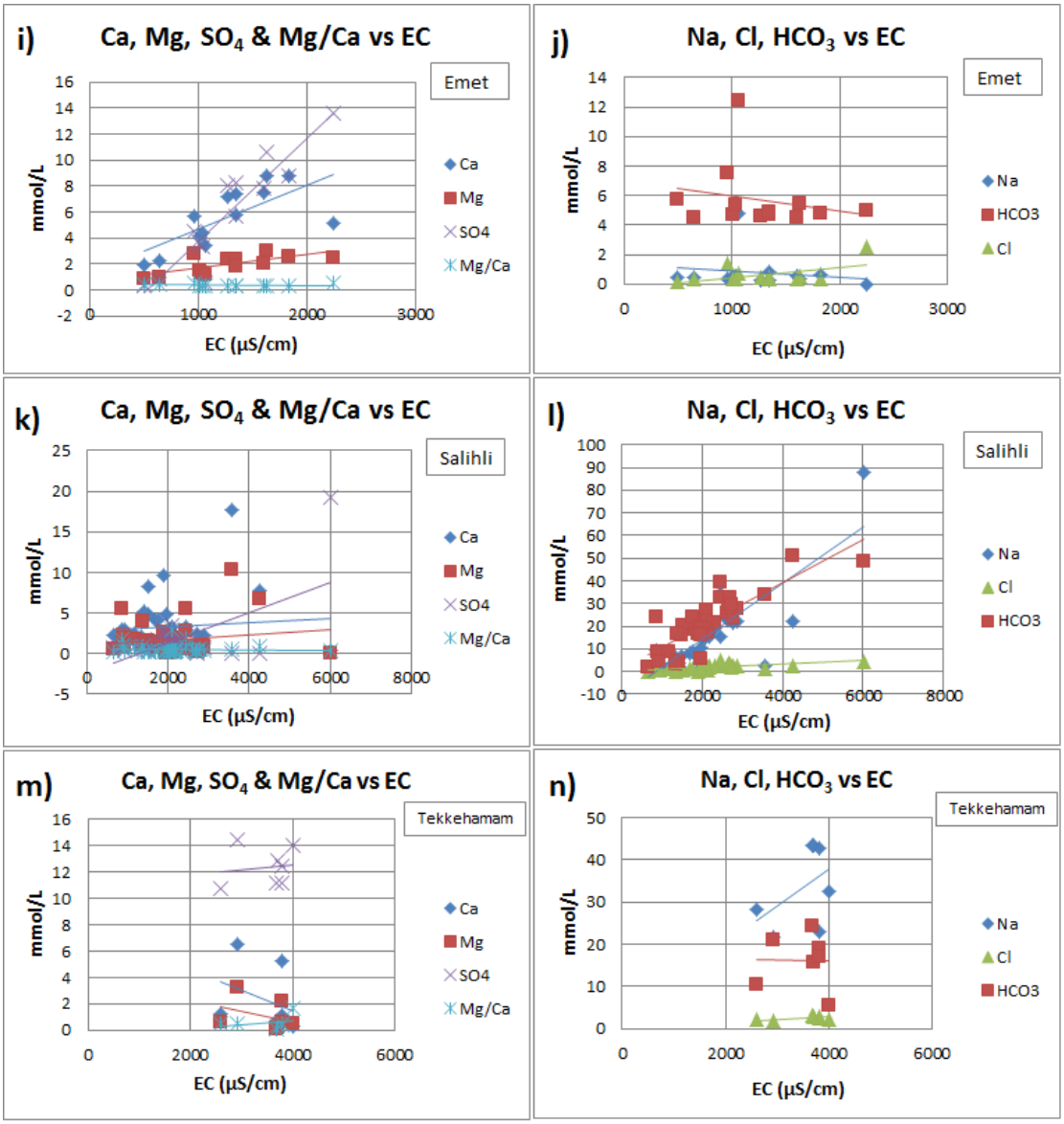

Figure 5.4 (cont'd): Concentration vs EC diagrams for geothermal fields of Emet (i, j), Salihli (k, l), Tekkehamam (m, n)

The geochemical characteristics of Group II differ slightly in each field. The common aspects of these fields are that they almost all have increasing SO_4, Na, and Cl concentrations with increasing EC (except the rather constant trend of SO_4 in Dikili and Na in Emet). When HCO_3 concentration is taken into account, in Balıkesir, Dikili, Sındırgı and Salihli fields it has an increasing trend, while in Edremit, Emet and Tekkehamam the trend is decreasing. In the case of Ca and Mg concentrations, the decreasing trend can be observed in Edremit (slightly decreases), Sındırgı and Tekkehamam, whereas in Emet and Salihli both of them increase in parallel with the increase of EC. For Balıkesir, Ca concentration slightly increases and Mg slightly decreases, contrarily for Dikili, Ca decreases and Mg increases. Except for the negative trend observed in Sındırgı, Mg/Ca ratio is almost constant in every field of Group II. Considering these examinations, the dissolution of sulphate minerals can be expected due to the increasing amount of SO_4 in all fields. On the other hand, the variations seen in HCO_3 concentrations among the fields can be explained by both dissolution and precipitation of carbonate minerals which also affect the changes in the concentrations of Ca and Mg. To be able to make more precise interpretations regarding the systems, the speciation – solubility calculations are performed.

5.2.2. Speciation – Solubility Calculations

Saturation index (SI) of Anhydrite, Gypsum, Aragonite, Calcite, Dolomite, and Magnesite minerals are calculated for each field of Group II with the aid of *PHREEQC* code. The calculation results are tabulated in Table 5.4, along with the calculated CO_2 partial pressure, and are illustrated in terms of SI vs. major anion plots in Fig. 5.5.

Table 5.4: Summary of results from speciation - solubility calculations of Group II fields (bh: borehole)

Geothermal Field	Sample	T(°C)	pH	log pCO_2	Saturation Index (SI)					
					Aragonite	Calcite	Dolomite	Magnesite	Gypsum	Anhydrite
Edremit	ED-3	62	7.76	-2.81	-0.32	-0.18	-1.09	-2.33	-1.55	-1.39
	ED-1	62	7.65	-2.82	-0.42	-0.27	-1.75	-2.90	-1.34	-1.18
	EDJ-3	59	7.65	-2.87	-0.53	-0.38	-1.93	-2.99	-1.38	-1.25
	EDJ-2	58	7.67	-2.85	-0.48	-0.34	-1.80	-2.91	-1.44	-1.31
	EDJ-5	55	7.99	-2.84	-0.16	-0.02	-0.72	-2.16	-2.03	-1.93
	DERM.	53	7.81	-2.84	-0.15	-0.01	-0.38	-1.84	-1.36	-1.28
	ENT.	51	7.95	-2.87	0.02	0.17	0.05	-1.59	-1.47	-1.41
	EDJ-7	51	7.61	-2.91	-0.63	-0.49	-2.21	-3.20	-1.32	-1.25
	EDJ-4	50	7.81	-2.85	-0.18	-0.04	-0.41	-1.86	-1.42	-1.36
	EDJ-8	43	8	-2.90	-0.69	-0.55	-1.37	-2.35	-2.49	-2.50
	YAGCI	42	8.13	-2.86	0.36	0.50	0.71	-1.32	-1.69	-1.70
	DSI-6	39	8.07	-2.75	0.84	0.98	2.54	0.02	-1.10	-1.15
	DOG.	32	8.14	-2.80	0.88	1.03	2.65	0.04	-1.23	-1.34
	DSI-9	32	8.09	-2.80	0.85	1.00	2.48	-0.10	-1.05	-1.16
	HAST.	31	8.06	-2.88	0.65	0.79	2.12	-0.26	-1.26	-1.39
	DSI-5	30	8.06	-2.83	0.57	0.72	2.16	-0.15	-1.34	-1.47
	DSI-7	21	8.14	-2.91	0.39	0.54	1.81	-0.38	-2.40	-2.62
	DSI-8	18	8.12	-2.86	0.64	0.78	2.40	-0.05	-1.76	-2.01
	EMINDSI	12	8.14	-2.92	0.47	0.62	1.73	-0.6	-2.07	-2.38
Balikesir	G-7	60.4	7.15	-1.42	0.20	0.35	0.77	-1.01	-1.19	-1.05
	G-8	57.8	7.42	-1.68	0.47	0.62	1.31	-0.75	-1.19	-1.07
	G-16	77.5	6.97	-1.19	0.03	0.17	0.43	-1.10	-1.28	-0.98
	EKS-1	42.7	7.26	-1.90	-0.08	0.06	1.00	-0.58	-2.47	-2.48
	EKS-2	18.8	4.16						-2.82	-3.06
	EKS-3	21.5	3.91						-3.27	-3.48
	MK-1	49.8	6.57	-0.90	-0.09	0.06	0.47	-1.07	-1.57	-1.51
	MK-2	34.4	6.87	-1.28	0.05	0.20	0.72	-1.05	-1.79	-1.88
	PMK-1	64.9	7.56	-2.01	0.34	0.48	1.31	-0.58	-1.38	-1.19
	PMK-2	55.5	7.34	-1.75	-0.03	0.12	0.61	-0.96	-1.60	-1.49
	BHS-1	94.6	7.29	-0.88	0.23	0.37	2.30	0.65	-2.15	-1.72
	BHS-2	82.9	6.95	-0.63	0.33	0.48	1.98	0.17	-1.65	-1.31
	SHS-1	98.5	7.01	-0.84	0.30	0.45	1.53	-0.18	-2.03	-1.56
	SHS-2	97.3	7.38	-1.20	1.13	1.28	2.78	0.23	-1.64	-1.18
	SHS-3	95.1	6.97	-0.83	0.23	0.38	1.45	-0.21	-2.05	-1.62
	SHS-4	87	6.72	-0.69	-0.15	0.00	0.78	-0.54	-2.07	-1.70
	EDR-1	57.6	7.83	-2.97	-0.11	0.04	-0.36	-1.85	-1.20	-1.08
	EDR-2	44.7	7.56	-2.44	-0.02	0.12	0.26	-1.38	-1.16	-1.16
	GDR-1	56.6	8.4	-3.54	0.10	0.25	-0.49	-2.19	-1.56	-1.45
	GDR-2	17.5	7.76	-2.68	-0.15	-0.01	0.54	-1.13	-2.96	-3.22
	BLY-1	59	8.21	-3.12	0.06	0.21	-0.42	-2.06	-1.77	-1.64
	BLY-2	58.1	8.1	-3.04	-0.10	0.04	-0.73	-2.22	-1.79	-1.66
	BLY-3	28.8	6.17	-1.47	-2.19	-2.04	-3.16	-2.72	-2.70	-2.84
	SLK-1	31.8	7.05	-1.56	-0.11	0.04	1.03	-0.59	-1.57	-1.69
	SLK-2	72.8	6.4	-0.55	-0.75	-0.60	-1.33	-2.10	-1.86	-1.60
	SLK-3	25.7	8.05	-3.02	-0.11	0.04	1.00	-0.66	-2.70	-2.88
Dikili	1-a Dikili Spa	65	7.3	-1.08	0.54	0.68	2.07	-0.02	-1.46	-1.27
	2-a Dikili Spa	40	7.3	-1.22	0.33	0.48	1.65	-0.36	-1.47	-1.51
	3-a Dikili Spa	40	7.3	-1.22	0.37	0.51	1.59	-0.46	-1.44	-1.47
	4-a Dikili Spa	66	7.1	-0.90	0.41	0.55	1.73	-0.23	-1.43	-1.24
	5-a Dikili Spa	65	7	-0.81	0.37	0.51	1.54	-0.39	-1.35	-1.16
	6-a Dikili Spa	73	7.2	-0.95	0.63	0.77	2.09	-0.06	-1.37	-1.12
	7-a Dikili Spa	34	7.4	-1.21	0.43	0.58	1.86	-0.29	-1.51	-1.60
	8-b Dikili Spa	72	6.2	-0.21	-0.58	-0.43			-1.29	-1.04

Table 5.4 (cont'd): Summary of results from speciation - solubility calculations of Group II fields (bh: borehole)

Geothermal Field	Sample	T(°C)	pH	log pCO_2	Saturation Index (SI)					
					Aragonite	Calcite	Dolomite	Magnesite	Gypsum	Anhydrite
Dikili	9-b Dikili Spa	41	6.7	-0.69	-0.26	-0.12	-0.86	-2.27	-1.34	-1.37
	10-b Dikili Spa	36	6.4	-0.59	-0.78	-0.64	-2.17	-3.10	-1.40	-1.48
	11-b Dikili Spa	65	6.8	-0.64	0.14	0.29	-0.31	-2.01	-1.38	-1.19
	12-b Dikili Spa	30	6.6	-0.61	-0.01	0.13	-0.63	-2.36	-1.07	-1.20
	13-b Near Dikili	32	7.9	-1.77	0.97	1.11			-1.36	-1.47
	15-b Plain near Dikili	24	6.7	-1.65	-1.27	-1.12	-1.52	-2.02	-2.75	-2.94
	16-b Sülüklü spr.	24	7.2	-1.82	-0.20	-0.05	0.68	-0.90	-2.53	-2.72
	18-c Agrobay-1. well	93	6.9	-1.01	0.20	0.34	0.80	-0.83	-0.99	-0.57
	19-c Agrobay-2, well	89	6.8	-1.00	0.00	0.15	0.88	-0.57	-1.00	-0.62
	21-a Kaynarca	42	8.1	-2.27	0.73	0.88	1.79	-0.62	-1.41	-1.43
	22-a Kaynarca	82	7.7	-1.61	0.80	0.95	1.39	-0.89	-1.35	-1.01
	23-a Kaynarca	48	8	-2.13	0.77	0.91	2.22	-0.18	-1.36	-1.33
	24-a Kaynarca	53	7.7	-1.81	0.56	0.70	0.87	-1.30	-1.32	-1.24
	25-a Kaynarca	80	7.8	-1.72	1.02	1.16	2.55	0.05	-1.23	-0.92
	26-a Kaynarca	74	7.4	-1.36	0.49	0.63	0.70	-1.30	-1.28	-1.02
	27-a Kaynarca	99	8.6	-2.39	1.64	1.78	3.20	0.15	-1.51	-1.04
	28-a Kaynarca	46	8.4	-2.54	1.06	1.20	2.29	-0.42	-1.46	-1.44
	29-a Kaynarca	83	7.4	-1.34	0.33	0.47	0.64	-1.17	-1.55	-1.21
	30-a Kaynarca	76	7.4	-1.36	0.55	0.69	0.89	-1.16	-1.41	-1.13
	31-b Kaynarca	88	7.4	-1.30	0.61	0.75	1.67	-0.39	-1.33	-0.95
	32-b Kaynarca	41	7.8	-2.01	0.51	0.66	1.52	-0.67	-1.28	-1.31
	33-b Kaynarca east	70	7.1	-1.13	0.16	0.30	0.71	-0.98	-1.24	-1.01
	34-b Kaynarca west	32	7.4	-1.77	0.68	0.83	2.46	0.05	-0.67	-0.79
	37-b Kaynarca, spring	79	7.6	-1.85	0.49	0.63	0.96	-1.02	-1.23	-0.92
	38-c Kaynarca well-1	67	6.9	-1.48	-0.34	-0.19	0.02	-1.19	-1.05	-0.85
	39-c Kaynarca well-3	87	8.2	-2.33	0.92	1.06	2.76	0.38	-1.49	-1.12
	40-c Kaynarca petrol	68	7	-1.29	0.04	0.19	0.76	-0.82	-1.03	-0.81
	41-a DG-1, well	98	9	-3.15	1.21	1.35	3.52	0.90	-2.06	-1.60
	42-a DG-3, well	45	7.7	-2.24	-0.93	-0.78	1.21	0.48	-3.21	-3.20
	44-c Kocaoba Spa	52	7.4	-2.20	0.09	0.23	0.07	-1.64	-0.77	-0.70
	45-b Kocaoba Spa	54	7.2	-1.89	0.03	0.17	0.40	-1.23	-0.80	-0.71
Sindirgi	H-1	96	7.79	-1.56	1.02	1.16	3.00	0.56	-2.08	-1.64
	H-2	58.2	7.51	-1.55	0.36	0.50	1.59	-0.35	-2.11	-1.98
	H-4	79.2	7.03	-0.97	0.12	0.26	1.04	-0.58	-2.03	-1.73
	H-5	85	6.59	-0.58	-0.28	-0.14	0.31	-0.88	-1.95	-1.59
	H-6	83.7	6.51	-0.52	-0.43	-0.29	-0.04	-1.09	-1.96	-1.62
	H-7	72	7.45	-1.40	0.43	0.58	1.80	-0.16	-2.13	-1.88
	H-8	96	7.43	-1.21	0.55	0.70	2.08	0.11	-2.16	-1.72
	H-9	81.3	7	-0.90	0.13	0.27	1.04	-0.57	-2.15	-1.82
	H-10	94	6.89	-0.74	0.26	0.40	1.66	-0.03	-1.89	-1.46
	H-11	55.5	7.07	-1.16	-0.17	-0.03	0.61	-0.82	-2.17	-2.07
	H-12	62	6.14	-0.36	-0.73	-0.59	-0.84	-1.68	-1.80	-1.64
	H-13	62	6.9	-0.98	0.02	0.17	0.35	-1.24	-2.04	-1.88
	H-15	95	7.46	-1.43	1.19	1.34	3.75	1.13	-2.19	-1.75
	H-16	96.6	6.8	-0.65	0.07	0.21	0.99	-0.51	-2.01	-1.56
	H-8A	95.2	7.12	-1.96	0.00	0.14	1.55	0.13	-2.19	-1.75
Emet	1	43	7.11	-1.62	0.38	0.52	1.72	-0.32	-0.67	-0.68
	2	54	7.1	-1.48	0.49	0.64	1.96	-0.14	-0.92	-0.82
	3	43	7.1	-1.61	0.27	0.41	1.56	-0.37	-0.93	-0.94
	4	38	6.9	-1.48	0.19	0.33	1.28	-0.61	-0.40	-0.46
	6	48	7	-1.49	0.03	0.18	1.24	-0.43	-1.63	-1.59
	8	46	6.47	-1.11	-0.32	-0.17	0.32	-1.01	-0.48	-0.46
	9	49	6.45	-1.07	-0.29	-0.14	0.37	-0.98	-0.46	-0.41

Table 5.4 (cont'd): Summary of results from speciation - solubility calculations of Group II fields (bh: borehole)

Geothermal Field	Sample	T(°C)	pH	log pCO_2	Saturation Index (SI)					
					Aragonite	Calcite	Dolomite	Magnesite	Gypsum	Anhydrite
Emet	11	33	7.8	-2.23	0.72	0.87	2.61	0.16	-2.16	-2.26
	12	39	6.7	-0.89	0.12	0.26	1.29	-0.52	-1.79	-1.84
	13	43	7.1	-1.61	0.19	0.33	1.47	-0.38	-0.51	-0.52
Salihli	1	55	6.53	-0.34	-0.11	0.03	1.14	-0.36	-2.28	-2.18
	2	60	6.93	-0.59	0.73	0.87	2.69	0.38	-1.94	-1.80
	3	44	6.39	-0.47	0.02	0.16	0.93	-0.75	-1.82	-1.82
	4	31	6.69	-0.73	0.52	0.66	1.83	-0.42	-1.73	-1.85
	5	42	7.31	-1.06	1.00	1.14	3.30	0.63	-1.23	-1.25
	6	55	7.43	-1.13	0.73	0.88	2.79	0.45	-2.40	-2.30
	7	29	6.35	-0.33	-0.25	-0.11	1.26	-0.23	-1.90	-2.04
	8	34	6.35	-0.21	-0.08	0.06	1.29	-0.34	-1.81	-1.90
	9	182 (bh)	8.31	-0.77	1.73	1.88	4.47	1.59	-1.84	-0.80
	10	27	6.01	-0.74	-1.37	-1.22	-1.25	-1.64	-1.63	-1.80
	11	31	6.83	-0.78	0.29	0.44	2.36	0.33	-1.97	-2.09
	12	155 (bh)	7.8	-0.64	1.99	2.14	5.36	2.14	-2.49	-1.62
	13	37	6.38	-0.10	0.45	0.6	2.39	0.24	-2.95	-3.02
	14	31.6	7.1	-1.08	0.36	0.51	1.69	-0.40	-1.63	-1.75
	15	59.3	7.6	-1.35	1.12	1.27	3.38	0.67	-1.68	-1.54
	16	41.5	6.2	-0.27	-0.21	-0.07	0.61	-0.85	-1.27	-1.30
	17	42.6	7.8	-1.66	1.33	1.48	3.68	0.67	-1.59	-1.60
	18	64.9	6.6	-0.39	0.04	0.19	1.00	-0.60	-2.48	-2.29
	19	56.3	6.7	-0.42	0.17	0.32	1.46	-0.31	-2.58	-2.47
	20	57	6.7	-0.56	0.64	0.79	2.37	0.13	-1.32	-1.21
	21	55	7.3	-1.08	0.93	1.08	2.93	0.39	-1.58	-1.48
	22	51.1	7.7	-1.56	1.21	1.36	3.50	0.66	-1.67	-1.60
	23	63.5	7.7	-1.38	1.33	1.48	3.77	0.87	-1.70	-1.53
	24	63.2	6.6	-0.39	-0.75	-0.60	0.58	-0.24	-2.98	-2.81
	25	35.1	7.3	-1.24	0.70	0.85	2.39	-0.03	-1.57	-1.65
	26	52	6.7	-0.43	0.45	0.60	2.07	0	-2.71	-2.64
	27	43	6.3	-0.49	-0.12	0.03	0.62	-0.93	-1.53	-1.54
	28	22	4.9	-0.05	-2.17	-2.02	-3.09	-2.71	-2.64	-2.85
	29	26	6.7	-0.87	0.40	0.54	1.69	-0.47	-0.81	-0.99
	30	54	7.5	-1.80	-0.34	-0.19	0.51	-0.77	-2.31	-2.22
	31	36.3	7.8	-1.78	-0.05	0.09	1.00	-0.65	-2.58	-2.65
	32	29.8	5.9	-0.68	-1.40	-1.26	-1.49	-1.83	-1.98	-2.11
	33	31.1	6.7	-0.82	0.22	0.37	1.86	-0.10	-1.48	-1.60
	34	27.5	7.1	-1.44	0.13	0.28	1.58	-0.31	-1.66	-1.81
	35	23.6	6.1	-1.14	-1.26	-1.12	-1.60	-2.11	-1.56	-1.75
	36	23.7	7.8	-2.80	0.18	0.32	1.17	-0.78	-1.63	-1.83
	37	28	8	-2.58	0.88	1.03	2.75	0.11	-1.58	-1.73
	38	26.8	7.5	-2.24	0.09	0.24	1.38	-0.47	-1.56	-1.72
Tekkehamam	TH-1	116	7.71	-1.63	0.40	0.55	2.15	0.40	-1.50	-0.90
	3	98	6.7	-0.58	0.08	0.22	1.14	-0.35	-1.00	-0.54
	4	99	7.6	-1.19	0.67	0.82	2.19	0.11	-1.55	-1.08
	5	60	7.9	-1.70	1.76	1.90	4.60	1.26	-0.63	-0.49
	6	72	7.7	-1.45	0.97	1.12	3.11	0.61	-1.21	-0.96
	7	55.5	6.45	-0.63	-0.16	-0.01	0.55	-0.89	-0.49	-0.39
	8	61.5	6.2	-0.20	0.00	0.14	1.10	-0.47	-0.41	-0.26
	9	73.5	7.1	-0.72	0.36	0.51	0.86	-1.02	-1.39	-1.13

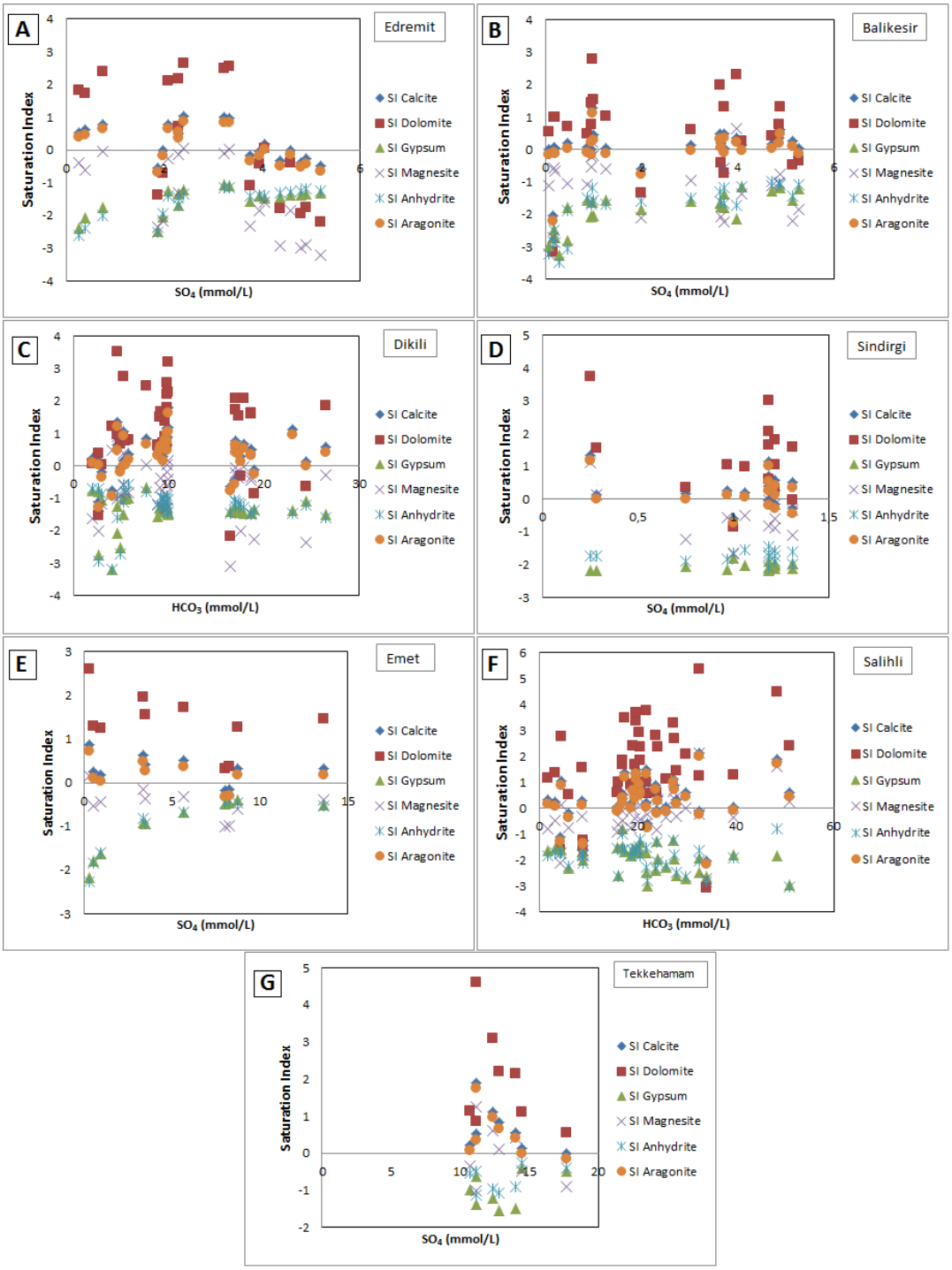

Figure 5.5: Evolution of saturation indices in the thermal waters of Edremit (A), Balıkesir (B), Dikili (C), Sındırgı (D), Emet (E), Salihli (F) and Tekkehamam (G) vs dominant anion concentrations

According to the SI calculations, most of the waters in Group II fields are undersaturated with respect to anhydrite, gypsum and magnesite, close to equilibrium or slightly oversaturated with respect to aragonite and calcite, and mostly oversaturated with respect to dolomite (Table 5.4, Fig. 5.5.). Since undersaturation points to the possibility of dissolution, and oversaturation implies the possibility of precipitation of the minerals, it can be said that anhydrite, gypsum and magnesite dissolution and aragonite, calcite, and dolomite precipitation is expected in these fields.

When the fields of Group II are examined in detail, it is observed that SI values of carbonate minerals mostly fall into both areas of the SI diagrams. For instance in Edremit (Fig. 5.5A), aragonite, calcite, dolomite and magnesite all have both positive and negative SI values that suggest dissolution and precipitation would take place for those carbonate minerals. In fact, the variations of Ca, Mg, HCO_3 seen in hydrogeochemical investigations in Fig. 5.4 can be explained with the variant mineral dynamics suggested by the SI results. In other words, if a decrease in HCO_3, Ca and/or Mg concentration is observed, the precipitation of the related carbonate mineral is effective in that field rather than dissolution. In the case of sulphate minerals, the increase in SO_4 concentration (Fig. 5.4) is in favour of the SI index results which imply the dissolution of SO_4-bearing minerals. In brief, the results of speciation - solubility calculations are consistent with the hydrogeochemical characteristics of Group II fields.

Given that the dissolution of Ca- and/or Mg-bearing minerals (dominantly sulphate and, to a lesser extent, carbonate minerals) is an effective hydrothermal process in Group II geothermal fields, the relative contribution of carbonate minerals' dissolution to the total dissolved calcium is estimated. As applied for Group I fields, the amount of calcium derived from dissolution of $CaSO_4$ minerals (gypsum or anhydrite) (as inferred from total dissolved sulphate), is subtracted from the total dissolved calcium concentrations. The (corrected) Ca concentration estimated via this calculation is also shown in Fig. 5.6. It can be observed that corrected Ca concentrations correlate negatively with SO_4. The negative trend of corrected Ca

with SO_4 indeed suggests that the dissolution is largely governed by sulphate (rather than carbonate) minerals. This trend can also be an indication of calcite and/or aragonite precipitation in parallel with gypsum and/or anhydrite dissolution. Moreover, the negative correlation between Mg and SO_4 in Edremit, Dikili, Sındırgı and Salihli waters suggests potential dolomite and/or magnesite precipitation, while the positive trend of Mg in Emet and Tekkehamam indicates the possibility of dolomite and/or magnesite dissolution in these fields along with calcite and aragonite precipitation. The almost constant trend of Mg in Balikesir points to the fact that both dissolution and precipitation can take place similar to the SI results of Balikesir in Fig. 5.5B.

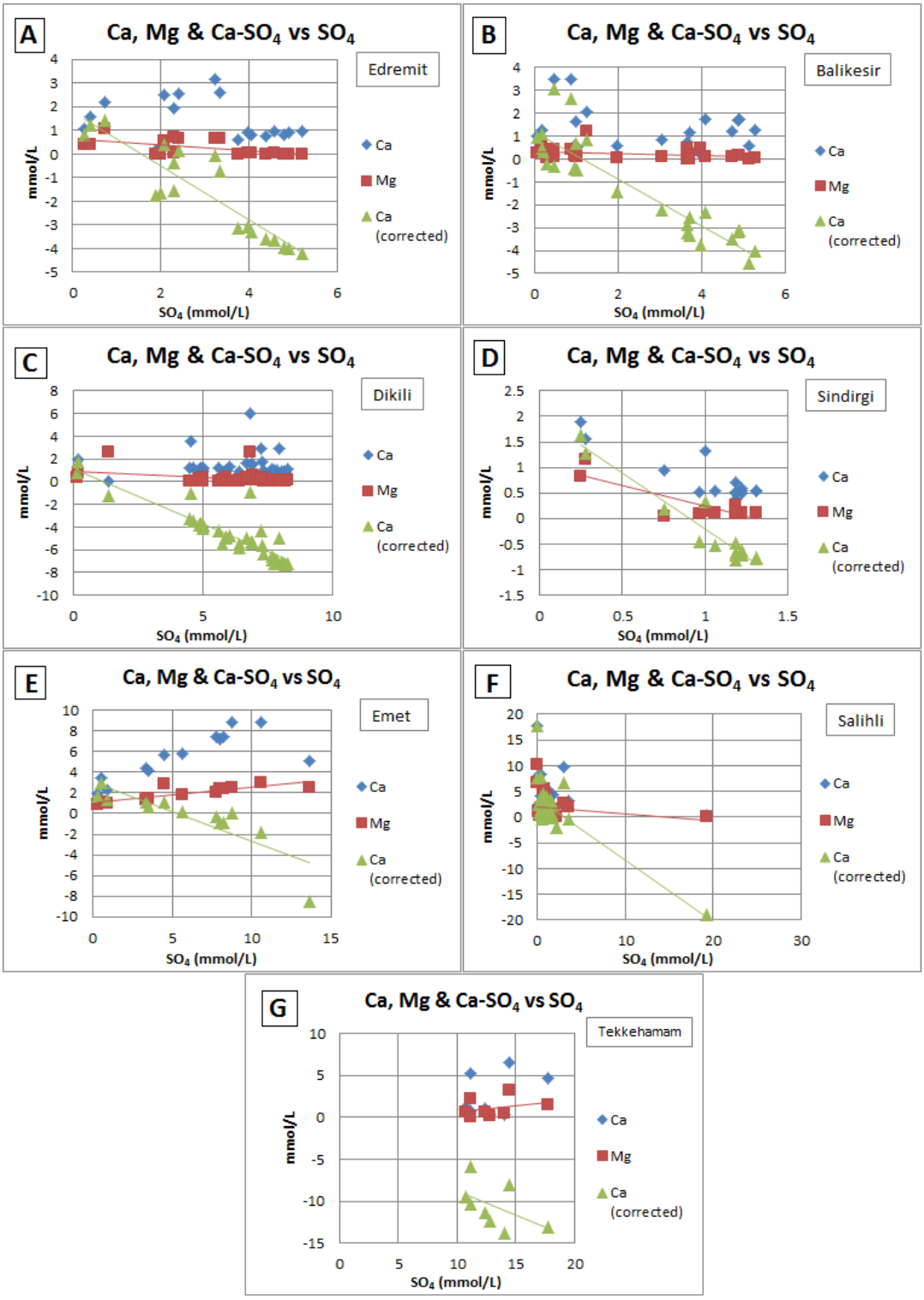

Figure 5.6: Evolution of analytic and corrected calcium concentrations and magnesium concentrations vs. total sulphate concentrations in the thermal waters of Edremit (A), Balıkesir (B), Dikili (C), Sındırgı (D), Emet (E), Salihli (F) and Tekkehamam (G).

It follows from the above discussion that dolomite and magnesite have characteristics for both dissolution and precipitation in Group II systems. Furthermore, Table 5.4 and Fig. 5.5 reveal that dolomite is likely to be precipitated and magnesite is prone to be dissolved; the relative contribution of these minerals to the system is investigated in Fig. 5.7 with calculations similar to the Ca correction calculations.

Initially, the distinction of chemical formulas between dolomite ($CaMg(CO_3)_2$) and magnesite ($MgCO_3$) is considered to be able to calculate the relative contribution of each mineral. Given that magnesium is the common element of these carbonate minerals, the calcium assumed to be derived from the dissolution of dolomite is subtracted from the total magnesium content of the system. It is important to note here that the calcium content used in these calculations is the corrected Ca (mentioned above) which represents the contribution from carbonate (and eliminates the contribution from sulphate) dissolution. The (corrected) Mg concentrations estimated with this calculation, which are shown in Fig. 5.7, have positive trend with increasing SO_4 in all the fields of Group II. This positive trend can be interpreted as the dissolution of magnesite and precipitation of dolomite which justify the SI results.

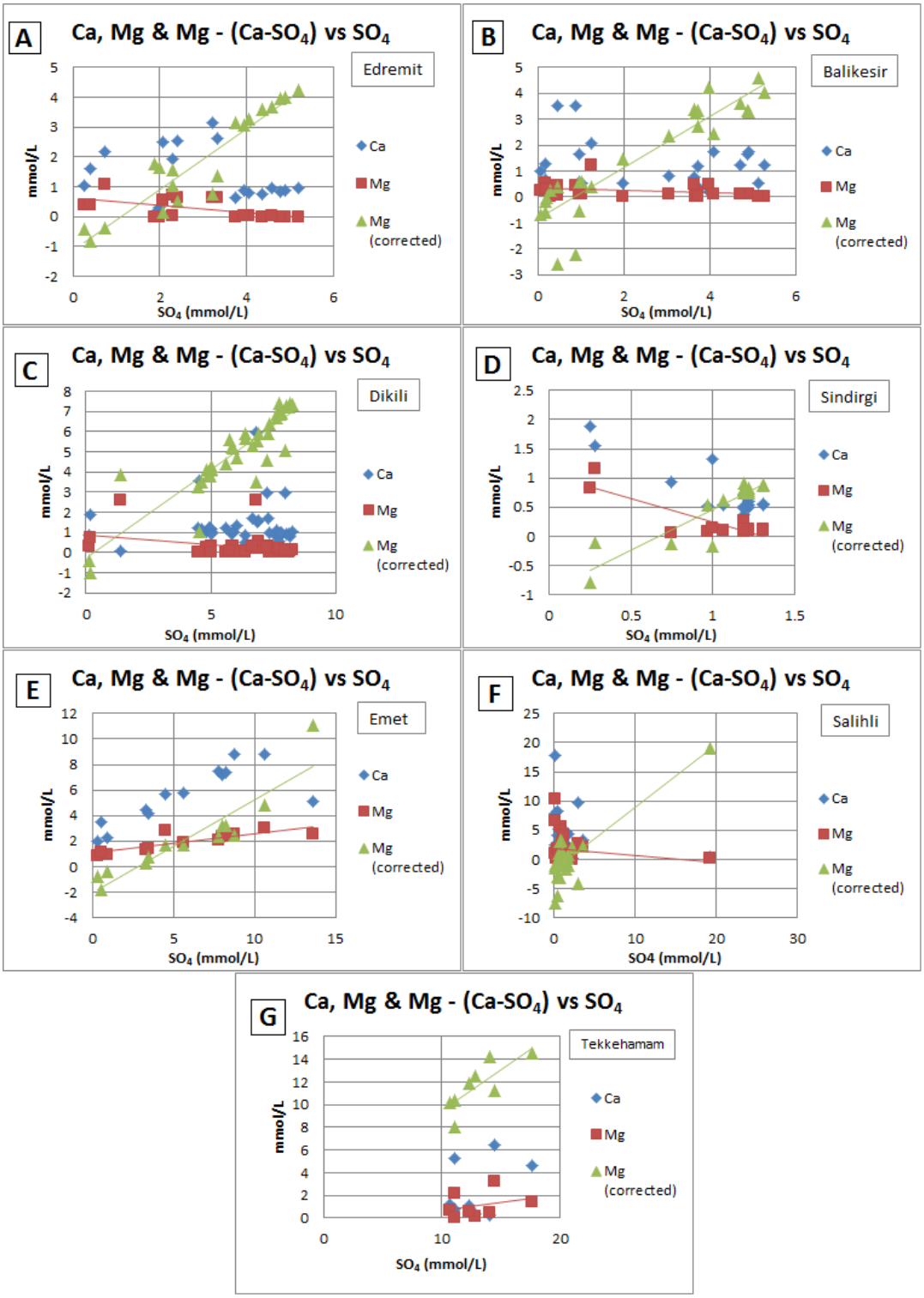

Figure 5.7: Evolution of analytic and corrected magnesium and calcium concentrations vs. total sulfate concentrations in the thermal waters of Edremit (A), Balıkesir (B), Dikili (C), Sındırgı (D), Emet (E), Salihli (F) and Tekkehamam (G) (see text for further explanation)

5.2.3. Mass – Balance Calculations

In the geothermal fields of Group II, the examination of hydrogeochemical characteristics and speciation-solubility calculations show that both dissolution and mineral precipitation might be controlling the trapping of CO_2 in the system.

For a further verification, mass-balance calculations (inverse modelling) have also been performed with the help of *PHREEQC* code for Group II geothermal fields, and the modelling results are tabulated in Table 5.5.

Table 5.5: Summary of results from mass-balance calculations of Group II geothermal fields

	Field	Initial Solution*	Final Solution*	Calcite mole transfer**	Dolomite mole transfer**
Mass-Balance Calculations	Edremit	EDJ-5	DERM	-0.499	0.030
	Balikesir	BLY-3	BHS-2	-0.279	0.772
	Dikili	15	7	0.0205	0.545
	Sindirgi	H-8A	H-12	0.689	-0.314
	Emet	11	13	-3.747	1.631
	Salihli	11	13	3.327	1.134
	Tekkehamam	8	TH-1	-2.380	-1.552

*Sample numbers are given in Table A.1

**Negative mass transfer corresponds to precipitation and positive to dissolution.

Since negative mass transfer values corresponds to precipitation and positive values to dissolution in mass-balance calculations, the results of Group II are consistent with the SI index results which suggest both dissolution and precipitation can be present for calcite and dolomite in the fields.

A striking feature of inverse modelling results in Table 5.5 is that in Edremit, Balıkesir and Emet fields calcite precipitation seems to be accompanied by dolomite dissolution which is an important sign for a possible occurrence, in the concerned fields, of dedolomitization process (dissolution of dolomite and precipitation of calcite induced by input of calcium ions through gypsum

dissolution). In this respect, when hydrogeochemical characteristics of Edremit, Balıkesir and Emet fields are re-examined, the EC diagrams (in Fig. 5.4) reveal an almost constant Mg/Ca ratio which is an indicator for the possibility of dedolomitization (referring to the equilibrium with both calcite and dolomite as explained in Chapter 2). In Edremit and Emet, the decreasing HCO_3 concentration is indirect evidence that the mass of precipitated calcite is larger than that of dissolved dolomite (see Chapter 2). In the saturation index plot of Edremit and Balıkesir (Fig. 5.5) samples fall into the areas of both undersaturation and oversaturation with respect to calcite and dolomite supporting the potential for dedolomitization. On the other hand, in Emet, the samples are close to the equilibrium with respect to calcite and aragonite, even though they seem to be oversaturated with dolomite, and given the fact that the continuous addition of CO_2 to the system lowers the saturation index values of carbonate minerals (especially dolomite) as shown in Fig. 5.8, the existence of dedolomitization process in this system is possible. Moreover, corrected Ca trends shown in Fig. 5.6 suggest calcite and/or aragonite precipitation in parallel with gypsum and/or anhydrite dissolution in all three fields, accompanied by dolomite and/or magnesite dissolution in Emet as inferred from the positive Mg trend. Another indicator for the dedolomitization process for Emet field is the Calcite/Dolomite ratio calculated during the inverse modelling. This ratio is around 2 (calcite mole transfer/dolomite mole transfer = 2.3, in Table 5.5) which is the ratio considered for the stoichiometry of the overall dedolomitization reaction meaning that for every dissolved dolomite 2 calcite minerals precipitate (see Chapter 2 and equation 5.1 in the following section 5.2.4). All these observations suggest dedolomitization as a potential process in those fields.

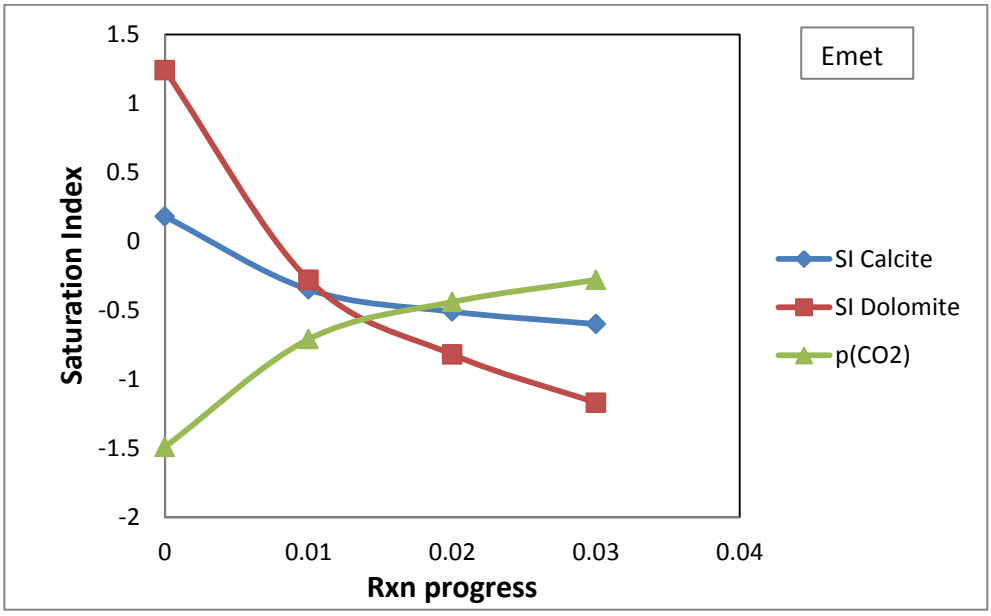

Figure 5.8: PHREEQC simulations of a less evolved Emet sample (sample no.6) water reacting with added CO_2 and gypsum (0.01 moles of each are added in 3 steps). The initial points are the calculated SI values of the sample. Previously applied by Keating et al. (2010).

5.2.4. Modelling Dedolomitization

As previously explained in Chapter 2, the main driving force in systems dominated by dedolomitization is not the addition of CO_2 but of calcium ions. Dissolution of gypsum or anhydrite within a carbonate aquifer is commonly the source for calcium ions inducing dedolomitization. The dedolomitization process triggered by the input of Ca^{2+} ions follows the below reaction

$$Ca^{2+} + CaMg(CO_3)_2 \leftrightarrow Mg^{2+} + 2CaCO_3 \quad \ldots\ldots\ldots\ldots\ldots\ldots \quad (5.1)$$

and creates a carbonate environment different than that caused by calcite dissolution:

$$CO_{2\,(aq)} + H_2O + CaCO_3 \leftrightarrow Ca^{2+} + 2HCO_3^- \quad \ldots\ldots\ldots\ldots\ldots\ldots \quad (5.2)$$

In order to distinguish the effects of CO_2 in systems dominated by dedolomitization from those dominated by calcite dissolution, Romanak et al. (2010) have

previously implemented a geochemical modelling using the *PHREEQC* code for a study of the Dockum aquifer in SACROC oil field, Texas. In this thesis study, this dedolomitization modelling is performed for the geothermal fields of Edremit, Balikesir and Emet due to the possibility of dedolomitization in these systems (Fig. 5.9).

For the modelling, a high HCO_3^- - low Ca^{2+} water sample from each of the corresponding field is used as the input for *PHREEQC* (the samples used in this study are YAGCI for Edremit, BHS-1 for Balıkesir and 11 for Emet). Then, to be able to construct the geochemical trends of dedolomitization, 30 mmoles of $CaSO_4$ is added to the solution in each step for a total of 30 steps in equilibrium with calcite and dolomite at various values of fixed partial pressure of CO_2 (P_{CO2}) (Fig. 5.9). The P_{CO2} values used in the model is within the range of those obtained from speciation-solubility calculations (Table 5.4) and also within the normal range for aquifers (~10^{-3} to 10^{-1} (Clark & Fritz, 1997)). Calcite dissolution is also modelled using the information from equation 5.2 which is the production of 1 mole of Ca^{2+} and 2 moles of HCO_3^- leading to a trendline with a slope of 0,5 on a chart of Ca^{2+} versus HCO_3^- (Fig. 5.9).

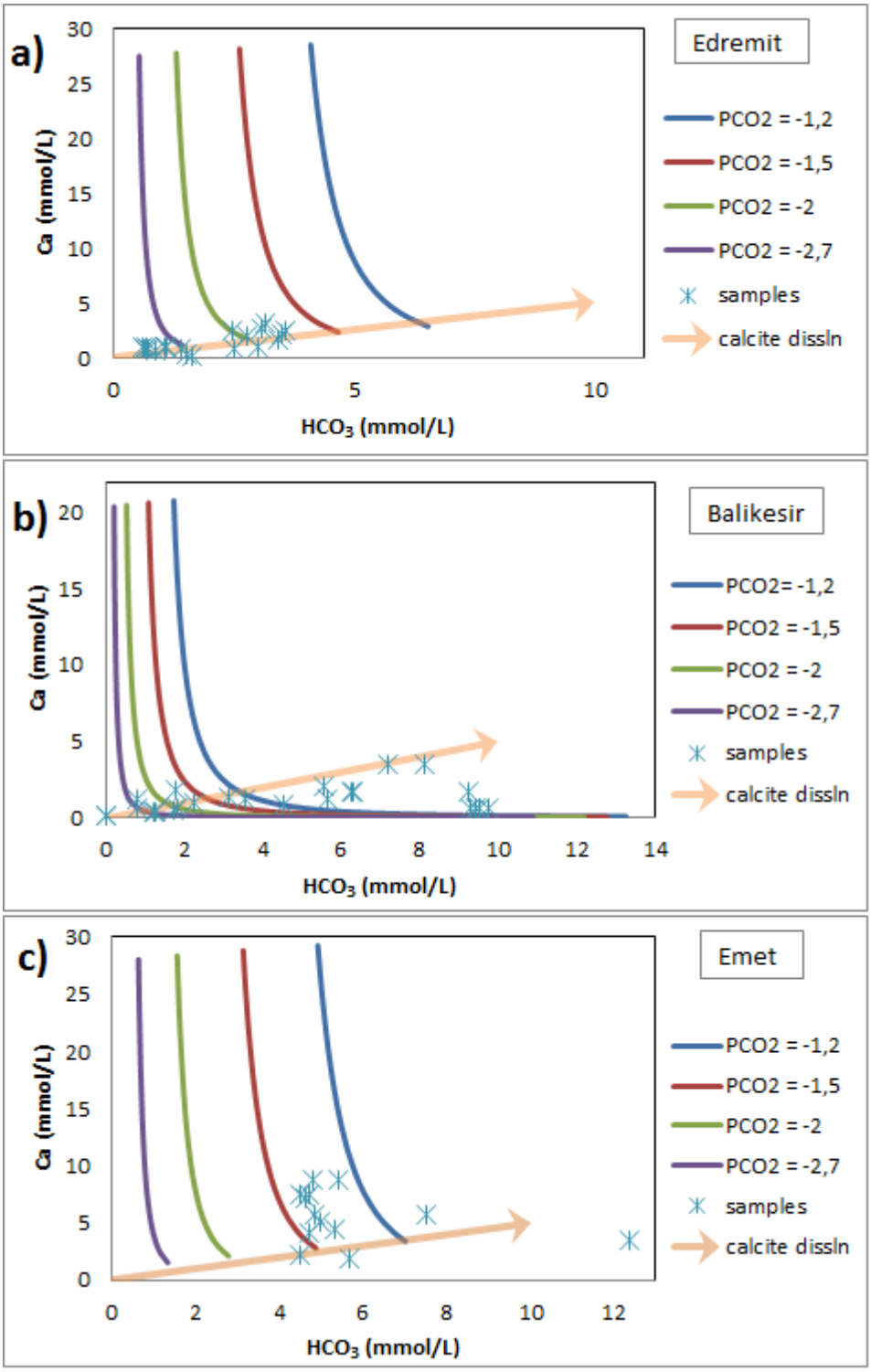

Figure 5.9: Modelling of dedolomitization and calcite dissolution for the geothermal fields of a) Edremit, b) Balikesir, c) Emet. Trends are modelled for different conditions of fixed PCO_2 at $10^{-1,2}$, $10^{-1,5}$, 10^{-2} and $10^{-2,7}$ as shown.

The results of the modelling show two different scenarios for the fields. While the water samples from Edremit and Balıkesir follow the trend for calcite dissolution, the samples from Emet mostly fall within the trends for dedolomitization. These outcomes indicate that the most likely process for Edremit and Balıkesir is calcite dissolution rather than dedolomitization; on the other hand, the hypothesis of the existence of dedolomitization for Emet is acceptable.

Regarding dedolomitization for Emet, if the model is further evaluated, it is observed that the dissolved HCO_3^- concentration decreases in the early stages of reaction since it is consumed during calcite precipitation process. As calcite precipitation proceeds, HCO_3^- concentration in the initial solution is used up and dedolomitization process starts to be the main supply of HCO_3^- for calcite precipitation. Even though Ca^{2+} is also consumed during the calcite precipitation process, due to the constant addition of $CaSO_4$ to the system, its concentration slightly increases.

When all the investigations are taken into consideration, it can be said that the trapping mechanism for Group II geothermal fields (Edremit, Balıkesir, Dikili, Sındırgı, Emet and Tekkehamam) is a combination of solubility and mineral trapping of CO_2. The He-CO_2 systematics of these fields (Mutlu et al., 2008) also suggest both precipitation and dissolution of carbonate minerals (Fig. 4.3). Additionally, in Emet, a special trapping mechanism is likely to occur, namely dedolomitization which is one of the most desirable methods for the storage of CO_2. The presence of gypsum bands in the Neogene lacustrine sediments in Emet is in support of the likelihood of dedolomitization in this field.

5.3. Solubility Trapping: Group III Type Geothermal Fields

Group III comprises the geothermal fields which have distinctive hydrogeological features leading them to be identified as a separate group. These are Çaldıran and Diyadin from eastern Anatolia, and the fields along the North Anatolian Fault Zone (NAFZ) which, from west to east, are Yalova, Efteni, Bolu**,** Mudurnu, Seben,

Kurşunlu, Hamamözü, Gözlek and Reşadiye. The hydrogeochemical characteristics, saturation index calculations and inverse modelling of the fields in this group suggest solubility trapping as the most effective mechanism in these systems.

5.3.1. Hydrogeochemical Characteristics

The table for hydrochemistry of the water samples taken from the fields of Group III is presented in Appendix-Tables A.3 and A.5. The variations in the concentrations of the major ions (Na, Ca, Mg, HCO_3, SO_4, and Cl) vs. electrical conductivity (EC) are shown in Fig. 5.10.

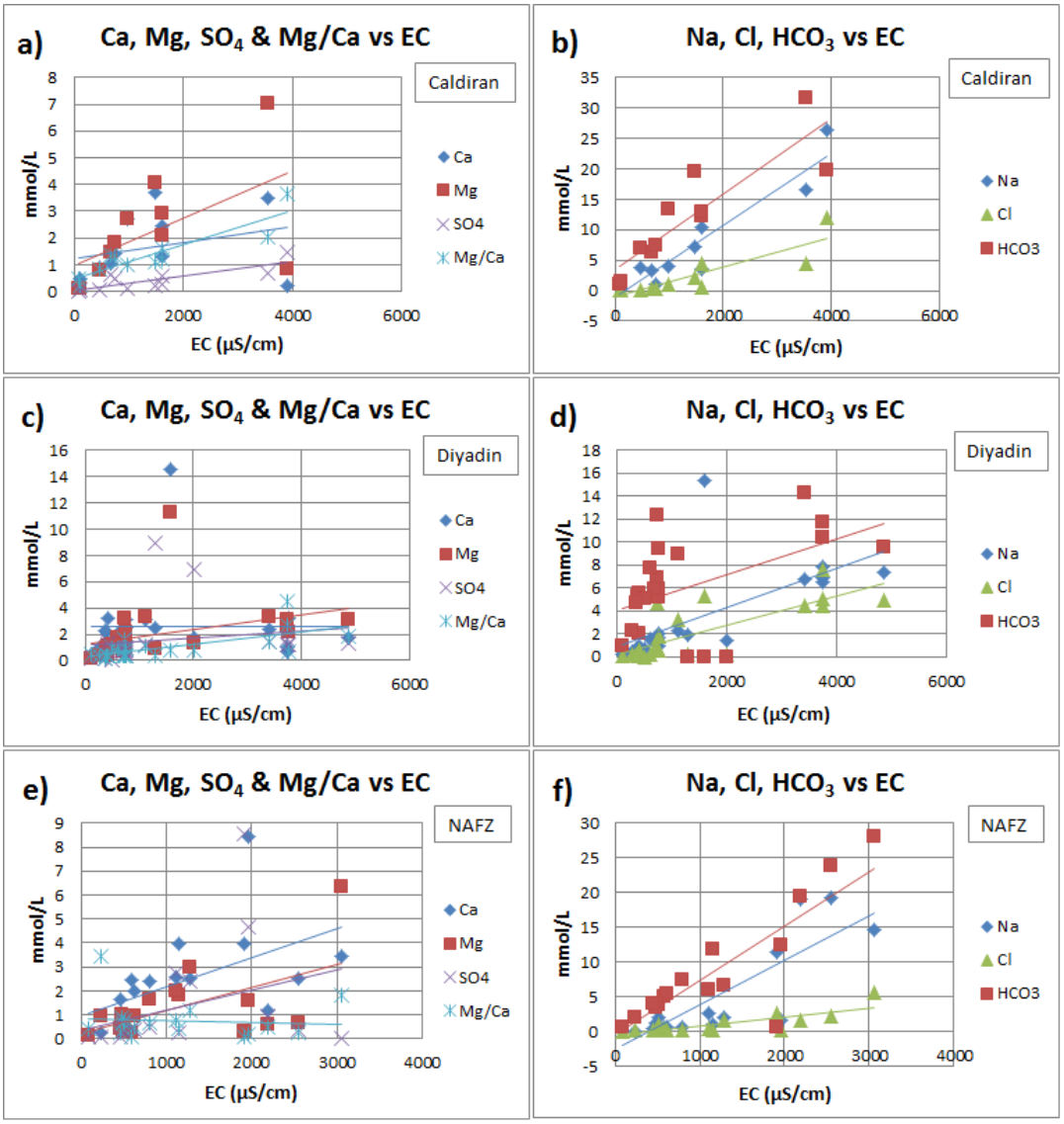

Figure 5.10: Concentration vs EC diagrams for geothermal fields of Çaldıran (a, b), Diyadin (c, d), NAFZ (e, f).

From Fig. 5.10, it is observed that the geothermal fields of Group III have very similar hydrogeochemical characteristics. Except Ca in Diyadin which is constant, all of the ions have increasing trends with increasing EC in all fields. Mg/Ca ratio remains constant in NAFZ geothermal fields and increases in Çaldıran and Diyadin. These examinations lead to the assumption that the rate of dissolution of the minerals is higher than that of their precipitation which results in the increase in the concentrations. For further analysis of the systems, speciation – solubility calculations are studied.

5.3.2. Speciation – Solubility Calculations

Saturation index (SI) calculations are carried out for Anhydrite, Gypsum, Aragonite, Calcite, Dolomite, and Magnesite minerals for each field of Group III with the assistance of *PHREEQC* code; the results are tabulated in Table 5.6, along with the calculated CO_2 partial pressure, and are illustrated in terms of SI vs. major anion diagrams in Fig. 5.11.

Table 5.6: Summary of results from speciation - solubility calculations of Group III fields

Geothermal Field	Sample	T(°C)	pH	log pCO_2	Saturation Index (SI)					
					Aragonite	Calcite	Dolomite	Magnesite	Gypsum	Anhydrite
Caldiran	ALT	23.62	6.51	-1.16	-1.13	-0.98	-0.66	-1.31	-2.13	-2.32
	AVC	12.86	7.88	-3.17	-1.04	-0.89	-1.00	-1.80	-4.28	-4.59
	AYR	36.15	7.02	-0.97	-0.62	-0.47	0.84	-0.24	-2.63	-2.70
	AYS	25.80	6.07	-0.64	-1.42	-1.27	-1.15	-1.50	-2.19	-2.37
	BUG	35.73	6.76	-0.94	0.01	0.16	1.62	-0.09	-2.33	-2.41
	BUS	20.33	5.85	-0.84	-2.00	-1.86	-2.45	-2.25	-2.11	-2.33
	KOC-I	15.98	6.18	-0.75	-1.06	-0.91	-0.69	-1.46	-2.66	-2.93
	KOC-II	25.08	6.71	-0.62	0.19	0.33	2.17	0.21	-1.98	-2.16
	KOC-III	14.59	5.63	-0.46	-1.76	-1.62	-2.06	-2.13	-2.29	-2.57
	YKR	14.16	5.62	-0.90	-2.75	-2.60	-4.15	-3.24	-3.18	-3.47
	ZYR	11.39	7.15	-2.37	-1.39	-1.24	-2.00	-2.47	-3.15	-3.47
Diyadin	BUR	19.51	5.4	-1.34	-3.47	-3.32	-6.02	-4.36	-1.66	-1.89
	DGM	11.07	4.56	-1.00	-4.64	-4.49	-8.28	-5.5	-1.90	-2.22
	DHS	21.5	8.43	-3.00	1.21	1.35	3.48	0.48	-1.82	-2.04
	DIB	48.25	6.98	-0.99	0.41	0.56	2.54	0.48	-1.65	-1.61
	DKC	11.19	6.44	-1.27	-1.03	-0.89	-1.09	-1.92	-1.51	-1.83
	DVS	11.4	5.4	-1.02	-2.85	-2.70	-4.78	-3.79	-1.31	-1.62
	EBU	25.77	3.17						-1.02	-1.19
	GBK	9.64	5.5	-0.95	-2.66	-2.52	-4.42	-3.63	-1.63	-1.97
	GOK	10.94	6.05	-1.11	-1.78	-1.63	-2.65	-2.73	-1.75	-2.07
	KEV	20.62	5.9	-0.84	-1.75	-1.61	-2.12	-2.17	-1.84	-2.06
	KOP	50.63	7.23	-1.37	0.44	0.58	2.70	0.63	-1.78	-1.72
	KUS	65.5	7.43	-1.42	0.49	0.63	3.24	1.19	-2.19	-2.00
	MKK	9.27	6.11	-0.98	-1.45	-1.30	-1.48	-1.90	-1.49	-1.83
	MLK	65.2	6.63	-0.69	0.28	0.43	1.99	0.15	-1.53	-1.34
	MNC	20.15	7.8	-2.70	-0.10	0.05	0.82	-0.88	-2.41	-2.64
	MNG	16.57	7.18	-2.51	-1.49	-1.35	-1.88	-2.21	-2.89	-3.15
	RAH	11.46	7.75	-2.37	0.11	0.25	1.63	-0.33	-2.86	-3.17
	TAZ	39.81	6.93	-1.07	0.11	0.25	1.95	0.16	-1.67	-1.71
	TSK	10.7	5.26	-0.78	-2.99	-2.85	-4.65	-3.52	-1.67	-2.00
	TUN	63.4	7.27	-1.28	0.43	0.58	2.87	0.87	-1.90	-1.73
	YES	12.01	7.68	-2.34	0.28	0.43	1.13	-1.00	-2.36	-2.67
	ZEG	17.82	3.15						-0.81	-1.06
NAFZ	Efteni-1a	43.2	6.5	-0.38	0.17	0.31	2.17	0.33	-3.33	-3.34
	Efteni-1b	17	8.6	-3.53	0.09	0.23	2.16	0.25	-3.51	-3.77
	Yalova-2a	61.2	7.6	-2.77	0.10	0.24	0.51	-1.16	-0.63	-0.47
	Yalova-2c	17.2	7.5	-2.10	0.23	0.38	0.89	-1.15	-1.88	-2.14
	Bolu-3a	42	6.2	-0.56	-0.23	-0.08	0.30	-1.14	-0.63	-0.65
	Bolu-3b	14.6	8	-3.45	-0.99	-0.84	-0.91	-1.76	-3.32	-3.60
	Mudurnu-4a	39.8	6.2	-0.59	-0.49	-0.34	0.22	-0.97	-2.01	-2.05
	Mudurnu-4d	15.1	7.1	-1.59	-0.11	0.04	1.03	-0.69	-1.93	-2.21
	Seben-5a	71.4	6.6	-0.40	0.09	0.24	1.49	-0.13	-1.97	-1.73
	Seben-5d	15	7.4	-1.97	0.08	0.23	1.46	-0.46	-1.21	-1.50
	Hamamözü-6a	42.5	7.4	-1.94	0.00	0.15	1.45	-0.23	-2.48	-2.49
	Hamamözü-6b	16.3	7.5	-2.08	0.15	0.29	1.40	-0.57	-2.04	-2.31
	Gözlek-7a	39.1	7.8	-2.33	0.12	0.26	1.58	-0.22	-2.61	-2.65
	Gözlek-7b	17.8	7.7	-2.19	0.47	0.62	2.44	0.16	-1.32	-1.58
	Reşadiye-8a	41.2	6.4	-0.32	0.30	0.45	1.85	-0.14	-1.44	-1.46
	Reşadiye-8b	15.3	7.3	-2.08	-0.52	-0.37	0.35	-0.97	-1.96	-2.24
	Kurşunlu-9a	57.4	7	-0.16	0.91	1.05	3.23	0.73	-2.53	-2.40
	Kurşunlu-9b	13.3	6.4	-0.63	-0.61	-0.47	-0.39	-1.62	-2.14	-2.43
	Kurşunlu-9c	13.2	8	-2.69	0.46	0.60	1.72	-0.58	-2.68	-2.98

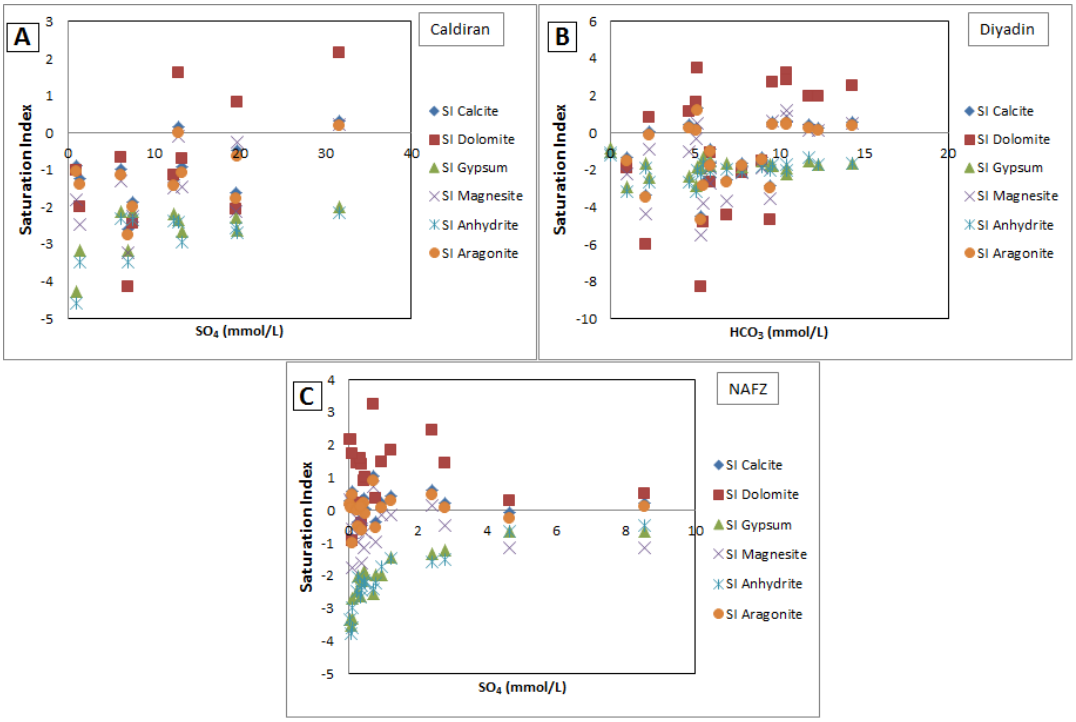

Figure 5.11: Evolution of saturation indices in the thermal waters of Çaldıran (A), Diyadin (B), and NAFZ (C) vs dominant anion concentrations

Speciation - solubility index calculations show that the waters of Group III are undersaturated with respect to anhydrite and gypsum, and – to a certain extent – magnesite, pointing to dissolution of these minerals. Calcite and aragonite show SI values close to equilibrium or indicative of dissolution. The fields in eastern Anatolia have waters mostly undersaturated, while those along NAFZ mostly oversaturated with respect to dolomite (Table 5.6, Fig. 5.11). In other words, SI values indicate that dissolution is the dominating process in the geothermal systems associated with eastern Anatolian fields. On the other hand, for the fields along the NAFZ, although both precipitation and dissolution seem to be the valid hydrogeochemical processes, the rate of dissolution appears to be exceeding that of precipitation as the concentrations of major anions and cations display increasing trends with increasing EC value as a measure of hydrogeochemical evolution (Fig. 5.10).

Although both carbonate and sulphate minerals in these waters are likely to be dissolved, it is important to evaluate the relative contribution of carbonate minerals' dissolution to the total dissolved calcium. Similar to the procedure done for other groups, the amount of calcium derived from dissolution of $CaSO_4$ minerals (gypsum or anhydrite) (as inferred from total dissolved sulphate), is subtracted from the total dissolved calcium concentrations. The (corrected) Ca concentration estimated with this calculation is shown in Fig. 5.12.

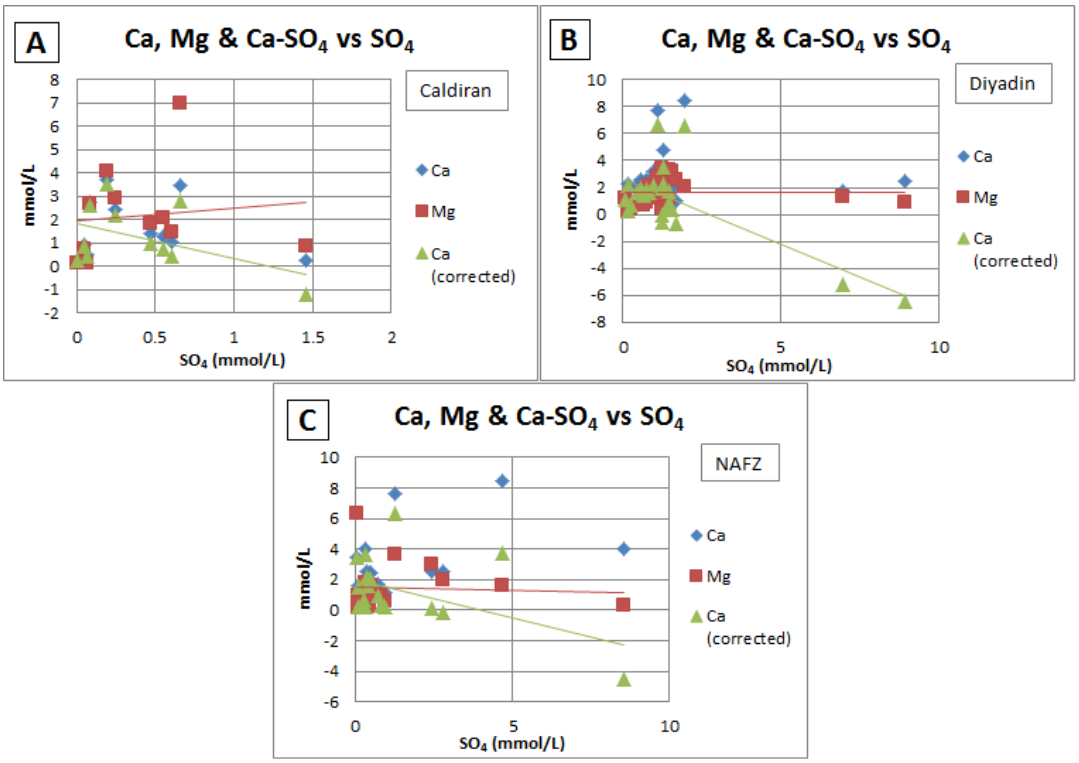

Figure 5.12: Evolution of analytic and corrected calcium concentrations and magnesium concentrations vs. total sulphate concentrations in the thermal waters of Çaldıran (A), Diyadin (B), and NAFZ (C).

As seen in Fig. 5.12, in all fields of Group III corrected Ca concentrations correlate negatively with SO_4. The negative trend of corrected Ca with SO_4, when combined with the results obtained from SI calculations, suggests that the dissolution process is dominated by sulphate, rather than carbonate minerals.

5.3.3. Mass – Balance Calculations

For the geothermal fields of Group III, dissolution is found out to be the most likely process for the trapping of CO_2 in these systems.

Mass-balance calculations (inverse modelling) have also been carried out utilizing *PHREEQC* code for Group III geothermal fields to further evaluate the mechanism of CO_2 storage and the modelling results are presented in Table 5.7.

Table 5.7: Summary of results from mass-balance calculations of Group III geothermal fields

Mass-Balance Calculations	Field	Initial Solution*	Final Solution*	Calcite mole transfer**	Dolomite mole transfer**
	Caldiran	1 (ALT)	8 (KOC-II)	-3.306	6.165
	Diyadin	1 (BUR)	15 (MLK)	0.365	1.773
	NAFZ	11	1	-3.087	5.616

*Sample numbers are given in Tables A.3 and A.5

**Negative mass transfer corresponds to precipitation and positive to dissolution.

Given that positive mass transfer values correspond to dissolution in mass-balance calculations, it is clear from Table 5.7 that dissolution is indeed the major process in Diyadin field. Dolomite dissolution is also clear for the fields of Çaldıran and NAFZ, although the negative values indicate precipitation for calcite. It is important, however, to note the relatively large amount of dolomite dissolution compared to calcite precipitation in Çaldıran and NAFZ fields, suggesting that the calcite precipitation does not contradict the validity of dissolution as the major hydrogeochemical process for Group III fields. Furthermore, the He-CO_2 systematics (Fig. 4.6 and Fig. 4.9) of these fields (Mutlu et al., 2012; de Leeuw et 2010) also suggest that dissolution of carbonate minerals is the dominant hydrogeochemical process.

CHAPTER 6

CONCLUSIONS AND RECOMMENDATIONS

Taken as the natural analogues for CO_2 storage sites, various geothermal fields from western, eastern and northern Anatolia are examined with respect to the hydrogeochemical processes and potential mechanisms controlling CO_2 trapping in these systems. The methods used for this study are the geochemical characterization of the system, speciation-solubility calculations, estimation of relative contribution of carbonate and sulphate minerals to the system, and modelling studies such as inverse modelling and dedolomitization modelling depending on the behaviour of the field. With the investigation of the results, three different groups of geothermal systems are identified with regard to the dominant CO_2 trapping mechanism:

1. First group is characterized by ***mineral trapping*** as the dominant trapping mechanism and is comprised by Kızıldere, Germencik, Balçova and Simav geothermal fields from western Anatolia. In these fields, increasing electrical conductivity (EC) of solutions (as a measure of hydrogeochemical evolution) is accompanied by decreasing Ca and Mg, and generally increasing SO_4 contents, pointing to the potential of precipitation of carbonate and dissolution of sulphate minerals. Saturation index (SI) calculations indeed reveal that majority of waters are oversaturated with respect to carbonate minerals dolomite and magnesite, and - to a certain extent - aragonite and calcite, and undersaturated with respect to anhydrite and gypsum. With the results showing dolomite ± calcite precipitation, mass-balance calculations (inverse modelling) verify mineral trapping as the dominant CO_2 trapping mechanism in these systems.

2. The second group is characterized by ***mineral ± solubility trapping*** and includes Edremit, Balıkesir, Dikili, Sındırgı, Emet, Salihli and Tekkehamam geothermal fields from western Anatolia. The hydrogeochemical differences observed between these fields and those categorized as Group I, lead to their identification as a separate group (Group II). This group has variable geochemical characteristics. The SO_4 concentrations have increasing trends with increasing EC in almost all fields (as is the case with the first group), suggesting the dissolution of sulphate minerals which is also supported by SI calculations. On the other hand, HCO_3, Ca and Mg concentrations have different trends in different fields, resulting in the anticipation of both dissolution and precipitation of carbonate minerals in the systems. SI calculations reveal that different water samples from individual fields show both undersaturation and oversaturation with respect to calcite, aragonite and dolomite, while dominantly undersaturation with respect to magnesite (as opposed to Group I fields). The occurrence of both dissolution and precipitation of carbonate minerals for this group is justified with the mass-balance calculations (inverse modelling). However for Edremit, Balıkesir and Emet fields, the results of mass-balance calculations combined with the previous studies indicate the possibility of dedolomitization which can be generated by calcite precipitation accompanied by dolomite dissolution. At this step, dedolomitization modelling is performed to differentiate the effects of CO_2 in systems dominated by dedolomitization from those dominated by calcite dissolution. The results of this modelling show that Edremit and Balıkesir follow the trend for calcite dissolution, while the samples from Emet mostly fall within the trends for dedolomitization. In brief, the trapping mechanism of the fields in this group is a combination of solubility and mineral trapping whereas for Emet, dedolomitization is also likely to occur.

3. The third group is characterized by ***solubility trapping***. The fields included in this group are Çaldıran and Diyadin from eastern Anatolia, and the fields along the North Anatolian Fault Zone (NAFZ), namely, Yalova, Efteni, Bolu**,** Mudurnu, Seben, Kurşunlu, Hamamözü, Gözlek and Reşadiye. The hydrogeochemical

character of this group is that all of the major anions and cations have increasing trends with increasing EC in almost all fields. This observation implies the dissolution of sulphate and carbonate minerals in these systems. SI calculations reveal that the waters are dominantly undersaturated with respect to carbonate and sulphate minerals. The mass-balance calculations verify dissolution as the major process, although calcite precipitation may also occur in some fields. In other words, solubility trapping is the main mechanism for the fields of Group III.

A striking observation relevant to the above mentioned grouping is that the mineral trapping (rather than dissolution) seems to be the dominant CO_2 trapping mechanism in fields with the highest reservoir temperatures such as Germencik and Kızıldere in the Büyük Menderes Graben, whereas in the fields with relatively lower temperatures dissolution is an effective process. Therefore, it can be concluded that reservoir's temperature condition determines the impact of CO_2 interactions.

The conclusions derived from this thesis study are relevant for CO_2 storage in deep saline aquifers. The geochemical investigations performed in this study provide an invaluable starting point for understanding the behavior of potential storage systems. For the prospective CO_2 storage projects in the long term, rate of mineral precipitation or dissolution of CO_2 should also be studied via kinetic modelling in addition to the thermodynamic studies performed in the thesis work. Moreover, more natural analogues must be studied in order to confirm and widen the knowledge of long-term CO_2-induced geochemical interactions.

REFERENCES

Akkuş, İ., Akıllı, H., Ceyhan, S., Dilemre, A., & Tekin, Z. (2005). *Türkiye Jeotermal Kaynakları Envanteri.* Ankara: Maden Tetkik ve Arama Genel Müdürlüğü.

Aksoy, N., Demirkıran, Z., & Şimşek, C. (2009). Sındırgı-Hisaralan (Balıkesir) jeotermal sahasının jeokimyasal özelliklerinin değerlendirilmesi. *Jeotermal Enerji Semineri*, (pp. 61-72). İzmir.

Appelo, C., & Postma, D. (2005). *Geochemistry, groundwater and pollution.* Amsterdam: A.A. Balkema Publishers.

Auqué, L., Acero, P., Gimeno, M., Gomez, J., & Asta, M. (2009). Hydrogeochemical modeling of a thermal system and lessons learned for CO2 geologic storage. *Chemical Geology, 268*, 324-336.

Avşar, Ö., Güleç, N., & Parlaktuna, M. (2013). Hydrogeochemical characterization and conceptual modeling of the Edremit geothermal field (NW Turkey). *Journal of Volcanology and Geothermal Research, 262*, 68–79.

Aydın, H., Mutlu, H., & Kazancı, A. (2013). Çaldıran (Van) jeotermal sahasının hidrojeokimyasal özellikleri. *11. Ulusal Tesisat Mühendisliği Kongresi - Jeotermal Enerji Semineri*, (pp. 71-90). İzmir.

Bingöl, E. (1969). Geology of the central and southeastern sections of the Kazdag Massif. *Mineral Exploration Institute of Turkey Bulletin, 72*, 102-123.

Bingöl, E., Akyürek, B., & Korkmazer, B. (1973). Biga yarımadası'nın jeolojisi ve karakaya formasyonunun bazı özellikleri. *MTA, cumhuriyetin 50.yılı yer bilimleri kongresi, tebliğler*, (pp. 70-76). Ankara.

Bozkurt, E. (2003). Origin of NE-trending basins in western Turkey. *Geodinamica Acta, 16*, 61–81.

Bozkurt, E., & Mittwede, S. (2001). Introduction to the Geology of Turkey—A Synthesis. *International Geology Review, 43*, 578-594.

Canik, B. (1972). *Düzce-Derdin hamamı civarının jeoloji ve hidrojeoloji etüdü.* Ankara: MTA Report 6359.

Canik, B., & Pasvanoğlu, S. (2003). Geothermal investigation of the Kesenözü thermal springs (Bolu-Turkey). *European Geothermal Congress* , (pp. 1-10). Szeged-Hungary.

CCP (2008). *CO_2 Trapping Mechanisms.* CO_2 Capture Project: Retrieved from http://www.co2captureproject.org/co2_trapping.html (last accessed on 14 August 2014)

Clark, I. D., & Fritz, P. (1997). *Environmental Isotopes in Hydrogeology*. Boca Raton: CRC Press.

CO_2CRC (2011). *Injection & storage.* The Cooperative Research Centre for Greenhouse Gas Technologie: Retrieved from http://www.co2crc.com.au/aboutccs/stor_trapping.html (last accessed on 14 August 2014)

CO_2GeoNet (2008). *What does CO_2 geological storage really mean?* The European Network of Excellence on the Geological Storage of CO_2: Retrieved from http://www.co2geonet.com/ (last accessed on 4 August 2014)

Craig, H. (1961). Isotopic variations in meteoric waters. *Science, 133*, 1702–1703.

Dagistan, H. (2007). Yenilenebilir Enerji ve Jeotermal Kaynaklarimiz. *Türkiye 10. Enerji Kongresi* (pp. 73-80). Ankara: MTA Genel Müdürlügü.

de Leeuw, G., Hilton, D., Güleç, N., & Mutlu, H. (2010). Regional and temporal variations in CO2/3He, 3He/4He and d13C along the North Anatolian Fault Zone, Turkey. *Applied Geochemistry, 25*, 524–539.

Dewey, J., & Şengör, A. (1979). Aegean and surrounding regions: complex multiplate and continuum tectonics in a convergent zone. *Geological Society of America Bulletin, 90*, 84-92.

Dominco, E., & Şamilgil, E. (1970). The geochemistry of the Kizildere geothermal field, in the framework of the Saraykoy-Denizli geothermal area. *Geothermics, 2*, 553–560.

Dürr, S. (1975). *Über Alter und geotektonische Stellung des Menderes-Kristallins/SW-Anatolien und seine Äequivalente in der mittleren Ägäis.* Habilitation Thesis, University of Marburg/Lahn.

Erzenoğlu, Z. (1989). *Amasya Gümüşhacıköy Hamamözü (Arkutbey) kaplıcası H-1 no'lu sıcaksu sondajı kuyu bitirme raporu.* Ankara: MTA Report 8714.

Escorcia, L., Gomez-Rivas, E., Daniele, L., & Corbella, M. (2013). Dedolomitization and reservoir quality: insights from reactive transport modelling. *Geofluids*, 1-11.

Filiz, Ş., Tarcan, G., & Gemici, Ü. (2000). Geochemistry of the Germencik geothermal fields, Turkey. *Proceedings World Geothermal Congress*, (pp. 1115-1120). Kyushu - Tohoku, Japan.

Gat, J., & Carmi, I. (1970). Evolution in the isotopic composition of atmospheric waters in the Mediterranean Sea area. *Journal of Geophysical Research, 75*, 3039–3048.

Gaus, I. (2010). Role and impact of CO2–rock interactions during CO2 storage in sedimentary rocks. *International Journal of Greenhouse Gas Control, 4*, 73-89.

Gemici, Ü., & Tarcan, G. (2002). Hydrogeochemistry of the Simav geothermal field, western Anatolia, Turkey. *Journal of Volcanology and Geothermal Research, 116*, 215-233.

Gemici, Ü., Tarcan, G., Çolak, M., & Helvacı, C. (2004). Hydrogeochemical and hydrogeological investigations of thermal waters in the Emet area (Kütahya, Turkey). *Applied Geochemistry, 19*, 105–117.

Gevrek, A., Şener, M., & Ercan, T. (1984-1985). Çanakkale -Tuzla jeotermal alanının hidrotermal alterasyon etüdü ve volkanik kayaçların petrolojisi. *Maden Tetkik ve Arama Dergisi, 103,104*, 55-81.

Giggenbach, W. (1991). Chemical techniques in geothermal exploration. *Application of geochemistry in geothermal reservoir development* (pp. 119-142). Rome: UNITAR/UNDP.

Gökgöz, A. (1998). *Geochemistry of the Kızıldere-Tekkehamam-Buldan-Pamukkale Geothermal Fields, Turkey.* Reykjavik, Iceland: Geothermal Training Programme, The United Nations University.

Gunter, W., Perkins, E., & McCann, T. (1993). Aquifer disposal of CO_2-rich gases: reaction design for added capacity. *Energy Conversion and Management, 34*, 941–948.

Güleç, N., Hilton, D. R., de Leeuw, G., Mutlu, H., Süer, S., & Çifter, C. (2006). Geochemical monitoring of the geothermal fluids along the seismically active North Anatolian Fault Zone (NAFZ), Turkey. *New Techniques in Earthquake Prediction Studies and Their Applicability in Turkey.* INGV-Palermo, Italy: Leopass-RAP4LEO-Leonardo da Vinci Project.

Güleç, N., Hilton, D., & Mutlu, H. (2002). Helium isotope variations in Turkey: relationship to tectonics, volcanism and recent seismic activities. *Chemical Geology, 187*, 129– 142.

Hovorka, S., Doughty, C., Knox, P., Green, C., Pruess, K., & Benson, S. (2001). *Evaluation of Brine-Bearing Sands of the Frio Formation, Upper Texas Gulf Coast for Geological Sequestration of CO_2.* Washington DC: National Energy Technology Laboratory.

IEA (2008). *Geologic Storage of Carbon Dioxide: Staying Safely Underground.* CO2CRC.

IPCC (2005). *Carbon Dioxide Capture and Storage: Special Report of the Intergovernmental Panel on Climate Change.* New York: Cambridge University Press.

IPCC (2007). Climate Change 2007: Synthesis Report. (p. 104). Geneva, Switzerland: Intergovernmental Panel on Climate Change [Core Writing Team, Pachauri, R.K and Reisinger, A.(eds.)].

Jeckelmann, C. (1996). *Genese Lokaler Thermal Wasser Vorkommen in der Region, Bergama/W-Türkei.* Zurich: Doktor der Naturwissenchaften der Eridgenössischen Technischen Hochshule.

Karahan, Ç. (2013). Jeotermal Enerji, Çevresel Etkileri Dikili-Kaynarca Jeotermal Rezervuarı ve Sondaj Uygulamaları. *Jeotermal Sempozyumu, Dikili Jeotermal Alanı.* MTA Ege Bölge Müdürlüğü.

Karakhanian, A., Djrbashian, R., Trifonov, V., Philip, H., Arakelian, S., & Avagian, A. (2002). Holocene-historical volcanism and active faults as natural risk factors for Armenia and adjacent countries. *Journal of Volcanology and Geothermal Research, 113*, 319–344.

Karakuş, H., & Şimşek, Ş. (2013). Tracing deep thermal water circulation systems in the E–W trending Büyük Menderes Graben, western Turkey. *Journal of Volcanology and Geothermal Research, 252*, 38–52.

Karamanderesi, İ. (2013). *Characteristics of Geothermal Reservoirs in Turkey.* İzmir: IGA Academy Report.

Keskin, M. (2007). Eastern Anatolia: a hot spot in a collision zone without a mantle plume. *Plates, Plumes, and Planetary Processes, Geological Society of America Special Paper, 430*, pp. 693–722.

Koçak, A. (1974). *Çavundur (Kurşunlu-Çankırı) kaplıca bölgesinin hidrojeoloji etüdü raporu.* Ankara: MTA Report 6373.

Koçyiğit , A., Yılmaz, A., Adamia, S., & Kuloshvili, S. (2001). Neotectonics of East Anatolian Plateau (Turkey) and Lesser Caucasus: implication for transition from thrusting to strike-slip faulting. *Geodinamica Acta, 14*, 177-195.

Lollar, B., & Ballentine, C. (2009). Insights into deep carbon derived from noble gases. *Nature Geoscience, 2*, 543 - 547.

Magri, F., Akar, T., Gemici, Ü., & Pekdeger, A. (2010). Deep geothermal groundwater flow in the Seferihisar–Balçova area, Turkey: results from transient numerical simulations of coupled fluid flow and heat transport processes. *Geofluids, 10*, 388–405.

Mahon, W., Klyen, L., & Rhode, M. (1980). Natural Sodium bicarbonate sulphate hot waters in geothermal systems. *Chinetsu (Journal Japanese Geothermal Energy Association), 17*, 11-24.

METI (2010). Japan's current situation and direction of progress after the economic crisis. In *White Paper on International Economy and Trade 2010.* Tokyo, Japan: Industrial Science and Technology Policy and Environmental Bureau, the Ministry of Economy, Trade and Industry (METI).

MIT Energy Initiative. (2014, January). *Otway Fact Sheet: Carbon Dioxide Capture and Storage Project*. Carbon Capture & Sequestration Technologies: Retrieved from https://sequestration.mit.edu/tools/projects/otway.html (last accessed on 31 July 2014)

MTA (2011). *Geothermal Energy Studies in MTA.* Ankara: Maden Tetkik ve Arama Genel Müdürlüğü.

MTA (2012). *Türkiye Jeotermal Enerji Potansiyeli.* Maden Tetkik ve Arama Genel Müdürlüğü: Retrieved from http://www.mta.gov.tr/v2.0/daire-baskanliklari/enerji/index.php?id=jeotermal_potansiyel (last accessed on 9 July 2014)

MTA-JICA (1987). *Pre-Feasibility Study on the Dikili Bergama Geothermal Development Project in the Republic of Turkey.* Ankara: Progress Report II, Final Report, M.T.A.

Mutlu, H. (1998). Chemical geothermometry and fluid–mineral equilibria for the Ömer–Gecek thermal waters, Afyon area, Turkey. *Journal of Volcanology and Geothermal Research, 80,* 303–321.

Mutlu, H. (2007). Constraints on the origin of the Balıkesir thermal waters (Turkey) from stable isotope (d18O, dD, d13C, d34S) and major-trace element compositions. *Turkish Journal of Earth Sciences, 16,* 13-32.

Mutlu, H., & Güleç, N. (1998). Hydrogeochemical outline of thermal waters and geothermometry applications in Anatolia (Turkey). *Journal of Volcanology and Geothermal Research, 85,* 495–515.

Mutlu, H., & Kılıç, A. (2009). Geothermometry applications for the Balıkesir thermal waters, Turkey. *Environmental Geology, 56,* 913–920.

Mutlu, H., Aydın, H., & Kazancı, A. (2013). Diyadin (Ağrı) jeotermal sahasına yönelik jeokimyasal ve izotopik bulgular. *11. Ulusal Tesisat Mühendisliği Kongresi - Jeotermal Enerji Semineri,* (pp. 47-67). İzmir.

Mutlu, H., Güleç, N., & Hilton, D. (2008). Helium–carbon relationships in geothermal fluids of western Anatolia, Turkey. *Chemical Geology, 247,* 305–321.

Mutlu, H., Güleç, N., Hilton, D., Aydın, H., & Halldórsson, S. (2012). Spatial variations in gas and stable isotope compositions of thermal fluids around Lake Van: Implications for crust–mantle dynamics in eastern Turkey. *Chemical Geology, 300-301*, 165–176.

Okay, A., & Satır, M. (2000). Upper Cretaceous Eclogite-Facies Metamorphic Rocks from the Biga Peninsula, Northwest Turkey. *Turkish Journal of Earth Sciences, 9*, 47-56.

Özcan, M., & Ünay, T. (1978). *Bolu-Seben-Kesenözü kaplıcası ve çevresi jeotermal enerji aramaları rezistivite etüdü raporu.* Ankara: MTA Report 8269.

Özdemir, Y. (2011). *Volcanostratigraphy and Petrogenesis of Süphan Stratovolcano.* Ankara: Ph.D. Thesis, Middle East Technical University.

Özdemir, Y., Karaoğlu, Ö., Tolluoğlu, A., & Güleç, N. (2006). Volcanostratigraphy and petrogenesis of the Nemrut stratovolcano (East Anatolian High Plateau): the most recent post-collisional volcanism in Turkey. *Chemical Geology, 226*, 189–211.

Özen, T., Bülbül, A., & Tarcan, G. (2012). Reservoir and hydrogeochemical characterizations of geothermal fields in Salihli, Turkey. *Journal of Asian Earth Sciences, 60*, 1–17.

Özen, T., Tarcan, G., & Gemici, Ü. (2005). Hydrogeochemical Study of the Selected Thermal and Mineral Waters in Dikili Town, İzmir, Turkey. *Proceedings World Geothermal Congress*, (pp. 1-12). Antalya.

Özgür, N. (2002). Geochemical signature of the Kizildere geothermal field, Western Anatolia, Turkey. *International Geology Review, 44*, 153-163.

Özgür, N. (2003). *Active geothermal systems in the rift zone of the Büyük Menderes, Western Anatolia, Turkey.* Isparta, Turkey: Süleyman Demirel

Üniversitesi, Research and Application Center for Geothermal Energy, Groundwater and Mineral Resources.

Palabıyık, Y., & Serpen, U. (2008). Geochemical assessment of Simav geothermal fi eld, Turkey. *Revista Mexicana de Ciencias Geológicas, 25*(3), 408-425.

Parkhurst, D., & Appelo, C. (1999). User's guide to PHREEQC (version 2)--A computer program for speciation, batch-reaction, one-dimensional transport, and inverse geochemical calculations. In *U.S. Geological Survey Water-Resources Investigations Report 99-4259* (p. 312).

Parkhurst, D., & Appelo, C. (2013). Description of input and examples for PHREEQC version 3—A computer program for speciation, batch-reaction, one-dimensional transport, and inverse geochemical calculations: U.S. Geological Survey Techniques and Methods. U.S. Geological Survey.

Pasvanoğlu, S., & Güler, S. (2010). Hydrogeological and Geothermal Features of Hot and Mineralized Waters of the Ağri - Diyadin (Turkey). *Proceedings World Geothermal Congress*, (pp. 1-10). Bali, Indonesia.

Romanak, K. D., Smyth, R. C., Yang, C., Hovorka, S. D., & Lu, J. (2010). Role of dedolomitization in the detection of anthropogenic CO2 in freshwater aquifers. *Water Rock Interaction 13 Conference* (pp. 1-4). Guanajuato, México: GCCC Digital Publication Series.

Rütters, H., Möller, I., May, F., Flornes, K., Hladik, V., Arvanitis, A., et al. (2013). *State of the Art of Monitoring Methods to evaluate Storage Site Performance.* (A. Korre, R. Stead, & N. Jensen, Eds.) CGS Europe report No. D3.3.

Salvi, S., Quattrocchi, F., Brunori, C., Doumaz, F., Angelone, M., Billi, A., et al. (1999). A Multidisciplinary Approach to Earthquake Research: Implementation of a Geochemical Geographic Information System for the Gargano Site, Southern Italy. *Natural Hazards, 20*, 255–278.

Scripps Institution of Oceanography. (2014). *The Keeling Curve.* Retrieved from https://scripps.ucsd.edu/programs/keelingcurve/ (last accessed on 8 September 2014)

Shukla, R., Ranjith, P., Haque, A., & Choi, X. (2010). A review of studies on CO2 sequestration and caprock integrity. *Fuel, 89*, 2651–2664.

Solomon, S. (2007). *Carbon Dioxide Storage: Geological Security and Environmental Issues – Case Study on the Sleipner Gas field in Norway* . Bellona Report .

Soong, Y., Jones, J., Harrison, D., Hedges, S., Goodman, A., & Baltrus, J. (2003). Mineral Trapping of CO2 with Oriskany Brine. *U.S. Department of Energy, National Energy Technology Laboratory*.

Söğüt, A. R., Güzel, A., Zedef, V., & Bayram, A. F. (2010). Some geological and hydrogeochemical characteristics of geothermal fields of Turkey. *Scientific Research and Essays, 5*, 3147-3151.

Süer, S., Güleç, N., Mutlu, H., Hilton, D., Çifter, C., & Sayın, M. (2008). Geochemical Monitoring of Geothermal Waters (2002–2004) along the North Anatolian Fault Zone, Turkey: Spatial and Temporal Variations and Relationship to Seismic Activity. *Pure and Applied Geophysics, 165*, 17-43.

Şahinci, A. (1970). *Mudurnu kaplıcası hidrojeoloji etüd raporu.* Ankara: MTA Report 4367.

Şengör, A. (1984). Structural classification of the tectonic history of Turkey. *Proceedings of Ketin Symposium*, (pp. 37-61). Ankara.

Şengör, A., & Yılmaz, Y. (1981). Tethyan evolution of Turkey: A plate tectonic approach. *Tectonophysics, 75*, 181-241.

Şengör, A., Görür, N., & Şaroğlu, F. (1985). *Strike-slip faulting and related basin formation in zones of tectonic escape: Turkey as a case study*, *Strike-slip*

Deformation, Basin Formation, and Sedimentation. Society of Economic Palaentologists and Mineralogists, Special Publication 37 (in honor of J.C. Crowell).

Şengör, A., Satır, M., & Akkök, R. (1984). Timing of the tectonic events in the Menderes Massif, western Turkey: implications for tectonic evolution and evidence for Pan-African basement in Turkey. *Tectonics, 3,* 693-707.

Şimşek, S. (1982). *Geology and geothermal energy possibilities oJthe Denizli-Saraykoy-Buldan area.* İstanbul: Ph.D. Thesis, Istanbul University, Earth and Sciences Faculty.

Şimşek, Ş. (2003). Present status and future development possibilities of Aydın-Denizli Geothermal Province. *International Geothermal Conference,* (pp. 11-16). Reykjavík.

Şimşek, Ş., & Güleç, N. (1994). Geothermal Fields of Western Anatolia: Excursion Guide. *International Volcanological Congress* (pp. 1-35). Ankara: IAVCEI.

Şimşek, Ş., Yıldırım, N., & Gülgör, A. (2005). Developmental and environmental effects of the Kızıldere geothermal power project, Turkey. *Geothermics, 34*, 239–256.

Tarcan, G. (2005). Mineral saturation and scaling tendencies of waters discharged from wells (>150 oC) in geothermal areas of Turkey. *Journal of Volcanology and Geothermal Research, 142,* 263– 283.

Tarcan, G., & Gemici, Ü. (2003). Water geochemistry of the Seferihisar geothermal area, İzmir, Turkey. *Journal of Volcanology and Geothermal Research, 126,* 225-242.

Tarcan, G., Gemici, Ü., & Aksoy, N. (2005). Hydrogeological and geochemical assessments of the Gediz Graben geothermal areas, western Anatolia, Turkey. *Environmental Geology, 47,* 523–534.

Tarcan, G., Gemici, Ü., & Aksoy, N. (2009). Hydrogeochemical factors effecting the scaling problem in Balçova geothermal field, İzmir, Turkey. *Environmental Geology, 58,* 1375–1386.

Tatar, O., Piper, J. D., Park, R., & Gürsoy, H. (1995). Palaeomagnetic study of block rotations in the Niksar overlap region of the North Anatolian Fault Zone, central Turkey. *Tectonophysics, 244*, 251-266.

Tezcan, A. (1975). Geophysical studies in Sarayköy–Kızıldere geothermal field, Turkey. *Proceedings of 2nd UN Symposium on the Development and Use of Geothermal Resources,* (pp. 1231–1240).

Wiersberg, T., Süer, S., Güleç, N., Erzinger, J., & Parlaktuna, M. (2011). Noble gas isotopes and the chemical composition of geothermal gases from the eastern part of the Büyük Menderes Graben (Turkey). *Journal of Volcanology and Geothermal Research, 208,* 112-121.

Yıldırım, N. D. (1997). Geochemical characteristic and re-injection of the Kizildere-Tekkehamam geothermal field. *GEOENV'97.* İstanbul.

Yıldırım, N., & Ölmez, E. (1999). Kızıldere (Denizli–Sarayköy) sahasında acilan yeni kuyular ile üretim kuyuları arasındaki hidrokimyasal ilişki. *Batı Anadolu Hammadde Kaynakları Sempozyumu Baksem 99.* İzmir.

Yilmaz, Y., Güner, Y., & Şaroğlu, F. (1998). Geology of the quaternary volcanic centers of the east Anatolia. *Journal of Volcanology and Geothermal Research, 85,* 173–210.

Yılmazdemir, K. (2011, January 12). *Sondajdan 90 C derecelik su çıktı.* Hürriyet: Retrieved from http://www.bolununsesi.com/icerik/haber.asp?id=19062 (last accessed on 15 July 2014)

Yılmazer, S. (2009). *Batı Anadolu'nun Olası Jeotermal Potansiyelinin Belirlenmesi.* Gayzer Yerbilimleri Ltd. Şti.

APPENDIX A

GEOCHEMICAL DATA COMPILED FROM PREVIOUS STUDIES

In this thesis study, various geothermal fields from western, eastern and northern Anatolia are chosen as natural analogues. The selection of the fields is based mainly on the available and reliable hydrogeochemical data from recent publications that have sufficient parameters. The compiled hydrogeochemical and isotopic data of these fields are tabulated in the following pages.

Table A.1: Chemical analyses of waters from geothermal fields of western Anatolia

Field	*Sample No.*	*Location*	T(°C)	*pH*	EC (µS/cm)	Na	K	Ca	Mg	HCO_3	SO_4	Cl	Mg/Ca
Kızıldere [a]	KD-6	Kızıldere	196[b]	8.97	5830	53.07	2.97	0.03	0.01	25.99	5.83	3.5	0.49
	KD-13	Kızıldere	195[b]	8.89	5940	56.55	3.53	0.05	0.01	24.99	8.05	3.61	0.21
	KD-14	Kızıldere	207[b]	8.96	6160	61.33	3.89	0.03	0.01	39.38	7.67	4.06	0.27
	KD-15	Kızıldere	205[b]	8.82	5890	58.29	3.53	0.03	0.01	23.99	7.6	3.95	0.21
	KD-16	Kızıldere	211[b]	8.94	5835	60.9	3.79	0.08	0.01	24.99	7.43	3.84	0.12
	KD-20	Kızıldere	201[b]	8.92	6180	59.81	3.58	0.04	0.01	18.99	7.39	3.95	0.15
	KD-21	Kızıldere	202[b]	9.02	5940	57.63	3.35	0.04	0.01	19.99	7.39	3.95	0.22
	KD-22	Kızıldere	202[b]	9.3	5830	55.46	3.58	0.03	0.01	25.99	7.59	3.84	0.33
	R-1	Kızıldere	242[b]	8.8	5820	67.68	6.27	0.07	0.01	50.38	8.24	3.78	0.14
	TH-2	Kızıldere	171[b]	9.4	4800	53.94	3.07	0.05	0.05	21.88	7.57	3.16	0.99
Tekkehamam [c]	TH-1	Well TH-1	116	7.71	4000	32.62	1.92	0.30	0.49	5.49	14.05	2.14	1.65
	3	Demirtas	98	6.70	2600	28.27	1.18	1.25	0.66	10.53	10.72	2.09	0.53
	4	Tekkehamam	99	7.60	3700	43.28	2.43	0.40	0.14	15.90	12.80	2.88	0.35
	5	Tekkehamam-1	60	7.90	3800	23.05	1.64	5.24	2.18	18.93	11.14	2.54	0.42
	6	Tekkehamam-2	72	7.70	3800	42.80	2.53	1.12	0.62	16.99	12.39	2.74	0.55
	7	İnalti magarasi	55.5	6.45		31.97	1.87	4.64	1.44	11.94	17.70	2.45	0.31
	8	Babacik pinari	61.5	6.20	2930	21.75	1.18	6.49	3.25	21.14	14.47	1.75	0.50
	9	Gerenlik gölü	73.5	7.10	3680	43.50	2.40	0.75	0.04	24.16	11.14	3.10	0.05
Germencik [d]	1	Balli Hot Spr	60	7.01	5763	52.68	2.97	1.10	1.97	38.48	0.62	34.67	1.80
	2	Alangullu Hot Spr	60	6.66	5838	52.15	3.20	1.72	1.03	39.76	0.69	34.19	0.60

Table A.1 (cont'd): Chemical analyses of waters from geothermal fields of western Anatolia

Field	*Sample No.*	*Location*	T(°C)	*pH*	EC (µS/cm)	Na	K	Ca	Mg	HCO_3	SO_4	Cl	Mg/Ca
Germencik [d]	3	Camur Hot Spr	50	6.9	5383	47.89	2.79	1.65	2.39	38.60	1.50	31.45	1.45
	4	Ilica Hot Spr	70	6.63	5783	48.59	2.81	1.42	2.22	38.81	0.63	32.75	1.56
	5	Ali Thermal Spr	60	7.6	5292	46.89	2.76	0.97	1.40	33.86	0.63	33.45	1.44
	6	OB_1 weirbox	200[b]	8.5	7000	89.17	2.17	0.08	0.04	34.79	0.69	49.28	0.52
	7	OB_1 weirbox	200[b]	8.5		58.94	1.15	0.16	0.04	21.70	0.39	44.74	0.26
	8	OB_2 weirbox	231[b]		7200	122.23	4.88	0.10	0.08	25.09	1.75	54.95	0.79
	9	OB_2 2.reservoir	231[b]	8.7		69.60	3.71	0.15	0.05	14.75	0.25	50.49	0.33
	10	OB_6 weirbox		8.38		80.47	4.35	0.01	0.02	30.61	0.29	55.57	1.65
	11	OB_6 reservoir	221[b]	6.05		54.81	3.38	0.96	0.02	26.03	0.40	40.05	0.02
	12	Cold Gw	17	7	1171	4.87	0.72	0.95	3.17	10.70	0.81	2.12	3.34
Balçova [e]	1 (DHDNS)	Balçova	114[b]	7.25	1490	12.64	0.60	1.33	0.77	9.39	1.93	3.61	0.58
	2 (DHDNR)	Balçova	116[b]	6.99	1514	13.06	0.62	1.34	0.76	9.44	2.14	3.75	0.57
	3 (GEWR)	Balçova	138[b]	6.33	1744	17.50	0.74	0.50	0.16	10.55	2.04	4.99	0.32
	4 (BD-2)	Balçova	129[b]	7.77	1842	19.99	0.93	0.33	0.09	10.88	1.94	5.64	0.27
	5 (BD-4)	Balçova	138[b]	8.01	2020	20.08	0.85	0.44	0.09	10.47	2.46	5.92	0.20
	6 (BD-5)	Balçova	117[b]	7.84	1850	19.26	0.73	0.53	0.13	9.39	1.78	5.61	0.24
	7 (B-4)	Balçova	86[b]	7.38	1900	16.48	0.70	0.59	0.22	10.83	2.20	4.43	0.38
	8 (B-5)	Balçova	105[b]	7.07	1595	16.07	0.66	0.57	0.30	10.00	1.99	4.17	0.53
	9 (B-10)	Balçova	92[b]	7.05	1950	16.93	0.75	0.75	0.30	10.44	3.29	4.99	0.40
	10 (B-11)	Balçova	92[b]	7.85	1619	15.83	0.65	0.48	0.23	9.83	3.12	4.80	0.47

Table A.1 (cont'd): Chemical analyses of waters from geothermal fields of western Anatolia

Field	*Sample No.*	*Location*	T(°C)	*pH*	EC (µS/cm)	Na	K	Ca	Mg	HCO_3	SO_4	Cl	Mg/Ca
Balçova[e]	11 (B-13)	Balçova	120[b]	7.48	1148	9.85	0.35	2.34	0.75	4.24	1.34	2.43	0.32
Salihli[f]	1	Urganli spa spr	55	6.53	2620	22.84	1.28	1.12	0.66	25.83	0.57	2.40	0.59
	2	Urganli spa well (U-1)	60	6.93	2870	22.23	1.25	2.27	0.95	27.52	0.72	2.37	0.42
	3	Sart Camur spa spr	44	6.39	1690	8.18	0.56	4.19	0.91	18.55	0.44	1.30	0.22
	4	Üfürük min well	31	6.69	1527	0.61	0.05	8.31	1.60	20.63	0.36	0.87	0.19
	5	Kursunlu Ts	42	7.31	2110	23.44	1.61	3.24	1.97	27.39	3.53	2.82	0.61
	6	Kursunlu Tw	55	7.43	2780	21.92	1.53	0.87	0.45	23.75	0.60	2.76	0.52
	7	Sazdere min spr	29	6.35	2450	15.35	0.84	2.97	5.51	32.63	0.81	2.68	1.86
	8	Sazdere Ts	34	6.35	2450	34.62	1.69	3.24	2.80	39.66	0.95	5.05	0.86
	9	KG-1 (Göbekli) Dw	182[g]	8.31	6020	88.17	2.02	0.32	0.13	48.35	19.19	4.65	0.40
	10	Sarikiz spr	27	6.01	906	1.13	0.15	2.25	2.35	8.92	1.08	0.45	1.04
	11	Alasehir Ts	31	6.83	874	9.53	0.31	3.04	5.55	24.11	0.67	1.89	1.82
	12	Caferbeyli Dw (SC-1)	155[g]	7.8	2700	29.58	1.79	1.05	0.25	32.50	0.35	3.24	0.24
	13	Alasehir Tw	37	6.38	4270	22.01	1.25	7.76	6.67	51.05	0.04	2.85	0.86
	14	K-1 well	31.6	7.1	2160	16.46	1.36	1.98	0.59	19.40	1.53	0.51	0.30
	15	K-2 well	59.3	7.6	2200	17.03	1.38	1.57	0.55	19.60	1.75	2.00	0.35
	16	K-4 well	41.5	6.2	1757	8.84	0.64	4.24	1.40	23.94	1.74	1.16	0.33
	17	K-5 well	42.6	7.8	2070	14.84	1.23	2.60	0.74	19.78	1.44	1.83	0.29
	18	K-6 well	64.9	6.6	2130	18.39	1.32	1.08	0.21	21.78	0.30	2.12	0.20
	19	K-7 well	56.3	6.7	2680	23.52	1.89	1.21	0.39	27.88	0.27	3.72	0.32

Table A.1 (cont'd): Chemical analyses of waters from geothermal fields of western Anatolia

Field	*Sample No.*	*Location*	T(°C)	*pH*	EC (µS/cm)	Na	K	Ca	Mg	HCO_3	SO_4	Cl	Mg/Ca
Salihli [f]	20	K-8 well	57	6.7	1967	10.52	0.80	4.78	1.54	20.49	1.47	1.38	0.32
	21	K-11 well	55	7.3	2200	15.64	1.31	2.17	0.68	20.40	1.62	2.45	0.31
	22	K-12 well	51.1	7.7	2160	16.50	1.33	2.11	0.66	17.39	1.37	1.78	0.31
	23	K-15 well	63.5	7.7	2330	19.28	1.61	1.74	0.53	21.75	1.62	2.28	0.30
	24	K-16 well	63.2	6.6	2100	16.91	1.28	0.18	0.53	22.04	0.57	1.81	3.02
	25	K-19 well	35.1	7.3	2010	14.80	1.22	2.44	0.72	19.04	1.50	1.83	0.29
	26	K-20 well	52	6.7	2730	22.56	1.31	2.53	0.93	29.75	0.11	1.95	0.37
	27	Sart thermal spr	43	6.3	1506	6.76	0.64	4.93	1.01	16.00	0.75	0.76	0.21
	28	Üfürük mineral spr	22	4.9	3560	2.47	0.30	17.71	10.28	34.00	0.04	1.52	0.58
	29	Kurşunlu mineral spr	26	6.7	1906	0.89	0.13	9.69	2.60	17.00	2.96	0.39	0.27
	30	Greenhouse well-1	54	7.5	1991	21.50	0.19	0.22	0.10	5.87	2.19	1.50	0.45
	31	Greenhouse well-2	36.3	7.8	1963	20.08	0.18	0.15	0.06	16.14	2.19	1.24	0.37
	32	Cold well in KGF	29.8	5.9	926	2.62	0.32	2.75	1.85	8.90	0.39	0.96	0.67
	33	Cold well in CGF	31.1	6.7	1381	2.89	0.15	4.91	4.04	16.90	1.12	0.93	0.82
	34	Cold well in CGF	27.5	7.1	1180	2.08	0.15	2.47	1.69	8.75	0.97	1.50	0.68
	35	Cold well in GGF	23.6	6.1	1409	3.69	0.19	5.18	1.51	4.20	0.63	0.51	0.29
	36	Kurşunlu stream	23.7	7.8	664	1.50	0.20	2.34	0.54	1.80	0.81	0.23	0.23
	37	Tabak stream	28	8	942	3.85	0.34	2.94	0.92	4.52	0.90	0.51	0.31
	38	Gediz river	26.8	7.5	1350	6.28	0.60	2.17	1.16	3.28	1.26	0.34	0.54

Table A.1 (cont'd): Chemical analyses of waters from geothermal fields of western Anatolia

Field	*Sample No.*	*Location*	T(°C)	*pH*	EC (µS/cm)	Na	K	Ca	Mg	HCO_3	SO_4	Cl	Mg/Ca
Sındırgı[h]	H-1	Sındırgı	96	7.79	1252	11.89	0.46	0.51	0.11	10.10	1.19	2.60	0.22
	H-2	Sındırgı	58.2	7.51	1378	11.98	0.50	0.53	0.11	10.00	1.31	2.62	0.21
	H-4	Sındırgı	79.2	7.03	1331	11.61	0.50	0.54	0.09	9.93	1.22	2.45	0.18
	H-5	Sındırgı	85	6.59	1287	11.63	0.46	0.60	0.12	10.06	1.22	2.40	0.20
	H-6	Sındırgı	83.7	6.51	1283	12.41	0.48	0.55	0.10	10.33	1.31	2.51	0.19
	H-7	Sındırgı	72	7.45	1388	11.85	0.48	0.49	0.11	10.01	1.22	2.43	0.21
	H-8	Sındırgı	96	7.43	1196	11.96	0.45	0.37	0.09	9.98	1.19	2.37	0.24
	H-9	Sındırgı	81.3	7	1487	14.00	0.39	0.52	0.08	10.73	0.97	1.95	0.16
	H-10	Sındırgı	94	6.89	1275	11.23	0.47	0.70	0.26	10.33	1.19	2.34	0.37
	H-11	Sındırgı	55.5	7.07	1252	11.73	0.44	0.48	0.12	10.00	1.19	2.40	0.24
	H-12	Sındırgı	62	6.14	1490	13.27	0.33	1.32	0.15	12.84	1.00	1.86	0.11
	H-13	Sındırgı	62	6.9	1225	11.39	0.23	0.94	0.05	9.78	0.75	1.52	0.05
	H-15	Sındırgı	95	7.46	597	1.50	0.05	1.88	0.83	6.71	0.25	0.34	0.44
	H-16	Sındırgı	96.6	6.8	1487	13.36	0.59	0.54	0.10	10.36	1.06	2.09	0.19
	H-8A	Sındırgı	95.2	7.12	428	0.20	0.04	1.56	1.16	0.95	0.28	0.17	0.75
Simav[i]	1	EJ-1	163	8.74	2300	22.03	1.41	0.29	0.20	11.12	4.91	2.26	0.70
	3	E6	160	8.84	2280	23.15	1.59	0.16	0.24	10.68	4.75	2.26	1.49
	4	E8	150	9.2	2300	22.75	1.49	0.21	0.19	9.48	4.64	2.28	0.90
	5	Eynal Spa spring	78	9.2	2200	23.03	1.24	0.04	0.16	9.64	4.42	2.00	4.02
	6	E4	98	7.07	2280	22.63	1.44	0.79	0.21	13.60	4.78	2.12	0.27

Table A.1 (cont'd): Chemical analyses of waters from geothermal fields of western Anatolia

Field	*Sample No.*	*Location*	T(°C)	*pH*	EC (µS/cm)	Na	K	Ca	Mg	HCO_3	SO_4	Cl	Mg/Ca
Simav [i]	7	Çitgöl dw	140	7.31	1460	12.55	0.91	1.37	0.37	9.16	2.83	1.35	0.27
	8	Çitgöl dw	162	7.91	1826	17.83	1.01	0.65	0.23	9.76	4.09	1.83	0.36
	9	Çitgöl spring	51	6.84	2090	19.69	1.01	1.39	0.50	10.44	5.15	2.26	0.36
	11	Naşa dw	90	7.03	1612	14.53	0.91	1.19	0.46	9.72	3.37	1.58	0.39
	13	Eynal spring [j]	60	8.2	1200	19.57	1.38	0.14	0.05	8.49	4.73	1.97	0.39
	14	Çitgöl spring [j]	83	7	1000	14.79	1.13	0.85	0.22	9.39	3.91	1.61	0.26
	15	Naşa spring [j]	64	6.6	1000	17.18	1.07	0.97	0.39	9.90	4.10	1.47	0.40
Emet [k]	1	Emet [i]	43	7.11	1350	0.82	0.13	5.76	1.86	4.84	5.64	0.31	0.32
	2	Emet [i]	54	7.1	1041	0.55	0.08	4.41	1.33	5.32	3.33	0.31	0.30
	3	Emet	43	7.1	1015	0.57	0.09	4.15	1.46	4.72	3.49	0.31	0.35
	4	Emet	38	6.9	1830	0.65	0.14	8.83	2.55	4.80	8.74	0.34	0.29
	5	Emet [i]	13	7.25	1606	0.58	0.11	7.46	2.04	4.48	7.81	0.37	0.27
	6	Emet	48	7	646	0.44	0.16	2.24	0.96	4.52	0.91	0.39	0.43
	7	Emet	15	7.2	962	0.40	0.05	5.66	2.83	7.52	4.51	1.41	0.50
	8	Emet	46	6.47	1269	0.27	0.03	7.19	2.37	4.64	8.04	0.48	0.33
	9	Emet	49	6.45	1346	0.30	0.03	7.42	2.38	4.72	8.25	0.48	0.32
	10	Emet	15	7.09	1636	0.37	0.02	8.82	3.02	5.44	10.61	0.56	0.34
	11	Emet [j]	33	7.8	500	0.43	0.05	1.95	0.86	5.70	0.30	0.16	0.44
	12	Emet [j]	39	6.7	1060	4.78	0.25	3.47	1.15	12.39	0.53	0.76	0.33
	13	Emet [j]	43	7.1	2250	14.79	1.82	5.09	2.51	5.00	13.63	2.48	0.49

Table A.1 (cont'd): Chemical analyses of waters from geothermal fields of western Anatolia

Field	*Sample No.*	*Location*	T(°C)	*pH*	EC (µS/cm)	Na	K	Ca	Mg	HCO_3	SO_4	Cl	Mg/Ca
Dikili [I]	1-a	Dikili Spa	65	7.3	2900	28.71	1.07	0.92	0.30	17.86	5.87	2.76	0.33
	2-a	Dikili Spa	40	7.3	2900	24.79	1.05	1.07	0.35	18.68	5.01	2.89	0.33
	3-a	Dikili Spa	40	7.3	2900	25.45	1.10	1.17	0.28	18.68	5.01	2.92	0.24
	4-a	Dikili Spa	66	7.1	2800	24.14	0.97	1.05	0.28	17.04	4.84	2.46	0.27
	5-a	Dikili Spa	65	7	2800	23.71	0.97	1.25	0.26	17.37	4.92	2.49	0.21
	6-a	Dikili Spa	73	7.2	2600	23.49	1.02	1.15	0.26	17.04	4.97	2.51	0.22
	7-a	Dikili Spa	34	7.4	3600	35.67	0.90	1.02	0.34	26.55	5.88	2.73	0.33
	8-b	Dikili Spa	72	6.2	2560	24.79	0.88	1.22	0.00	16.96	5.00	2.50	0.00
	9-b	Dikili Spa	41	6.7	2670	21.47	0.91	1.23	0.02	18.99	5.59	2.82	0.01
	10-b	Dikili Spa	36	6.4	2540	21.97	0.98	1.17	0.01	16.50	4.63	2.93	0.01
	11-b	Dikili Spa	65	6.8	2600	24.03	0.99	1.21	0.01	17.60	4.49	2.38	0.01
	12-b	Dikili Spa	30	6.6	3030	24.70	1.06	3.54	0.03	24.40	4.55	25.19	0.01
	13-b	Near Dikili	32	7.9	3200	22.88	0.80	1.32	0.00	22.99	6.04	3.15	0.00
	15-b	Plain near Dikili	24	6.7	495	2.28	0.20	0.86	0.31	2.61	0.13	1.37	0.36
	16-b	Sülüklü spr.	24	7.2	631	19.36	0.18	1.91	0.75	4.90	0.18	10.49	0.39
	18-c	Agrobay-1, well	93	6.9	2140	18.05	0.82	1.55	0.19	5.83	6.88	2.09	0.13
	19-c	Agrobay-2, well	89	6.8	2150	18.44	0.82	1.57	0.53	5.28	6.92	2.14	0.34
	21-a	Kaynarca	42	8.1	2700	24.79	0.92	0.82	0.06	9.80	8.18	2.05	0.07
	22-a	Kaynarca	82	7.7	2500	23.05	0.92	0.80	0.02	9.60	7.65	1.94	0.02
	23-a	Kaynarca	48	8	2700	24.79	0.95	0.92	0.16	9.80	8.06	2.05	0.17

Table A.1 (cont'd): Chemical analyses of waters from geothermal fields of western Anatolia

Field	*Sample No.*	*Location*	T(°C)	*pH*	EC (µS/cm)	Na	K	Ca	Mg	HCO_3	SO_4	Cl	Mg/Ca
Dikili [I]	24-a	Kaynarca	53	7.7	2500	23.49	0.87	0.97	0.02	9.60	7.84	2.03	0.02
	25-a	Kaynarca	80	7.8	2600	23.05	0.84	1.10	0.14	9.80	7.65	2.00	0.12
	26-a	Kaynarca	74	7.4	2600	23.49	0.87	0.92	0.02	9.90	8.13	2.00	0.02
	27-a	Kaynarca	99	8.6	2500	23.49	0.84	0.82	0.02	10.00	7.74	1.97	0.02
	28-a	Kaynarca	46	8.4	2600	24.79	0.87	0.82	0.04	10.00	7.73	2.05	0.05
	29-a	Kaynarca	83	7.4	2600	22.62	0.84	0.52	0.02	8.90	6.40	1.97	0.03
	30-a	Kaynarca	76	7.4	2700	23.05	1.00	0.90	0.02	9.60	5.02	2.00	0.02
	31-b	Kaynarca	88	7.4	2530	22.74	0.94	0.85	0.10	9.19	6.40	1.73	0.12
	32-b	Kaynarca	41	7.8	2623	22.41	0.76	1.05	0.12	9.10	8.29	1.92	0.12
	33-b	Kaynarca east	70	7.1	2560	20.20	0.74	1.01	0.10	9.41	7.78	1.83	0.10
	34-b	Kaynarca west	32	7.4	1901	10.47	0.40	5.96	2.61	7.62	6.83	6.93	0.44
	37-b	Kaynarca, spring	79	7.6	410	21.36	1.05	0.99	0.04	4.64	7.35	2.26	0.04
	38-c	Kaynarca well-1	67	6.9	2040	16.31	0.61	1.68	0.32	2.97	6.67	6.35	0.19
	39-c	Kaynarca well-3	87	8.2	2360	21.53	0.98	0.55	0.19	5.28	7.73	2.23	0.34
	40-c	Kaynarca petrol	68	7	2320	18.83	0.82	1.71	0.32	5.47	7.30	2.31	0.19
	41-a	DG-1. well	98	9	1800	15.79	0.82	0.27	0.09	4.62	5.76	1.44	0.35
	42-a	DG-3. well	45	7.7	5500	32.06	2.23	0.08	2.59	4.11	1.36	43.16	31.48
	44-c	Kocaoba Spa	52	7.4	1763	11.27	0.36	2.97	0.09	2.00	7.96	1.52	0.03
	45-b	Kocaoba Spa	54	7.2	1430	10.12	0.40	2.94	0.25	2.61	7.25	0.98	0.09

Table A.1 (cont'd): Chemical analyses of waters from geothermal fields of western Anatolia

Field	*Sample No.*	*Location*	T(°C)	*pH*	EC (µS/cm)	Na	K	Ca	Mg	HCO_3	SO_4	Cl	Mg/Ca
Balıkesir [m]	G-7	Gönen	60.4	7.15	2410	20.84	0.74	1.67	0.13	6.28	4.87	7.05	0.08
	G-8	Gönen	57.8	7.42	2390	21.52	0.73	1.74	0.14	6.34	4.89	7.02	0.08
	G-16	Gönen	77.5	6.97	2930	21.23	0.75	1.22	0.10	5.68	4.71	7.23	0.08
	EKS-1	Gönen	42.7	7.26	329	0.53	0.05	1.28	0.53	3.15	0.17	0.24	0.42
	EKS-2	Gönen	18.8	4.16	171	0.40	0.04	0.16	0.09	0.00	0.45	0.41	0.55
	EKS-3	Gönen	21.5	3.91	113	0.29	0.05	0.08	0.04	0.00	0.28	0.27	0.50
	MK-1	Manyas	49.8	6.57	1570	11.31	0.76	3.51	0.43	8.15	0.87	7.85	0.12
	MK-2	Manyas	34.4	6.87	877	3.86	0.28	3.50	0.44	7.20	0.46	2.39	0.12
	PMK-1	Pamukcu	64.9	7.56	1972	16.36	0.51	1.18	0.17	3.55	3.72	6.18	0.14
	PMK-2	Pamukcu	55.5	7.34	1433	13.85	0.36	0.82	0.12	4.56	3.03	3.71	0.15
	BHS-1	Bigadic	94.6	7.29	2820	30.73	1.89	0.21	0.48	17.23	3.97	5.83	2.30
	BHS-2	Bigadic	82.9	6.95	3330	29.51	1.80	0.76	0.49	18.19	3.64	5.83	0.64
	SHS-1	Sindirgi (Hisaralan)	98.5	7.01	1454	13.99	0.53	0.55	0.12	9.46	1.01	2.30	0.22
	SHS-2	Sindirgi (Hisaralan)	97.3	7.38	1422	14.01	0.53	1.65	0.13	9.27	0.97	2.30	0.08
	SHS-3	Sindirgi (Hisaralan)	95.1	6.97	1451	13.84	0.53	0.56	0.14	9.52	0.96	2.33	0.24
	SHS-4	Sindirgi (Hisaralan)	87	6.72	1631	13.67	0.53	0.57	0.17	9.30	0.96	2.32	0.30
	EDR-1	Edremit	57.6	7.83	1354	11.86	0.13	1.25	0.03	0.80	5.28	1.68	0.03
	EDR-2	Edremit	44.7	7.56	968	8.65	0.10	1.75	0.12	1.77	4.07	1.46	0.07
	GDR-1	Edremit	56.6	8.4	1260	13.31	0.15	0.56	0.00	0.82	5.14	1.71	0.01
	GDR-2	Edremit	17.5	7.76	208	0.23	0.02	1.00	0.26	2.27	0.06	0.14	0.26

Table A.1 (cont'd): Chemical analyses of waters from geothermal fields of western Anatolia

Field	*Sample No.*	*Location*	T(°C)	*pH*	EC (µS/cm)	Na	K	Ca	Mg	HCO_3	SO_4	Cl	Mg/Ca
Balıkesir m	BLY-1	Balya	59	8.21	1240	11.47	0.11	0.41	0.00	1.30	3.65	2.23	0.01
	BLY-2	Balya	58.1	8.1	1234	11.72	0.11	0.39	0.00	1.23	3.72	2.24	0.01
	BLY-3	Balya	28.8	6.17	252	1.04	0.04	0.66	0.35	1.82	0.17	0.27	0.54
	SLK-1	Susurluk	31.8	7.05	685	2.73	0.19	2.07	1.21	5.57	1.25	0.30	0.59
	SLK-2	Susurluk	72.8	6.4	1605	16.55	0.34	0.56	0.02	9.76	1.98	1.61	0.04
	SLK-3	Susurluk	25.7	8.05	207	0.87	0.05	0.54	0.30	1.74	0.21	0.31	0.56
Edremit n	ED-3	Edremit	62	7.76	1060	8.40	0.09	0.62	0.01	0.89	3.75	1.35	0.01
	ED-1	Edremit	62	7.65	1310	10.22	0.14	0.90	0.00	0.70	4.89	1.75	0.00
	EDJ-3	Edremit	59	7.65	1260	9.92	0.13	0.82	0.00	0.64	4.79	1.64	0.00
	EDJ-2	Edremit	58	7.67	1200	9.44	0.13	0.77	0.00	0.72	4.37	1.61	0.01
	EDJ-5	Edremit	55	7.99	756	6.09	0.08	0.32	0.00	1.52	1.98	1.30	0.01
	DERM.	Edremit	53	7.81	1300	9.92	0.13	0.95	0.03	1.08	4.58	1.75	0.03
	ENT.	Edremit	51	7.95	1200	9.35	0.12	0.80	0.03	1.43	4.06	1.66	0.04
	EDJ-7	Edremit	51	7.61	1380	10.70	0.15	0.97	0.00	0.61	5.20	1.78	0.00
	EDJ-4	Edremit	50	7.81	1110	8.35	0.09	0.90	0.03	1.10	3.96	1.44	0.03
	EDJ-8	Edremit	43	8	751	6.39	0.12	0.12	0.00	1.64	1.87	1.41	0.03
	YAGCI	Edremit	42	8.13	874	6.70	0.08	0.75	0.02	2.51	2.29	1.33	0.03
	DSI-6	Edremit	39	8.07	1080	4.70	0.09	2.62	0.66	3.08	3.33	1.50	0.25
	DOG.	Edremit	32	8.14	934	3.48	0.08	2.55	0.66	3.56	2.39	1.33	0.26
	DSI-9	Edremit	32	8.09	1060	3.57	0.09	3.14	0.66	3.16	3.23	1.61	0.21

Table A.1 (cont'd): Chemical analyses of waters from geothermal fields of western Anatolia

Field	*Sample No.*	*Location*	T(°C)	*pH*	EC (µS/cm)	Na	K	Ca	Mg	HCO_3	SO_4	Cl	Mg/Ca
Edremit[n]	HAST.	Edremit	31	8.06	817	2.13	0.09	2.50	0.58	2.46	2.08	1.52	0.23
	DSI-5	Edremit	30	8.06	962	3.57	0.10	1.95	0.70	2.79	2.29	1.47	0.36
	DSI-7	Edremit	21	8.14	466	1.00	0.05	1.05	0.39	3.00	0.25	0.59	0.37
	DSI-8	Edremit	18	8.12	975	1.70	0.05	2.17	1.07	3.51	0.74	2.85	0.49
	EMINDSI	Edremit	12	8.14	438	0.61	0.04	1.60	0.38	3.43	0.39	0.48	0.24

All concentrations are mmol/L.

If not otherwise specified, discharge temperatures for springs, well-head temperatures for wells are given.

spr:spring. min:mineral. ts:thermal springs. tw:thermal well. dw:deep well

KGF: Kurşunlu geothermal field, CGF: Caferbeyli geothermal field, GGF: greenhouse geothermal field

[a]Şimşek et al. (2005).

[b]reservoir temperature.

[c]Simsek. (1982); except TH-1 from Yildirim et al. (1997) in Gökgöz (1998).

[d]Filiz et al. (2000).

[e]Tarcan et al. (2009).

[f]Tarcan et al. (2005) and Özen et al. (2012).

[g]bottom hole temperature.

[h]Aksoy et al. (2009).

[i]Gemici & Tarcan (2002).

[j]MTA (1996).

[k]Gemici et al. (2004).

[l]Özen et al. (2005).

[m]Mutlu (2007).

[n]Avşar et al. (2013).

Table A.2: Isotopic compositions waters from geothermal fields of western Anatolia

Sample No.	Sample location	$CO_2/^3He$ ($x10^9$)	$\delta^{13}C(CO_2)$ ‰ (PBD)	δD (‰SMOW)	$\delta^{18}O$ (‰SMOW)	References
B-48	Tuzla (spr)	45.5±0.3	0.35	-23.02	-4.01	Mutlu et al., 2008
B-73	Kestanbol-1 (well)	1.66±0.01	-3.59	-42.07	-7.99	Mutlu et al., 2008
B-64	Kestanbol-2 (spr)	15.7±0.1	-3.37			Mutlu et al., 2008
B-86	Çan (well)	1.72±0.02	-4.1	-65.43	-10.46	Mutlu et al., 2008
B-124	Gönen (well)	33.6±0.2	-1.52	-76.89	-11.96	Mutlu et al., 2008
B-77	Manyas (well)	34.3±0.2	-6.61	-60.88	-11.01	Mutlu et al., 2008
B-118	Hisaralan (spr)	220 ±2	-8.04	-68.49	-11.61	Mutlu et al., 2008
B-90	Seferihisar (spr)	892 ±20	-3.79	-35.97	-6.11	Mutlu et al., 2008
B-101	Balçova (well)	95.1 ±0.8	-3.65	-40.96	-7	Mutlu et al., 2008
B-13	Germencik (spr)	3865 ±80	-1.89	-45.04	-4.68	Mutlu et al., 2008
B-109		1934 ±24	-2.35			Mutlu et al., 2008
B-40	Kızıldere (well)	305±2	-0.62	-61.65	-7.68	Mutlu et al., 2008
B-117	Gazlıgöl (well)	5450± 150	-2.58	-89.86	-13.13	Mutlu et al., 2008
B-59	Ömer (well)	23.540 ±2.060	-0.66	-86.16	-13.11	Mutlu et al., 2008
BM-1	Pamukkale	12	-3.5	-59.6	-8.87	Güleç, 1988 (for $CO_2/^3He$); Ercan et al., 1994; Şimşek, 2003
BM-2	Kızıldere (R1 well)	180		-52.9	-4.31	Şimşek, 2003; Wiersberg et al., 2011
	Kızıldere (KD6 well)	180		-56.2	-6.13	Şimşek, 2003; Wiersberg et al., 2011
	Kızıldere (KD13 well)	280		-54.1	-5.31	Şimşek, 2003; Wiersberg et al., 2011
	Kızıldere (KD14 well)	780				Wiersberg et al., 2011
	Kızıldere (KD15 well)	300		-55.5	-5.23	Şimşek, 2003; Wiersberg et al., 2011

Table A.2 (cont'd): Isotopic compositions waters from geothermal fields of western Anatolia

Sample No.	Sample location	$CO_2/^3He$ ($x10^9$)	$\delta^{13}C(CO_2)$ ‰ (PBD)	δD (‰SMOW)	$\delta^{18}O$ (‰SMOW)	References
BM-2	Kızıldere (KD16 well)	920				Wiersberg et al., 2011
	Kızıldere (KD21 well)	510		-55.2	-5.65	Şimşek, 2003; Wiersberg et al., 2011
	Kızıldere (KD22 well)	430				Wiersberg et al., 2011
BM-3	Tekkehamam	90	— 1.2			Güleç, 1988; Ercan et al., 1994 (for $\delta^{13}C$)
		100		-53.5	-6.13	Wiersberg et al., 2011
		110		-54.7	-6.18	Wiersberg et al., 2011
BM-4	Ortakçı		-5.39	-51.1	-8.17	Karakuş & Şimşek, 2013
BM-5	Gedik		-5.23	-42.8	-7.1	Karakuş & Şimşek, 2013
BM-6	Güvendik	138	0.45	-37.7	-6.82	Karakuş & Şimşek, 2013
BM-7	Salavatlı	322	-0.2	-45	-1.36	Özgür, 2002
BM-8	Serçeköy	774	-0.45	-47.9	-2.95	Karakuş & Şimşek, 2013
BM-9	İmamköy		-1.29	-37.5	-6.31	Karakuş & Şimşek, 2013
BM-10	Yılmazköy	752	0.02	-47.8	-2.95	Karakuş & Şimşek, 2013
BM-12	Germencik (OB17 well)	1100	-0.33	-39	-1.46	Karakuş & Şimşek, 2013
	Germencik (OB14 well)			-38.9	-1.24	Karakuş & Şimşek, 2013
BM-13	Çamur	2086	-2.2	-40.6	-2.73	Karakuş & Şimşek, 2013
BM-14	Gümüş		-1.24	-22.6	-4.09	Karakuş & Şimşek, 2013
BM-15	Sazlıköy		-0.65	-32.3	-6.07	Karakuş & Şimşek, 2013
BM-16	Tuzburgaz		-3.69	2.7	-0.02	Karakuş & Şimşek, 2013
BM-17	Karina		-2.41	3	0.73	Karakuş & Şimşek, 2013

Table A.2 (cont'd): Isotopic compositions waters from geothermal fields of western Anatolia

Sample No.	Sample location	$CO_2/^3He$ ($x10^9$)	$\delta^{13}C(CO_2)$ ‰ (PBD)	δD (‰SMOW)	$\delta^{18}O$ (‰SMOW)	References
2	K-2 well			-50.92	-7.24	Özen et al., 2012
3	K-4 well			-50.3	-7.67	Özen et al., 2012
4	K-5 well			-51.11	-6.22	Özen et al., 2012
5	K-6 well			-53.83	-6.97	Özen et al., 2012
6	K-7 well			-53.24	-6.23	Özen et al., 2012
7	K-8 well			-49.88	-8.12	Özen et al., 2012
8	K-11 well			-51.09	-7.55	Özen et al., 2012
9	K-12 well			-60.69	-6.49	Özen et al., 2012
10	K-15 well			-51.56	-6.66	Özen et al., 2012
11	K-16 well			-51.98	-7.51	Özen et al., 2012
12	K-19 well			-50.54	-7.5	Özen et al., 2012
13	K-20 well			-50.19	-7.37	Özen et al., 2012
15	Sart thermal spr			-47.37	-7.88	Özen et al., 2012
16	Üfürük mineral spr			-41.69	-8.62	Özen et al., 2012
17	Kurşunlu mineral spr			-46.77	-9.73	Özen et al., 2012
18	Greenhouse well-1			-61.08	-7.37	Özen et al., 2012
19	Greenhouse well-2			-62.77	-8.87	Özen et al., 2012
20	Cold well in KGF			-41.79	-7.71	Özen et al., 2012
21				-52.53	-9.12	Özen et al., 2012
22				-54.12	-9.5	Özen et al., 2012

Table A.2 (cont'd): Isotopic compositions waters from geothermal fields of western Anatolia

Sample No.	Sample location	$CO_2/^3He$ ($x10^9$)	$\delta^{13}C(CO_2)$ ‰ (PBD)	δD (‰SMOW)	$\delta^{18}O$ (‰SMOW)	References
23	Cold well in KGF			-54.14	-9.52	Özen et al., 2012
24	Cold well in CGF			-46.41	-8.03	Özen et al., 2012
25						Özen et al., 2012
26				-46.55	-9.13	Özen et al., 2012
27	Cold well in GGF			-50.19	-9.38	Özen et al., 2012
28				-50.02	-9.26	Özen et al., 2012
29				-49.35	-9.46	Özen et al., 2012
30				-50.95	-9.68	Özen et al., 2012
E-7	Eynal (well)			-65.3	-9.34	Palabıyık & Serpen, 2008
Eynal	Eynal (hot spr)			-62.1	-8.94	Palabıyık & Serpen, 2008
E-1	Eynal (well)			-60.9	-9.08	Palabıyık & Serpen, 2008
ÇİTGÖL-2	Çitgöl-Naşa (well)			-55.9	-9.23	Palabıyık & Serpen, 2008
Naşa-2	Çitgöl-Naşa (hot spr)			-66.7	-9.62	Palabıyık & Serpen, 2008
Nadarçam	Çitgöl-Naşa (cold spr)			-57.1	-9.19	Palabıyık & Serpen, 2008
1	Dikili Spa			-41.5	-6.3	MTA-JICA, 1987
2				-44.4	-5.8	MTA-JICA, 1987
8				-43.5	-6.4	Jeckelman, 1996
9				-41.5	-5.9	Jeckelman, 1996
10				-45	-6.4	Jeckelman, 1996
11				-45.9	-6.3	Jeckelman, 1996

Table A.2 (cont'd): Isotopic compositions waters from geothermal fields of western Anatolia

Sample No.	Sample location	$CO_2/^3He$ ($x10^9$)	$\delta^{13}C(CO_2)$ ‰ (PBD)	δD (‰SMOW)	$\delta^{18}O$ (‰SMOW)	References
12	Dikili Spa			-47.1	-6.5	Jeckelman, 1996
13				-39	-4.7	Jeckelman, 1996
14				-31.7	-5.2	Jeckelman, 1996
15	Plain near Dikili			-33.8	-5.9	Jeckelman, 1996
16	Sülüklü fountain			-32.6	-5.4	Jeckelman, 1996
17	Plain near Dikili			-46.8	-6.2	Jeckelman, 1996
22	Kaynarca			-39.3	-6.3	MTA-JICA, 1987
23				-37.4	-4.9	MTA-JICA, 1987
24				-39.3	-6.1	MTA-JICA, 1987
26				-39.3	-6.1	MTA-JICA, 1987
27				-43	-6.4	MTA-JICA, 1987
28				-37.5	-4.8	MTA-JICA, 1987
31				-41.8	-5.9	Jeckelman, 1996
32				-38.2	-4.8	Jeckelman, 1996
33				-35.5	-5.6	Jeckelman, 1996
34	Kaynarca east			-30.7	-5	Jeckelman, 1996
35	Kaynarca west			-34.7	-5.7	Jeckelman, 1996
41	DG-1 well			-39.2	-5.9	MTA-JICA, 1987
42	DG-3 well			-35.5	-5.4	MTA-JICA, 1987
45	Kocaoba Spa			-46.3	-7.5	Jeckelman, 1996

Table A.2 (cont'd): Isotopic compositions waters from geothermal fields of western Anatolia

Sample No.	Sample location	$CO_2/^3He$ ($x10^9$)	$\delta^{13}C(CO_2)$ ‰ (PBD)	δD (‰SMOW)	$\delta^{18}O$ (‰SMOW)	References
46	Near Kocaoba			-37	-6.4	Jeckelman, 1996
G-7	Gönen		0	-76.83	-12.12	Mutlu, 2007
G-8			0	-77.05	-12.78	Mutlu, 2007
G-16			0.7	-77.39	-12.5	Mutlu, 2007
EKS-1			-1.7	-60.91	-11.94	Mutlu, 2007
EKS-2			-17.7	-55.95	-11.21	Mutlu, 2007
MK-1	Manyas		-3.6	-61.36	-9.91	Mutlu, 2007
MK-2			-8.4	-58.05	-10.77	Mutlu, 2007
PMK-1	Pamukcu		-8.9	-63.81	-10.67	Mutlu, 2007
PMK-2			-11.2	-58.47	-9.92	Mutlu, 2007
BHS-1	Bigadic		-2	-71.1	-9.94	Mutlu, 2007
BHS-2			-1.2	-71.8	-9.86	Mutlu, 2007
SHS-1	Sindirgi (Hisaralan)		-4.7	-68.49	-11.61	Mutlu, 2007
SHS-2			-4.8	-69.02	-11.78	Mutlu, 2007
SHS-3			-4.7	-69.28	-11.53	Mutlu, 2007
SHS-4			-3.4	-68.85	-11.73	Mutlu, 2007
EDR-1	Edremit		-10.5	-55.15	-10.05	Mutlu, 2007
EDR-2			-14.7	-53.38	-10.03	Mutlu, 2007
GDR-1			-7.2	-52.1	-9.61	Mutlu, 2007

Table A.2 (cont'd): Isotopic compositions waters from geothermal fields of western Anatolia

Sample No.	Sample location	$CO_2/^3He$ ($x10^9$)	$\delta^{13}C(CO_2)$ ‰ (PBD)	δD (‰SMOW)	$\delta^{18}O$ (‰SMOW)	References
BLY-1	Balya		-6.6	-76.8	-12.5	Mutlu, 2007
BLY-2			-6.7	-75.89	-12.91	Mutlu, 2007
SLK-1	Susurluk		-1.4	-63.16	-11.05	Mutlu, 2007
SLK-2			-1.8	-72.37	-12.36	Mutlu, 2007
ED-3	Edremit			-52.19	-9.19	Avşar et al., 2013
ED-1				-52.22	-9.47	Avşar et al., 2013
EDJ-5				-50.45	-7.6	Avşar et al., 2013
EDJ-7				-47.15	-7.24	Avşar et al., 2013
EDJ-4				-49.7	-8.26	Avşar et al., 2013
EDJ-8				-45.94	-7.18	Avşar et al., 2013
DSI-6				-47.55	-7.95	Avşar et al., 2013
TOTAL				-48.69	-7.91	Avşar et al., 2013
DOGANDERE				-43.28	-7.91	Avşar et al., 2013
DSI-9				-47.07	-7.76	Avşar et al., 2013
HASTANE				-43.26	-6.71	Avşar et al., 2013
DSI-7				-43.06	-6.95	Avşar et al., 2013
DSI-8				-38.72	-7.24	Avşar et al., 2013
EMINKUYU				-38.77	-6.88	Avşar et al., 2013
EMINDSI				-39.63	-8.11	Avşar et al., 2013

spr: spring, KGF: Kurşunlu geothermal field, CGF: Caferbeyli geothermal field, GGF: greenhouse geothermal field

Table A.3: Chemical analyses of waters from geothermal fields of eastern Anatolia

Field	*Sample No.*	*Location*	T(°C)	*pH*	EC (µS/cm)	Na	K	Ca	Mg	HCO_3	SO_4	Cl	Mg/Ca
Diyadin [a]	BUR	Burgulu spr	19.51	5.40	413	0.97	0.86	1.23	0.38	2.05	1.25	0.54	0.31
	CRK	Köprü hot spr	25.79	2.38	1591.9	15.33	7.76	14.55	11.30	0.00		5.33	0.78
	DGM	Davut cold spr	11.07	4.56	390	0.69	0.23	2.13	0.85	5.33	0.45	0.08	0.40
	DHS	Diyadin spr	21.50	8.43	759	2.08	0.04	2.56	1.03	5.16	0.58	1.78	0.40
	DIB	Dibekli hot spr	48.25	6.98	3415	6.79	1.79	2.32	3.33	14.34	1.46	4.51	1.43
	DKC	Davut cold spr	11.19	6.44	758	0.89	1.23	3.16	1.20	5.90	0.96	1.83	0.38
	DVS	Davut cold spr	11.40	5.40	413	0.73	0.47	3.18	1.07	5.49	1.46	0.54	0.34
	EBU	Boyalan spr	25.77	3.17	2007	1.48	1.81	1.75	1.30	0.00	6.97	0.25	0.74
	GBK	Göğebakan cold spr	9.64	5.50	725	1.45	0.24	2.63	0.86	6.88	0.75	0.87	0.33
	GOK	Göğebakan cold spr	10.94	6.05	692	1.38	0.14	2.19	0.71	5.90	0.65	0.65	0.32
	KEV	Rahmankulu spr	20.62	5.90	606	1.58	0.02	2.06	1.77	7.78	0.65	0.20	0.86
	KOP	Köprü hot spr	50.63	7.23	4868	7.42	1.77	1.72	3.12	9.59	1.35	4.96	1.81
	KUS	Köprü hot spr	65.50	7.43	3738	6.55	1.88	0.70	3.12	10.41	1.25	4.40	4.45
	MKK	Mollakara cold spr	9.27	6.11	1104	2.30	1.55	3.15	3.37	8.93	1.25	3.22	1.07
	MLK	Mollakara spr	65.20	6.63	3757	6.94	1.94	3.18	2.12	11.72	1.25	7.56	0.67
	MNC	Diyadin spr	20.15	7.80	267	0.48	0.13	0.96	0.36	2.29	0.25	0.17	0.37
	MNG	Mollakara spr	16.57	7.18	114	0.18	0.05	0.42	0.20	0.98	0.15	0.08	0.48
	RAH	Rahmankulu spr	11.46	7.75	505	0.74	0.05	1.20	1.24	5.08	0.09	0.03	1.03
	TAZ	Tazekent hot spr	39.81	6.93	737	6.55	1.79	1.95	3.19	12.29	1.56	4.65	1.64
	TSK	Taskesen cold spr	10.70	5.26	748	1.63	0.15	2.51	2.19	9.42	0.82	0.56	0.87

Table A.3 (cont'd): Chemical analyses of waters from geothermal fields of eastern Anatolia

Field	*Sample No.*	*Location*	T(°C)	*pH*	EC (µS/cm)	Na	K	Ca	Mg	HCO_3	SO_4	Cl	Mg/Ca
Diyadin [a]	TUN	Köprü hot spr	63.40	7.27	3744	7.86	2.02	0.97	2.60	10.41	1.67	5.11	2.70
	YES	Boyalan cold spr	12.01	7.68	359	0.69	0.04	2.26	0.33	4.67	0.15	0.23	0.14
	ZEG	Burgulu spr	17.82	3.15	1301	1.94	0.33	2.49	0.88	0.00	8.95	0.17	0.35
	AD-2[b]	Yılanlı hot spr	70.00			6.44	1.96	3.57	2.36	14.60	1.27	3.58	0.66
	MT-2[b]	Yılanlı hot spr	78.00			9.40	1.88	8.51	2.07	27.42	1.97	5.13	0.24
	MT-3[b]	Yılanlı hot spr	76.00			10.05	1.62	7.73	2.76	27.32	1.10	5.56	0.36
	MT-4[b]	Yılanlı hot spr	72.00			7.70	1.98	4.79	1.38	18.40	1.28	4.17	0.29
Çaldıran [c]	ALT	Altıyol	23.62	6.51	667	3.28	0.14	1.05	1.44	6.23	0.60	0.25	1.38
	AVC	Avcıbaşı	12.86	7.88	95	0.30	0.08	0.23	0.11	0.98	0.01	0.03	0.48
	AYR	Ayrancı	36.15	7.02	3915	26.33	4.80	0.23	0.85	19.67	1.46	12.02	3.67
	AYS	Ayrancı	25.80	6.07	1616	10.51	1.96	1.29	2.07	12.29	0.55	4.57	1.60
	BUG	Buğulu	35.73	6.76	1607	3.65	0.62	2.47	2.93	12.86	0.24	0.47	1.19
	BUS	Buğulu	20.33	5.85	747	1.14	0.33	1.42	1.84	7.54	0.47	0.31	1.29
	KOC-I	Koçovası	15.98	6.18	991	3.89	0.70	2.73	2.70	13.28	0.09	0.96	0.99
	KOC-II	Koçovası	25.08	6.71	3545	16.55	2.99	3.48	7.01	31.55	0.66	4.49	2.02
	KOC-III	Koçovası	14.59	5.63	1482	7.10	1.44	3.70	4.06	19.50	0.19	2.12	1.10
	YKR	Aşağıçanak	14.16	5.62	477	3.76	0.55	0.89	0.76	6.97	0.05	0.11	0.85
	ZYR	Ziyaret	11.39	7.15	103	0.46	0.02	0.50	0.12	1.39	0.07	0.03	0.23

All concentrations are mmol/L.

[a]Mutlu et al. (2013). [b]drilled wells of MTA. [c]Aydın et al. (2013).

Table A.4: Isotopic compositions waters from geothermal fields of eastern Anatolia

Sample No.	Sample location	$CO_2/^3He$ ($x10^9$) [a]	$\delta^{13}C(CO_2)$ ‰ (PBD)	δD (‰SMOW)	$\delta^{18}O$ (‰SMOW)	References
AYR	Ayrancı-Çaldıran	0.089	5.21	-89.7	-11.43	Mutlu et al., 2012
BUG	Buğulu-Çaldıran	89	2.94	-91	-13.49	Mutlu et al., 2012
CAM-1	Çamlık-Başkale	16,622	5.22	-77.4	-9.76	Mutlu et al., 2012
CAM-2			3.63	-81.5	-10.7	Mutlu et al., 2012
CAY	Çaybağı-Saray	37,742	1.82	-72.2	-3.41	Mutlu et al., 2012
CKR	Çukur-Güroymak	84	2.58	-68.8	-9.98	Mutlu et al., 2012
DVT	Diyadin	3660	4.61	-90.9	-11.29	Mutlu et al., 2012
DYD		28,779	4.79	-92.1	-11.52	Mutlu et al., 2012
GRM	Germav-Hizan	0.00024	-17.5	-72.4	-10.89	Mutlu et al., 2012
HAD	Taşkapı-Erciş		4.04	-79	-10.12	Mutlu et al., 2012
KOK	Kokarsu-Bitlis	83	4.04	-68.9	-10.65	Mutlu et al., 2012
NHL	Nemrut caldera	20	1.89	-64.5	-9.57	Mutlu et al., 2012
PAT	Patnos-Ağrı	14,708	3.13	-82.7	-11.36	Mutlu et al., 2012
TAS-1	Taşkapı-Erciş	889	4.36	-81.3	-11.37	Mutlu et al., 2012
TAS-2			5.55	-82.3	-11.26	Mutlu et al., 2012
TAT	Tatvan-Bitlis		2.27	-65.8	-9.76	Mutlu et al., 2012
TUT	Tutak-Van	114	4.6	-86.5	-12.12	Mutlu et al., 2012
YUR	Yurtbaşı-Gürpınar	10,292	3.13	-89.4	-12.68	Mutlu et al., 2012

[a]Uncertainty for the $CO_2/^3He$ ratio is estimated at ±5%.

Table A.5: Chemical analyses of waters from geothermal fields along the NAFZ

Field	*Sample No.*	*Location*	T(°C)	*pH*	EC (µS/cm)	Na	K	Ca	Mg	HCO_3	SO_4	Cl	Mg/Ca
NAFZ [a]	Efteni-1a	Efteni	43.2	6.5	3053	14.75	0.33	3.47	6.34	28.01	0.03	5.64	1.83
	Efteni-1b	Efteni	17	8.6	229	0.09	0.00	0.27	0.95	2.18	0.07	0.20	3.45
	Yalova-2a	Yalova	61.2	7.6	1917	11.40	0.13	3.99	0.33	0.74	8.54	2.65	0.08
	Yalova-2c	Yalova	17.2	7.5	584	0.74	0.05	2.47	0.25	5.02	0.43	0.39	0.10
	Bolu-3a	Bolu	42	6.2	1957	1.78	0.41	8.43	1.60	12.39	4.65	0.31	0.19
	Bolu-3b	Bolu	14.6	8	88	0.13	0.05	0.27	0.12	0.67	0.08	0.14	0.45
	Mudurnu-4a	Mudurnu	39.8	6.2	1150	1.04	0.18	3.97	1.81	11.98	0.28	0.23	0.46
	Mudurnu-4d	Mudurnu	15.1	7.1	793	0.78	0.10	2.42	1.65	7.57	0.47	0.25	0.68
	Seben-5a	Seben	71.4	6.6	2187	19.10	0.82	1.17	0.58	19.44	0.95	1.72	0.49
	Seben-5d	Seben	15	7.4	1105	2.61	0.15	2.57	1.97	6.00	2.77	0.39	0.77
	Hamamözü-6a	Hamamözü	42.5	7.4	514	2.00	0.15	0.95	0.74	3.90	0.25	1.02	0.78
	Hamamözü-6b	Hamamözü	16.3	7.5	613	0.70	0.05	1.97	0.95	5.42	0.39	0.31	0.48
	Gözlek-7a	Gözlek	39.1	7.8	495	3.35	0.13	0.50	0.33	4.08	0.32	0.42	0.66
	Gözlek-7b	Gözlek	17.8	7.7	1280	2.09	0.10	2.52	3.00	6.60	2.39	1.61	1.19
	Reşadiye-8a	Reşadiye	41.2	6.4		34.80	1.33	7.59	3.66	29.78	1.23	22.68	0.48
	Reşadiye-8b	Reşadiye	15.3	7.3	481	1.26	0.08	1.07	0.99	3.57	0.78	0.20	0.92
	Kurşunlu-9a	Kurşunlu	57.4	7	11160	107.09	6.68	1.67	0.99	97.38	0.70	21.86	0.59
	Kurşunlu-9b	Kurşunlu	13.3	6.4	2550	19.36	1.13	2.52	0.66	23.80	0.36	2.37	0.26
	Kurşunlu-9c	Kurşunlu	13.2	8	455	0.48	0.03	1.65	0.41	4.15	0.09	0.23	0.25

All concentrations are mmol/L. Data represent the average of nine sampling periods.

[a]Süer et al. (2008).

Table A.6: Isotopic compositions waters from geothermal fields along the NAFZ

Sample No.	Sample location	$CO_2/^3He$ ($x10^9$) [a]	$\delta^{13}C(CO_2)$ ‰ (PBD) [a]	δD (‰SMOW) [b]	$\delta^{18}O$ (‰SMOW) [b]	References
Efteni-1a	Efteni	8,700	-1.55	-82.9	-11.3	Süer et al. , 2008; de Leeuw et al., 2010
Efteni-1b				-80.1	-11.5	Süer et al. , 2008; de Leeuw et al., 2010
Yalova-2a	Yalova	32	1.52	-75.8	-11.3	Süer et al. , 2008; de Leeuw et al., 2010
Yalova-2c				-59	-9.1	Süer et al. , 2008; de Leeuw et al., 2010
Bolu-3a	Bolu	1,300	-0.18	-82.8	-11.5	Süer et al. , 2008; de Leeuw et al., 2010
Bolu-3b				-79.4	-11.9	Süer et al. , 2008; de Leeuw et al., 2010
Mudurnu-4a	Mudurnu	55	-2.46	-84.7	-12	Süer et al. , 2008; de Leeuw et al., 2010
Mudurnu-4d				-80.4	-11.2	Süer et al. , 2008; de Leeuw et al., 2010
Seben-5a	Seben	11,000	-0.34	-89	-12.1	Süer et al. , 2008; de Leeuw et al., 2010
Seben-5d				-68.4	-8.9	Süer et al. , 2008; de Leeuw et al., 2010
Hamamözü-6a	Hamamözü	35	-0.54	-87.4	-12	Süer et al. , 2008; de Leeuw et al., 2010
Hamamözü-6b				-74.5	-10.1	Süer et al. , 2008; de Leeuw et al., 2010
Gözlek-7a	Gözlek	120	-0.04	-94.2	-12.8	Süer et al. , 2008; de Leeuw et al., 2010
Gözlek-7b				-76.7	-10	Süer et al. , 2008; de Leeuw et al., 2010
Reşadiye-8a	Reşadiye	77,000	-1.92	-92.9	-12.7	Süer et al. , 2008; de Leeuw et al., 2010
Reşadiye-8b				-84.3	-12.1	Süer et al. , 2008; de Leeuw et al., 2010
Kurşunlu-9a	Kurşunlu	260,000	0.92	-88.3	-8.5	Süer et al. , 2008; de Leeuw et al., 2010
Kurşunlu-9b				-81.3	-10.5	Süer et al. , 2008; de Leeuw et al., 2010
Kurşunlu-9c				-77.4	-9.8	Süer et al. , 2008; de Leeuw et al., 2010

Data represent the average of nine sampling periods. [a]de Leeuw et al. (2010). [b]Süer et al. (2008).